Quantum Electrodynamics of an atom in front of a dielectric slab

A thesis submitted to University of Sussex
for the degree of Doctor of Philosophy
in the School of Science and Technology

2009

Ana María Contreras Reyes
Supervisor: Claudia Eberlein

Physics and Astronomy

Declaration

I hereby declare that this thesis describes my own original work, except where explicitly stated. No part of this work has previously been submitted, either in the same or different form, to this or any other University in connection with a higher degree or qualification.

Signed: . . . . . Date: . . . . . .

Contents

Acknowledgements

I owe my eternal gratitude to Claudia Eberlein for being an excellent supervisor to all extent. Thanks for her encouragement and for giving me the opportunity of working with her. I appreciate her vast knowledge and skill, her invaluable advice and the accurate motivation in going to conferences where I could receive important feedback. I am very grateful to the *Consejo Nacional de Ciencia y Tecnología* (CONACyT) for financial support for my doctoral studies; without it, this work would have been impossible.

A very special thanks goes out to Luis Mochan (ICF-UNAM), who first introduced me to the world of research and the Casimir forces that so much captivated me. His chats and enthusiasm always had a strong impact in my academic life.

I thank Carlos Villarreal (IF-UNAM), colleague and friend, for enhancing my career with his advice. I especially appreciate his encouragement to do my DPhil at Sussex, where I have had the opportunity to develop.

I must also acknowledge Prof. Gabriel Barton, who represents to me an inspiring figure. Thanks for his support, specially when my supervisor was absent, his stimulating discussions helped me to find the way.

Thanks to my friends who made more enjoyable my stay in Sussex, particularly Estela and Flor, for their companionship and support during these four years in Sussex; because we laughed and cried together a lot of times thus providing me with an enriched experience.

I thank Robert Zietal for critical discussions, and my friends James, Martin, Costas, Jim, and Peter for proofreading this manuscript.

And last, but most important, I would like to thank my parents and siblings for their unconditional and constant support. It was very hard to stay away from them for so long, but with their words they filled my soul with joy and drew a smile in my face every time I needed it. I apologize for not being there in the bad days, but I know they support me in this dream. To them I dedicate this thesis.

To the memory of my dear friend Ian Linington, with whom I shared the *theorists box* and the dream of becoming great scientists one day.

Abstract

Quantum electrodynamic theory (QED) in the vicinity of macroscopic structures has achieved new importance due to its applicability, particularly in nanotechnology. There are many powerful methods for studying QED near media with diverse properties and geometries. However, applying them to a particular problem generally necessitates extensive numerical calculations. This is not the case for simple systems of high symmetry, in which the electromagnetic field can be quantised by explicit mode expansion, allowing exact analytic calculations.

In the present thesis, we calculate the energy-level shift of a ground state atom near a non-dispersive and non-dissipative dielectric slab. The shift is due to the interaction of the atom with electromagnetic field fluctuations, which in turn are affected by the presence of the slab. Thus, a quantisation of the electromagnetic field in the presence of a layered system is required. We derive the field modes, which comprise of a continuous set of travelling modes (with incident, reflected and transmitted parts) and trapped modes, subject to repeated total internal reflection and emerge as an evanescent field outside the slab, they only exist at certain discrete frequencies. The shift is obtained by means of second-order perturbation theory. It splits up naturally into two contributions, due to the different nature of the modes, and a problem arises when we have to add them all. We have come up with a convenient method of summing over all modes, and its validity has been demonstrated by proving the completeness. The calculation of the shift follows as an application of our method. The result is analysed asymptotically for various regions, reducing to simple formulas that can be utilised in recent experiments, in which the thickness of the substrate matters.

Notation

Variable	Definition	Equation
$\mathbf{r}_o = (0, 0, z_o)$	Atom position	-
$\mathcal{Z}$	Surface-atom distance	-
L	Slab thickness	-
$\varepsilon(\mathbf{r})$	Dielectric permitivity	-
$\mathbf{k}$	Wave vector in free-space	(2.25)
$\mathbf{k}_\mathrm{d}$	Wave vector in dielectric	(2.26)
λ	Polarisations: TE, TM	-
ν	Mode, with polarisation λ and wave vector $\mathbf{k}$	-
$\hat{\mathbf{e}}_\mathrm{TE}$	TE polarisation vector	(2.17)
$\hat{\mathbf{e}}_\mathrm{TM}$	TM polarisation vector	(2.18)
N	Normalisation constant for travelling modes	(2.30)
M_{TE}	Normalisation constant for TE trapped modes	(2.49)
M_{TM}	Normalisation constant for TM trapped modes	(2.56)
R_λ	Reflection coefficient	(2.31)
T_λ	Transmission coefficient	(2.31)
r_λ	Fresnel coefficient (single interface)	(2.32)
L^S_{TE}	Decay coefficient for S trapped modes	(2.41)
L^A_{TE}	Decay coefficient for A trapped modes	(2.42)
L^S_{TM}	Decay coefficient for S trapped modes	(2.50)
L^A_{TM}	Decay coefficient for A trapped modes	(2.51)
α	Fine structure constant $\alpha = e^2/4\pi\epsilon_o\hbar c$	-

Chapter 1

General Introduction

1.1 The Casimir-Polder Force

It might come as a surprise that the ability of a gecko to walk across ceilings — in apparent defiance of gravity — is simply a manifestation of the zero-point energy. Amazingly, that talent does not rely on any sticky secreted substance or any other special biological effect, as would be the case for some other climbing animals. This ability arises from the intermolecular forces produced between their tiny foot hairs and the surfaces upon which they walk [1], even if they are smooth polished glass. This attractive force is known as the van der Waals force and it is also responsible for other curious phenomena in nature. A closely related attractive force, whose nature too comes from the fluctuations of the vacuum field is the so-called Casimir-Polder force — the force between an atom and a perfect conductor — as first predicted by Casimir and Polder in 1948 [2]. To date it is still a source of interesting research, probably due to its wide applicability particularly in nano-technology. This interesting quantum vacuum effect is the main subject of the present dissertation, and our motivation and particular interests in the matter will be manifested in the next section. First of all, we shall start with a brief review on the history of its discovery, including both the relevant theoretical and experimental contributions to date[1].

[1] For a general review on quantum vacuum effects, see for instance Ref. [3]

1.1.1 History

For a better understanding of the nature of the Casimir-Polder force, it is convenient to go back to the origin of its discovery, to the point where these ideas emerged: the more basic problem of the interaction between two neutral molecules, which is well known as *van der Waals* forces. This has been a more widely studied phenomenon and an extensive number of books devoted to this interaction can be found in the literature. For instance, one can find a very good description of such interactomic forces in Ref. [4–6].

Besides the more obvious forces that involve charged or dipolar molecules and arise straightforwardly from their electrostatic interaction, there is one that exists between all neutral but polarisable atoms and molecules. This force has been given many names, but the most widely used is *dispersion force*, in relation to the dispersion of light in the visible and UV regions of the spectrum. The literature on this specific subject is also very extensive, and one of the most recent and complete reviews on dispersion forces can be found in Ref. [7].

The dispersion forces represent one of three contributions to the van der Waals force and may be considered the most important contribution to the total force between atoms and molecules[2]. They are responsible for many interesting phenomena in nature such as adhesion, capillarity, surface tension [8], adsorption of inert gas atoms to solid surfaces [9], wetting properties of liquid on surfaces [10], the properties of gases, liquids and thin films, the strengths of solids and the structures of condensed macromolecules such as proteins and polymers [4].

These long-range forces may be repulsive or attractive. As will be explained in more detail later in this section, the interaction between two bodies is affected by the presence of other bodies nearby. In this sense, this force is not analogous to Coulombic interactions, where the superposition principle may be utilised. This is known as the *non-additivity* of an interaction.

The dispersion force has a quantum mechanical origin but there is a simple intuitive

[2]The other two contributions are the *induction force* and the *orientation force*.

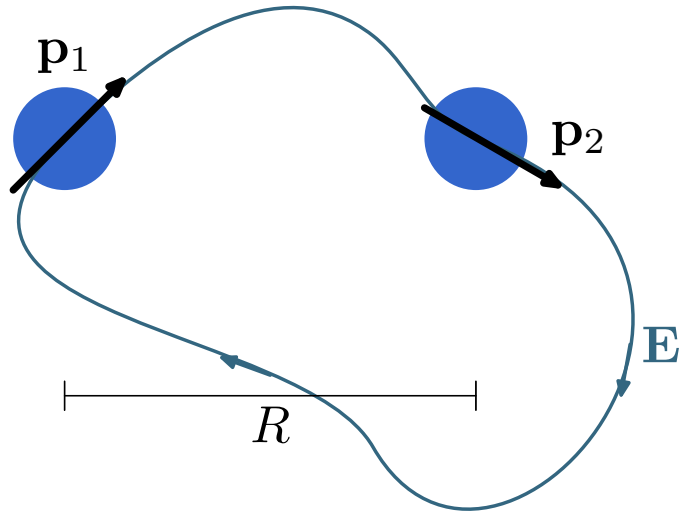

Figure 1.1: Two neutral molecules located a distance R apart. A fluctuating dipole $\mathbf{p}_1$ in one of them, produces an electric field $\mathbf{E}$ which induces a dipole $\mathbf{p}_2$ in the second molecule.

explanation that gives us a qualitative understanding of this physical problem [5]. Let us consider two neutral and non-polar molecules separated by a distance R, as it is shown in Fig. 1.1. Even though these molecules are neutral and have on average zero dipole moment, by the Heisenberg uncertainty principle we know that the position of the electrons belonging to each molecule is a fluctuating quantity and thus, a spontaneous fluctuating dipole $\mathbf{p}_1$ could exist in, lets say, the molecule 1. In other words, although $\langle p_1 \rangle_t = 0$, in general $\langle p_1^2 \rangle \neq 0$ because instantaneously $\mathbf{p}_1 \neq 0$. What is more interesting to note is that this fluctuating dipole produces an electric field $\mathbf{E}$ that can polarise the second molecule, inducing a dipole $\mathbf{p}_2 = \alpha_2 \mathbf{E}$. In this expression α_2 is the polarisability, which is a function of the frequency, and the electric field is given by $\mathbf{E} = \mathbf{T}\mathbf{p}_1$, where $\mathbf{T}$ is the dipolar interaction tensor, which is proportional to $1/R^3$. From classical electrodynamics it is known that the interaction energy for an induced dipole is given by[3] $U = -\mathbf{p}_2 \cdot \mathbf{E}/2$ (see for instance Eq. (4.93) in [11]), obtaining thus $U = -\alpha_2 \langle p_1^2 \rangle / R^6$, which is the above mentioned dispersion energy[4]. As expected, this interaction increases as much as the fluctuations $\langle p_1^2 \rangle$ do, depending on how quickly the molecule 1 gets

[3] For time-independent $\mathbf{E}$ fields.

[4] Since $\mathbf{p}_1$ has an arbitrary direction, one may take the average of the squared dipolar tensor $T_{ij} = (3R_iR_j - R^2\delta_{ji})/R^5$, thus $\langle T_{ij}T_{ik} \rangle = (2/R^6)\delta_{jk}$

polarised. We can therefore say that $\langle p_1^2 \rangle$ is proportional to α_1, thus obtaining an interaction energy $U \propto -\alpha_1 \alpha_2 / R^6$.

The instantaneous interaction of these two dipoles gives rise to an attractive force between the two molecules, which decays as R^{-7}. The exact result was derived by London in 1930 [12] by using quantum mechanical perturbation theory. His theory emerged due to his concern about the incorrect treatment that had been given to the dispersion forces at that time, indiscriminately based on additive central forces, which is not true at all. He also emphasized that the elementary units of the dipole-dipole interactions are not spherically symmetrical central forces, but have rather to be built up by highly anisotropic force centres [13]. The dispersion energy that he obtained for two identical molecules is given by

$$U = -\frac{3}{4} \frac{\alpha_o^2 h\nu}{(4\pi\epsilon_o)^2} \frac{1}{R^6}, \tag{1.1}$$

where α_o is the electronic polarisability of a Bohr atom. In 1963 McLachlan [14] presented a more generalised theory of van der Waals forces, obtaining one expression that included all the three contributions: induction, orientation and dispersion forces. His formula is written in terms of the polarisabilities of the interacting molecules (as in the example given above) and the dielectric permittivity of the medium in which they are embedded, which can be easily related to measurable properties so that the calculation of the interaction can be performed. In fact, London's formula can be seen as a particular case of McLachlan's theory; merely by treating molecules as simple harmonic oscillators, one can recover London's result.

A further interesting effect that one may consider is the one due to *retardation*[5]. As it has been shown, the force between two molecules will depend on the separation between them. If they are close enough to each other (as we have considered so far), their interaction arises from the electrostatic force between the fluctuating dipoles. Nevertheless, if they are located an appreciable distance apart, the time taken for the

[5]For a deeper review on this subject see for instance Chapter 5 in Ref. [5]

electric field produced by the first molecule to travel to the second molecule and get back becomes comparable to the period of the fluctuating dipole. This implies that by the time the **E** field comes back to the first molecule, it may find the fluctuating dipole pointing out in a different direction, which means that it would be less favourable for an attractive interaction[6]. When this happens, the dispersion energy begins to decay even faster with distance and goes from R^{-6} to R^{-7}. For example, for two Bohr atoms this change starts at distances greater than 100 nm. This is called the *retardation effect*.

But how did scientists realise that it was important to take into account the retardation of the electromagnetic field? The original idea was suggested by Overbeek, in 1948. He was studying colloidal solutions and realised that in order to account for the stability of suspensions of large particles it was necessary to include such retardation. Inspired by that insight, Casimir and Polder obtained the retarded dispersion energy between two molecules, and their results were published in a series of three papers [2, 15, 16]. They considered the interaction with the radiation field and used fourth order perturbation theory to conclude that the energy depends on the molecules polarisability α_m and is given by,

$$U = -\frac{23\hbar c}{4\pi}\frac{\alpha_m^2}{R^7}. \tag{1.2}$$

Later on, other attempts to calculate the force between two neutral but polarisable molecules were made. Among them we can find an approach given by Power and Zienau in [17]. In their approach they use a Hamiltonian in which each atom is replaced by an electric dipole. Other simpler formulations were given by Dzialoshinskii [18], Mavroyannis and Stephen [19] and MacLachlan [14].

The consequences of retardation become more important in the presence of other media — where the speed of light is slower — and it is particularly interesting when macroscopic bodies or surfaces come into play. The simplest example of this can be illustrated by the typical problem of an atom in front of a perfect conductor (see Fig.

[6]The maximum strength is obtained when there is no retardation, i.e., no change in orientation.

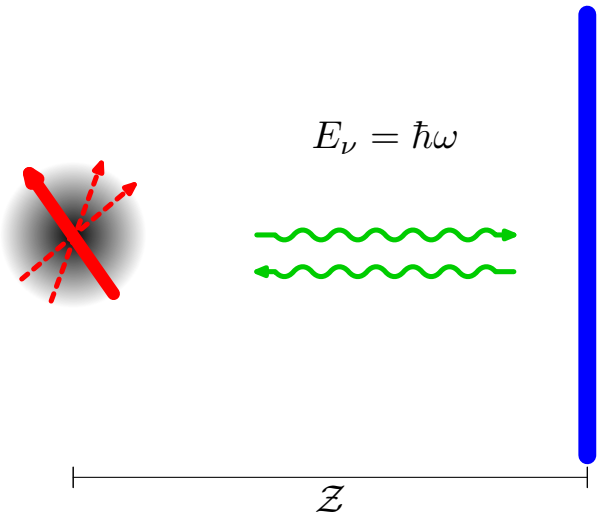

Figure 1.2: Atom located a distance $\mathcal{Z}$ in front of a perfect mirror, in the retarded regime, where the time a photon travels a round trip to the interface must be taken into account. The figure shows schematically how the fluctuating dipole changes during that time.

1.2). This problem was also solved by Casimir and Polder [2]. Following basically the same mechanism — as an illustration of the more complicated calculation for the interaction between two molecules — they found that the interaction energy decreases with distance as

$$U = -\frac{3\hbar c}{8\pi}\frac{\alpha_a}{\mathcal{Z}^4}, \tag{1.3}$$

where $\mathcal{Z}$ is the atom-surface separation and α_a is the static polarisability of the atom. The equation above gives rise to the famous Casimir-Polder force, in their honour. We have included in Appendix A a derivation of the formula above.

In the calculation of the force between an atom and a interface, one has to take into account the fact that the principle of additivity that is allowed in Coulombic interactions does not apply in this case. The non-additivity is a result of the fact that neighbouring atoms influence the interaction between any pair of atoms, and this is simply because the polarisability of an atom changes when it is surrounded by other atoms. This can be understood by going back to our example (Fig. 1.1). If we consider a third atom, it will feel an electric field produced by the first atom, and thus a dipole will be induced in it as well, and that must have an effect on the second atom. In summary, the field

from atom 1 reaches atom 2 both directly from atom 1 and by reflection from atom 3. Obviously the problem gets more complicated if several atoms are involved and the additivity procedure breaks down. However, a naïve deduction of the Casimir-Polder potential is presented in [20], in which a ground-state atom at a distance $\mathcal{Z}$ from a dielectric half-space consisting of N continuously distributed atoms per unit volume, is considered. Taking the interaction between the atom outside the dielectric and one atom inside being proportional to $-1/r^7$ (exactly as in Eq. (1.2)), one can thus add up all the pairwise interactions to obtain

$$U = -\frac{69\hbar c}{160\pi}\frac{\alpha_a}{\mathcal{Z}^4}, \tag{1.4}$$

which is surprisingly similar to the exact result, despite the fact that we are assuming pairwise additivity. This is not a problem in the Lifshitz theory [21], which treats large bodies as continuous media and the forces can be derived in terms of bulk properties such as dielectric constants. This theory, developed in 1956 and based on complicated quantum field theory, currently represents a very powerful and widely used formulation. It is especially devoted to the calculation of another related force: the famous Casimir force [22], which is the attractive force between two parallel plates (perfectly conducting, in the original derivation by Casimir). In his paper, he calculates the dispersion force between two half-spaces at finite temperature. The force is obtained through the average of the stress tensor of the fluctuating electromagnetic field at the surfaces of the half-spaces. The essential idea in this calculation is to relate the current fluctuations to the imaginary part of the permittivity[7] via the fluctuation-dissipation theorem. One could cite hundreds of papers in which the Lifshitz formula has been applied to several systems; including the controversial problem of finite temperature [23], surface roughness [24], and spatial dispersion [25], and even reformulated and generalised [26, 27]. As a particular case, Lifshitz used his approach to calculate the force between a wall and an atom by taking the latter as a dilute gas of atoms.

[7]The permittivity is a complex function of frequency, with the real and imaginary parts responsible for dispersion and absorption, respectively.

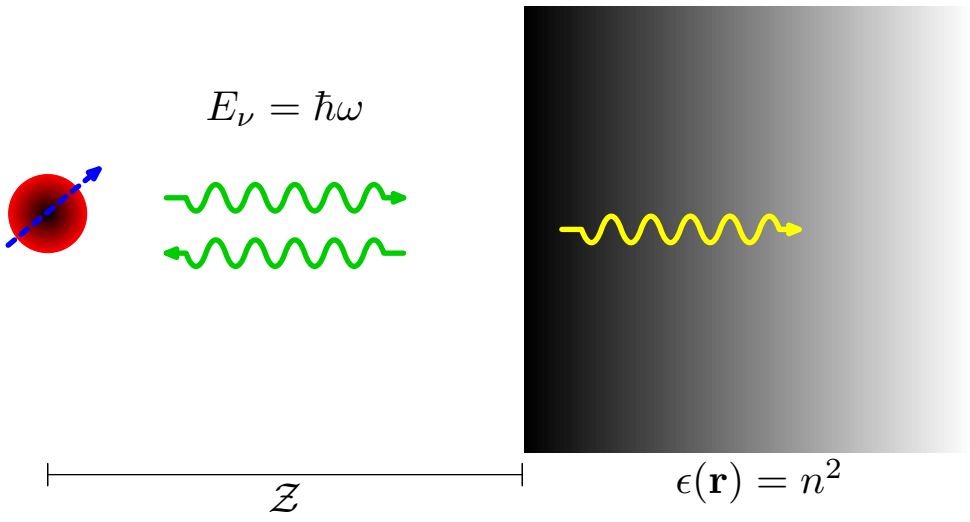

Figure 1.3: Atom in front of a dielectric half-space, in the retarded regime.

Many other variations have been provided to the problem of atom-surface interactions. Among them we can first mention the problem regarding an ideal wall and its interaction with excited atomic energy eigenstates [28], and with an electron [29]. If we instead want to get more realistic by describing the wall by an imperfect reflector, the next step would be to consider a dielectric wall, as illustrated in Fig. 1.3. Pioneering work was done by Mavroyannis in 1956, who studied the interaction of neutral molecules with dielectric walls [30]. Notice that in this situation the photons reaching the interface can also be transmitted through it, and hence they must be included in the calculation. Moreover, we shall take into account the waves coming from the dielectric, and thus, the evanescent waves outside the half-space.

This system could be turned into a more complicated problem if one wishes to include other physical properties and use more sophisticated models to describe the metallic surface. For instance, Babiker and Barton used the hydrodynamic model in order to describe the metallic interfaces in a more realistic way, and calculated the frequency shifts of an atom near a plasma surface [31].

Unsurprisingly, if one wishes to go further in the geometry of the system or include other properties, i.e. absorption [32], one might not be able to solve the problem

analytically anymore, due to the expected complexity that perturbative calculations based on normal-mode QED involves. For that reason, other methods based on linear-response theory have been utilised [33]; presumably overcoming those difficulties and extending results in such a way that practicability is gained. Nevertheless, the results obtained through these methods are given in terms of Green functions, and the problem lies in obtaining them. Thus, the price paid for this apparent wide applicability implies extensive numerical calculations for each particular problem.

1.1.2 Experimental observation

We have given so far a brief overview on the theoretical approaches that lead us to the famous formula for the Casimir-Polder force, beginning with the one that describes the interaction between two neutral and non-polar atoms (most commonly known as van der Waals) to finally obtain a formula for the dispersion energy between a perfectly reflecting plate and an atom, which is the origin of the motivation of this thesis. As theory and experimental research must go always together, we shall give a short list of the experiments built through the last thirty years, when they started to be successful, concentrating on those devoted to the study of atom-surface interactions.

It might be surprising to find numerous experimental papers in the literature, though what is truly astounding is that after 60 years of the discovery of the Casimir forces[8] new results and more interesting ideas are still produced, which can now be extended to other areas of physics and most importantly, that can be applied to improve technologies.

Many attempts have been made to detect this force; by using different types of experiments people have been able to measure first in the non-retarded regime (sometimes referred to in the literature as van der Waals interaction), and later in the retarded regime, the so-called Casimir-Polder interaction, which corresponds to greater atom-surface separations.

One of the first records that can be found on measuring the van der Waals interaction

[8]See the feature article in Physics Today, published by Lamoreaux [34].

between neutral atoms and a surface is an experiment performed by Raskin and Kusch [35], and later by Shih and Raskin for molecules [36]. By passing a thermal atomic beam near a metallic cylinder[9], they studied the deflection of the atomic beam. In a similar scheme, the deflection of atoms passing between two metal plates was monitored by observing the atom flux losses due to the sticking of atoms to the plates, finding a strong enhancement of the force when excited atoms were utilised [37].

A different type of experiment was performed in 1992 by Haroche and co-workers via spectroscopic means [38]. They used high resolution spectroscopy on Rydberg atoms inside a micron-sized parallel-plate metallic cavity to measure the energy shift due to the van der Waals interaction.

However, the first experiment that went further in distance into the retarded regime and certainly provided a confirmation of the Casimir-Polder force as predicted by quantum electrodynamics was performed by Hinds and his co-workers at Yale University [39]. In this elegant experiment, they studied the deflection of ground-state sodium atoms passing through a parallel plate cavity, of order microns in size. They measured the intensity of the beam transmitted through the cavity as a function of the separation between the cavity plates. The reason for this reflection is due to the variation of the vacuum field with position within the cavity. Thus the atoms are pushed towards the cavity walls, experiencing a Casimir-Polder force.

Other modern techniques have been used in order to get more precise experimental results. Advances in laser cooling [40] were applied ten years ago to increase the sensitivity of measurements by better control of atomic trajectories. That is the case of the atom-scattering experiment performed by Landragin *et al.* [41], in which a laser beam is incident on the surface of a dielectric from the inside at a sufficiently shallow angle, such that total reflection leads to an exponentially decaying electric field at its exterior. This artefact is called an evanescent-wave mirror, and the central purpose of the experiment is to place an atom in the vicinity of such a body, interacting therefore with this evanescent field and leading to an optical potential. If the laser frequency is

[9]Note that in such experiments the minimum atom-surface separation obtained is so small that the cylinder surfaces can be regarded as planar.

larger than the relevant atomic transition frequency (blue detuning), then this potential is repulsive; thus, one can in principle create the required compensating force which can be controlled by varying the laser frequency and intensity. Hence, the dispersion forces on ground-state atoms can be measured by monitoring the reflection of the atoms incident on evanescent-wave mirrors.

Other experiments were built on the idea of another wave phenomenon: diffraction, in which the van der Waals interaction is studied by measuring the diffraction intensity of atoms passing through a transmission grating [42, 43].

Experiments to measure the Casimir-Polder force by using ultracold atoms [41, 44–48] form a new age of experiments that are worth reviewing in more detail, since they could offer a much better precision and are sensitive to other geometrical characteristics of the system that have not been taken into account before. As an example, it has been recently suggested by Dalvit *et al.* [49] that using cold atoms would be useful to probe quantum-vacuum geometrical effects.

In the next section of this chapter the motivation and outline of this work is provided and thus it will certainly be appropriate to get back to the most recent experimental contribution. In that way, the practical reasons of our interest into this specific subject will become apparent. But first of all, let us conclude this section by showing from a more theoretical point of view the origin of this interesting phenomenon.

1.1.3 A different perspective

One of the most famous and intriguing vacuum effects, very closely related to those explained in the previous section, is the Lamb shift [50]. It was discovered in 1947 and its explanation, in words of Dirac, "changed fundamentally the character of theoretical physics" [51]. However, such vacuum effects were first explored in terms of intermolecular interactions due to their more intuitive character with relatively down-to-earth considerations having to do with the stability of colloids, as it has been explained.

The Schrödinger equation for hydrogen atoms predicts that the energy levels depend only on the quantum number n. From the Dirac equation it can be concluded that

states with the same n and same total angular momentum quantum number j, such as $2s_{1/2}$ and $2p_{1/2}$ remain degenerate. Nevertheless, experiments performed in the 1930's showed that the energy in such states differ slightly, but they were not accurate enough to draw formal conclusions. It was not until 1947 when Lamb and Retherford [50], utilizing microwave techniques, proved that those two energy states are actually non-degenerate and moreover, that the difference between them is approximately 1000 MHz.

Schwinger and Oppenheimer suggested that the explanation might be the shift of energy levels by the interaction of the electron with the radiation field. Since the Dirac theory ignores this interaction, one could partially understand the problem by modifying the Schrödinger equation to include the coupling of the atom to the radiation field.

Since the Lamb shift is a non-relativistic effect we can consider the Hamiltonian

$$H = H^{\mathrm{rad}} + H^{\mathrm{atom}} - \frac{e}{m}\mathbf{A}\cdot\mathbf{p} + \frac{e^2\mathbf{A}^2}{2m}, \tag{1.5}$$

where H^{rad} is the field Hamiltonian and H^{atom} is the Hamiltonian operator for the atomic electron. As it will be explained with more detail in Chapter 3, $\mathbf{A}$ is the electromagnetic vector potential and we make use of the electric dipole approximation.

It is clear that we are dealing with a quantum electrodynamic effect because in classical theory $\mathbf{A} = 0$ in vacuum and thus it would not contribute to perturb the atomic levels. However, when the field is quantised, standard perturbation theory gives the shift in the atomic level i due to the interaction $-(\mathbf{A}\cdot\mathbf{p})e/m$

$$\Delta E = -\frac{e^2}{m^2}\sum_{\nu}\sum_{j\neq i}\frac{|\langle j;1_\nu|\mathbf{p}\cdot\mathbf{A}(\mathbf{r},t)|i;0\rangle|^2}{E_j - E_i + \omega_\nu}. \tag{1.6}$$

The state $|i;0\rangle$ represents an atom in the state i and the field in vacuum state of no photons, and the state $|j;1_\nu\rangle$ represents an atom in the state j and the field with one photon in mode ν. If we quantise the field by normal-mode expansion of $\mathbf{A}$, in terms of the creation and annihilation operators, we can make further simplifications. After

some algebraic manipulations we get[10]

$$\Delta E_i = -\frac{2\alpha}{3\pi m^2}\sum_j |p_{ij}|^2 \int_0^\infty \frac{dE\ E}{E_i - E_j - E}, \tag{1.7}$$

which is infinite. This is problematic, as it presumably corresponds to the Lamb shift, which should be small instead, as the experiments had shown. This problem remained without answer until Bethe [52], after a Conference in Shelter Island and by using some ideas by Kramers, solved this dilemma. He identified the most strongly (linearly) divergent term in the level shift with the energy of a free electron due to its coupling to the field, and subtracted it from the above expression. This procedure is called renormalization, and it could be shown that such a difference corresponded to the observable Lamb shift. The result was still divergent, but only logarithmically divergent. Thus, by introducing a cut off in the upper limit of integration (assuming that the main part of the Lamb shift was due to the interaction of the electron with vacuum field modes of frequency small enough to justify a non-relativistic approach), Bethe obtained a level shift for the 2s state of H of ~ 1040 MHz, in agreement with experiments. It is interesting to recall that Bethe's estimate was considered by Feymann[11] "the most important discovery in the history of QED".

The way to connect this with the van der Waals forces follows from interpreting them as a result of the fluctuations of the zero-point energy, which is actually the idea that London originally followed.

Now, if the fluctuations of the electromagnetic field are constrained, i.e. by the presence of conducting media, the vacuum effects are enhanced. This manifests itself macroscopically in a modification of both the rate of spontaneous emission and the Lamb shift. The latter is the one that we have been referring to as the Casimir-Polder force, and it will be particularly interesting if we also add other constraints to this system. In this work we are especially interested in the variation of the force due to a finite slab. A more detailed description of the geometry we are interested in, together

[10] For a more detailed description of this procedure see Ref. [3].
[11] In his Nobel Lecture, see Ref. [53]

with the reasons for why it is important to solve such a problem, will be given in the following sections.

1.2 Motivation and outline

Section 1.1.2 reviewed a series of experiments that have been relevant in order to show the existence of the Casimir-Polder interaction. Nevertheless, nowadays simply detecting such forces is not as interesting and challenging as, for example, probing their wide ranging applicability and discovering other unusual behaviour[12].

As experiments become increasingly precise, corrections, such as finite temperature, roughness and other geometrical details, etc., become more important in the theoretical calculations. The levels of precision are becoming commonplace now more so than ever due to the motivations in developing nanotechnology and furthering quantum science [56, 57]. That is the case of the so-called *microtraps*, which when used in conjunction with chip technology, have promising areas of application like quantum information processing with neutral atoms, integrated atom optics, matter-wave interferometry, precision force sensing, and most importantly for the theoretical purpose of this thesis; studies of the interaction between atoms and surfaces. Thus, the control and manipulation of cold atoms have become fundamental, and it seems feasible to control them on the μm length scale by utilizing such microstructured surfaces, also known as atoms chips. In very general terms, magnetic traps on atom chips are commonly produced either by microfabricated current-carrying wires or by poled ferromagnetic films attached to some dielectric or metallic surface. Therefore, more sophisticated theories that include such geometries are required. For instance, Eberlein and Zietal obtained results for an atom in front of a cylinder [58], which would simulate the wires in those microstructures.

Furthermore, one can identify another characteristic of the system that has become sensitive to modern experiments, which is the thickness of the layer of material that

[12] Recently, people have been intrigued by the possibility of using left-handed metamaterials in order to detect repulsive Casimir forces. See for instance Ref. [54, 55]

is located near the atom in such microtraps. This is because, typically, the dielectric substrate utilised in those experiments contains a very thin top layer of other material. So far, in rigorous theories, this finite thickness has been neglected and the system has been treated as a semi-infinite half-space. Nevertheless, we believe that it is important to develop more accurate approaches and take the thickness correction into account.

In section 1.2.2, we will give a brief review on the theoretical work done so far involving an atom near a dielectric slab. To date, only some limiting cases for specific numerical examples have been obtained explicitly. We instead want to provide an exact analytical expression, which can be utilised practically in current experimental research.

In the following section we shall review the very latest experiments that have been developed using cold atoms techniques. This is essential in order to support our motivation for performing this thesis, and to make evident the importance of our calculations.

1.2.1 Experimental application

Trapping neutral particles is not a new field. The first neutral atoms were trapped in 1985 [59] in the magnetic field of electromagnets. Later on, the idea was extended to gases of alkali-metal atoms, which were magnetically trapped and cooled down below the critical temperature for Bose-Einstein condensation. For this achievement, the Nobel Prize was awarded to Cornell, Wieman and Ketterle [60, 61]. With these experiments a new generation of Casimir-Polder force measurements emerged. They realised that, by using cold atoms, potentially very high precision experiments could be performed[13]. Therefore they employed the Bose-Einstein Condensates (BEC), which consist of a cloud of ultracold atoms that are joined into a single quantum-mechanical state[14]. The advantage of using a BEC is that it is much easier to deal with rather than trying to manipulate a single atom.

A pioneering experiment was performed by Cornell's group [65]. To measure the Casimir-Polder force they created a horizontal cigar-shaped BEC of rubidium atoms several microns in diameter and set it within a magnetic trap, so it would oscillate

[13] And thus the possibility of investigating fundamental forces at the submicron scale [62].
[14] For a general review on BEC's see for instance Ref. [63, 64].

vertically. This trap was located just below a plate, in such a way that the oscillation frequency changed. This is because the Casimir-Polder force pulls more strongly on the upper edge of the cloud than on the lower one. This experiment was carried out at a range of distances between 6 and 10 microns (including the region where thermal effects become important [66]) and the force could be calculated from the frequency measurements. The dielectric surface utilised in this experiment was made of silica. However, in their second experiment, to measure the temperature dependence [66], they used a dielectric substrate topped with $\sim 100\mu m$ thick opaque layer of graphite. The beauty of this experiment emerges from the fact that is one of the first applications of BEC's, surprising due to the actual complexity of the condensate. The perturbation on the frequency of center-of-mass oscillation of the BEC detected was first predicted theoretically by Antezza *et al.* [67].

A similar experiment, in which ground-state rubidium atoms were utilised, was performed by Mohapatra and Unnikrishnan [68]. The purpose of this experiment was to measure the van der Waals force between them and a metallic surface (cobalt), by using a technique that involved the reflection of laser-cooled atoms from magnetic thin-film atom mirrors.

Following the same line there is an experiment performed by Spreeuw and co-workers [69]. Their experiment was the first in which modified radiative properties in the vacuum near a dielectric surface were observed. They used a magneto-optical trap to create a cloud of cold ^{87}Rb atoms, and observed a distance-dependent absorption linewidth when locating the atoms near a glass surface (with refractive index $n = 1.51$).

Several experiments have been developed to date, intending to measure the Casimir-Polder force with high precision[15], becoming thus more evident the success on accurate measurements. It might therefore be worth trying to understand how to trap and manipulate ultracold atoms (and degenerate quantum gases) in magnetic micropotentials. Fortagh and Zimmermann [70] have recently published a review, in which they give an overview on fabrication techniques and history of pioneering experiments. Also, though

[15]For instance, in experiments by Hinds group [39], it was obtained that $U_{theory}/U_{exp} = 1.02 \pm .13$

in less detail, they devote a section to atoms in the proximity of the microtrap surface, which is of particular interest to us.

As we explained earlier, atoms interact with fluctuations in the electromagnetic field. In this case, the fluctuations are modified in the vicinity of a trap surface, and this has other important consequences that some people have already analysed. The reason is that magnetic field fluctuations in a microtrap can induce transitions between internal spin states, which produce decoherence and loss of the atom[16]. This effect was predicted by Henkel *et al.* [71] and first observed by Ed Hind's group [72] for a cylindrical wire and by Cornell's group [73] for a thick metal slab.

Since trapped atoms are very sensitive to magnetic field fluctuations, such effects have recently been a subject of great interest, especially the spin-flips produced near surfaces. The problem has been analysed several times and the length-scales of the system that appear to be most important are: the thickness of the metal, the atom-surface distance and the skin depth. Thus, the lifetime of the atom has been calculated in terms of those variables for different interesting regimes. Very importantly for our purposes, they emphasize the results obtained when a thin slab is used, stressing that it characterizes more precisely what has been done recently in the lab, i.e. most microtraps used today have a film, not an infinitely thick surface. It is important to remark that although the nature of this problem has completely different physics, the reason we are including these experiments is because in them the thickness becomes an important parameter. As the combined Casimir-Polder interaction and the one produced by fluctuating magnetic fields will both be responsible for the behaviour of the atom, a correct theoretical calculation of the energy-shift, including such thickness, is essential.

The stability of magnetically trapped BEC was studied by Lin *et al* in [47]. They gave experimental values for the loss rate of ^{87}Rb atoms near a thin surface. In this experiment, a 2 μm-thick copper layer with a final top layer of 100 nm Au was utilised. The latter was deposited by electron beam evaporation (all of these on a substrate of nitride-coated silicon). The behaviour of the atom was studied at small distances of

[16] Only low-field-seeking states are confined in the magnetic trap

Table 1.1: Latest experiments

Authors	atom-surface separation $\mathcal{Z}$	Thickness L of top layer	Material of top layer	atoms used	Ref.
Obrecht *et al.*	$10\mu m$	$100\mu m$	graphite	^{87}Rb	[66]
Jones *et al.*	$\sim 30\mu m$	$200nm$	Gold	^{87}Rb	[72]
Lin *et al.*	$.5 - 10\mu m$	$100nm$	Gold	^{87}Rb	[47]
Leanhardt *et al.*	$\sim 70\mu m$	$1.25\mu m$	Gold	^{23}Na	[74]
Sukenik *et al.*	$\sim .5\mu m$	$40nm$	Gold	^{23}Na	[39]

.5μm - 10μm from the microfabricated silicon chip.

At this stage, it has become more evident that the accuracy of recent experiments allow high sensitivity to length scales of the system that were not taken into account before. That includes, undoubtedly, the film thickness i.e., in a microtrap.

The table 1.1 shows the Casimir-Polder experiments that are relevant for our purpose; where a thin layer of material is placed on the top of the dielectric substrate commonly used. In this way, one can note that the thickness of the material near the atom should not be treated as infinite, since it is of the order of the atom-surface separation.

1.2.2 Variations of this problem

We are interested in the calculation of the Casimir-Polder interaction of an atom with a dielectric slab. In this way, we would like to generalise the analytical formulae derived by Wu and Eberlein for the simpler case of a dielectric half-space [75, 76]. The geometry of an atom in front of a dielectric slab, even though seems to be quite simple, has been studied earlier but only simpler problems have been analysed (i.e. spontaneous emission), and no analytical formulae have been obtained so far.

Only a few papers, in which quantum electrodynamic concepts based on normal mode expansion of the quantised electromagnetic field are used, can be found in the literature. We shall first mention Khosravi and Loudon's work [77], who in an extension to their calculation for a dielectric half-space [78], utilised exactly the same model we

are using and quantised the field in order to evaluate the vacuum field fluctuations and spontaneous emission rates as functions of positions both inside and outside the slab. However, some calculational errors were made, including the normalisation constant for the TM polarisation and the density of modes. This affected particularly the results for a thin slab, as affirmed in [79].

Żakowicz and Błędowski [79], re-calculated the spontaneous emission by using the same quantum approach and standard perturbation theory. Unlike in [77], they utilised different parametrization of the travelling modes, by the outgoing waves. This was done with the purpose of describing angular properties of spontaneous emission. They corrected the normalisation constant miscalculated in Ref. [77], and regarding the second mistake, they obtained the energy density of trapped modes for the situation under consideration, as needed for their calculation of the radiation intensity distribution. They realised that in the region far away from the slab their density of modes would become very much simpler (but only in that region), and such a density of modes was the same as that adopted by Khosravi for the calculation in the whole space, with no proper arguments provided. That made their results doubtful, and actually their oversimplification caused their calculated decay rates to be incorrect. We shall come back to this point and provide more details in the following chapter.

Another related piece of work was done later on by Urbach and Rikken [80]. They calculated the spontaneous emission rate of an atom from inside a dielectric slab, bounded by two dielectric half-spaces. Their interest in this specific model had the purpose of being applied to the electron-hole recombination in GaAs slabs studied in [81] and to experiments in [82] for the radiative transition rate of Eu^{3+} complexes in polystyrene films on various dielectric substrates. Thus, they obtain numerical results for those particular problems.

A slightly different geometry was studied by Zhou and Spruch [83]. They considered two multilayered plane parallel walls of arbitrary thickness and permittivities and analysed their van der Waals (and retarded) interaction with a particle, either atom or electron, located between them; treating each multilayered wall as a single wall de-

scribed by an effective reflection coefficient. They quantised the surface modes in order to evaluate this force, and taking certain limits, they recovered well known results and provided others not previously obtained, in such a way that they could give quantitative estimates of the errors due to approximating a wall of finite thickness by one of semi-infinite thickness. Since they consider the limits to obtain the atom-wall interaction, we shall compare our final expressions with theirs, which consist of a double integral, unlike the explicit formulae that we are able to obtain. Bostrom and Sernelius [84] extended this calculation by examining the van der Waals energy of an atom placed between thin metal films at finite temperature. In order to study the effect of finite thickness, they evaluated their result numerically for ground-state hydrogen and helium atoms between silver films.

As was explained in the previous section, the Casimir-Polder theory is based on quantum electrodynamics, in which the electromagnetic field is quantised in terms of normal modes. Thus, the coupling energy for a ground-state atom with the field can be calculated in lowest order of perturbation theory, and the retarded van der Waals force arises as the gradient of this energy. This elegant approach is very convenient if we are dealing with systems of high symmetry, because the electromagnetic field can be quantised by explicit mode expansion (in a relatively easy way) facilitating exact analytical calculations. However, this formalism becomes far more complicated if we want to apply it to other geometries.

On the other hand, by taking into account imperfect reflectors in a cavity [85] would become apparent that it is not easy to obtain the field modes for dielectric cavities. In fact, it would not be favourable to use a normal-mode expansion. For this reason, a new range of very powerful general methods for studying quantum electrodynamics near dielectrics, reflecting, or absorbing boundaries, emerged [7]. The main problem is that applying them to a particular problem usually requires extensive numerical calculations. Since those different methods are based on different assumptions, their range of applicability varies in each case. In order to understand the main idea in such calculations, let us get back to Lifshitz theory. As we said, he expressed the

dispersion force in terms of response functions. They can be achieved by expressing the results obtained by normal-mode expansion in terms of the Green tensor of the electromagnetic field, which contains all the relevant information of the system, like its shape. This implies that we could, in principle, calculate the Casimir force for any geometry. We can also extend this linear response formalism to the force on an atom. Thus, in this approach, the coupling energy is expressed in terms of the linear response functions of the atom and the electromagnetic field [33],

$$U(\mathbf{r}) = \frac{\hbar\mu_o}{2\pi}\int_o^\infty \mathrm{d}\eta\, \eta^2\alpha(\mathrm{i}\eta)\mathrm{Tr}\ \mathbf{G}^{(1)}(\mathbf{r},\mathbf{r},\mathrm{i}\eta), \tag{1.8}$$

i.e., the atomic polarisability $\alpha(\omega)$ and the scattering Green tensor of the electromagnetic field. The latter is related to the susceptibilities via the dissipation-fluctuation theorem. It is worth emphasizing that the concepts of linear-response theory no longer use an explicit quantisation and employ the fluctuation-dissipation theorem from the beginning. The simplest case of a ground-state atom placed in front of a perfectly conducting half-space was first obtained by McLachlan in [14] and then extended for a dielectric half-space in [86] by the same author, and by Agarwal later on [87, 88] employing, in addition, Master equation techniques. A slight variation of this problem was investigated by Wylie and Sipe in [89] in which a ground-state atom interacting with a dielectric two-layer system was considered, and then extended to atoms in excited energy eigenstates [90]. Many other modifications to this problem have been studied to date, but we will not refer to them since they are not particularly of interest to us. This formalism has been successfully widely used in parallel with the more elegant formalism that gives us a QED treatment in terms of normal modes. Nevertheless, as the essential point is to construct expressions for the shift in terms of the appropriate response functions of the interface (i.e. through the complex impedances), only numerical results for specific cases can be obtained explicitly. For example, in [89] their general expressions are utilised to get the energy shift and transition rates of an atom close to a dielectric waveguide made of ZnO/sapphire.

More recent work following the same approach was carried out in [33]. In this paper, Buhmann *et al.* study the van der Waals force acting on a ground-state atom in the presence of planar, dispersive and absorbing magneto-dielectric bodies. Considering an arbitrary planar multilayer system (described in terms of generalised reflection coefficients, which depend on the complex permittivities of the layers), they obtain a general expression that can be applied to the case of an atom in front of a magneto-dielectric plate and between two such plates, and then analyse the result for limiting cases such as thick and thin plates in the long- and short-distance regimes. By simply discarding the magnetic properties from their expressions, we will be able to compare with our results.

As we are utilising the quantum approach and perturbation theory to calculate the energy-level shift on an atom in front of a dielectric slab, in the following chapter we shall quantise the electromagnetic field as in [79]. In chapter 3, we will obtain the shift analytically, and hence the final result will be expressed as a very handy formula with high applicability to current experiments.

Chapter 2

Field quantisation in the presence of a dielectric slab

The reason an atom changes its atomic properties, such as the rate of spontaneous emission and energy levels, is because it couples to the fluctuating electromagnetic field. It is well-known that in order to study the quantum theory of a free electromagnetic field, it is convenient to expand the electromagnetic field in terms of plane waves. Such expansion coefficients oscillate sinusoidally and quantisation is achieved by changing those time-dependent coefficients to quantum operators. This quantisation of the field will certainly depend on the constraints, i.e. the presence of any material media. In the present work, the constraint under consideration is a dielectric slab, and thus we shall proceed with a complete quantisation of the field in the presence of such a slab. This has been done previously by Khosravi and Loundon [77]. Thereby, we know that for this case the solutions to the field equations — the normal modes of the electromagnetic field — are divided into travelling and trapped modes, and together these form a complete set of orthogonal transverse modes for this system. The first class consists of incoming, reflected and transmitted parts, exactly as for a single interface geometry. The second type, the trapped modes, behave as in a dielectric waveguide. This means that they experience repeated total internal reflections and come out as an evanescent field on either side of the slab. We intend, in the first two sections of the present chapter, to

give further explanation and details on how these modes are obtained. However, it is important to emphasize from this early stage the fact that travelling modes have a continuous range of frequencies, unlike the trapped modes, which only appear at certain discrete frequencies. This will have important consequences that we shall discuss in the following.

The main purpose of this dissertation is to work out the energy-level shift of an atom in front of a dielectric slab, and hence the Casimir-Polder force. We will explain in detail hereafter, that the second-order perturbation-theory procedure required for this calculation will lead us to a sum over all electromagnetic field modes. The problem that one encounters is summing over all modes with their correct relative weightings, i.e. density of states. This is not normally problematic, and the usual way to solve it is by looking at the modes infinitely far away from a scatterer and then infer the correct weighting by reference to the electromagnetic field modes in free space. In the case of a slab we shall need to proceed with more insight.

As one can imagine, because of the contrasting nature of the spatial modes of this system, the crucial difficulty emerges when one has to decide how to add the continuous spectrum of travelling modes, in terms of an integral, and the discrete set over trapped modes, that corresponds to a sum, because there is no obvious way to know how to add them together.

Khosravi and Loudon [77] included the factor $2\pi/L$ in front of the trapped modes and did not give any reasons or formal derivations. This appeared doubtful to us, as it did for Żakowicz and Błędowski [79], who revisited the problem of spontaneous emission. They claimed that Khosravi and Loudon had probably not correctly taken into account the density of trapped modes, which they concluded to be important for thin slabs and close to the dielectric-vacuum interfaces. They also claimed to have corrected that mistake, but they only calculated the density of modes for their own purposes and did not produce a general expression, so unfortunately, their result is not very useful for our calculation.

Due to the uncertainty in the validity of the results obtained so far, the first purpose

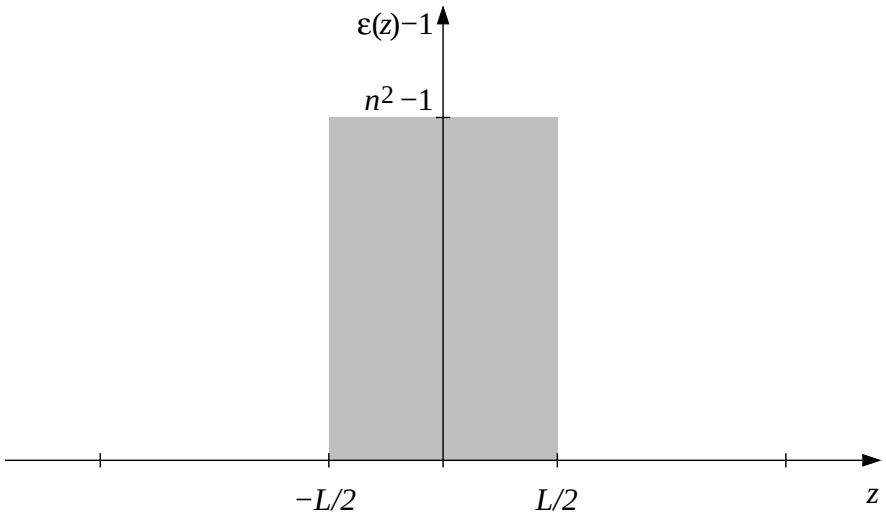

Figure 2.1: Non-dispersive and non-dissipative dielectric slab, characterised by a refractive index n and a thickness L.

of the present work is to derive the electromagnetic field modes of the system and discuss their general properties; establishing both travelling and trapped modes. This will be achieved in section 2.2. Then, we shall deduce the correct way of summing over all the electromagnetic mode functions. We will show that the most convenient method will follow from the proof of the completeness of the modes, as it involves the same sum over modes. Section 2.4 will be devoted to this proof. In chapter 3 we will then apply this result to the calculation of the energy shift, facilitating the procedure. But first of all, let us start with the description of the model to be utilised.

2.1 Description of the system

The system under consideration consists of a dielectric slab of finite thickness L surrounded by vacuum, as is shown in Fig. 2.1. We consider a non-dispersive and non-absorbing dielectric, as a good model for an imperfectly reflecting material. In such a way, one can still use a simple model for the material, characterizing the slab by its refractive index n, which is real and the same for all frequencies. Although we know that any real material has to be transparent at infinite frequencies, this model is better than the unrealistic perfect reflector, because it allows imperfect reflectivity and evanescent

waves.

Even though this seems to be an oversimplified model, it can be applied to systems whose dynamics are determined by a finite frequency range, for which the dielectric response of the material can be approximated by a constant [91]. This is the case for Casimir-Polder problems, in which the relevant frequencies are of the order of $2\pi/\mathcal{Z}$. This is a very small number because the atom-surface separation $\mathcal{Z}$ is normally much greater than the optical wavelengths, and hence only the static dielectric response $\varepsilon(\omega = 0)$ matters for the interaction.

Moreover, the model works fine for the description of the atom-surface interaction away from absorption resonances of the material. This means that the model can be utilised unless an important transition in the atom lies in a region of strong dispersion of the dielectric, in such a way that the atom would strongly couple to a surface excitation of the dielectric.

We have placed our system in such a way that it is translation-invariant in the x and y direction. Hence, the dielectric permittivity of the configuration only depends on the z direction and it is given by

$$\varepsilon(\mathbf{r}) = \begin{cases} n^2 & \text{for} \quad -L/2 \leq z \leq L/2 \\ 1 & \text{for} \quad |z| \geq L/2 \end{cases}$$

2.2 Electromagnetic field modes

The behaviour of the electromagnetic field is described by the Maxwell equations [11]

$$\nabla \cdot \mathbf{D} = \rho, \tag{2.1}$$

$$\nabla \cdot \mathbf{B} = 0, \tag{2.2}$$

$$\nabla \times \mathbf{E} + \frac{\partial \mathbf{B}}{\partial t} = 0, \tag{2.3}$$

$$\nabla \times \mathbf{H} - \frac{\partial \mathbf{D}}{\partial t} = \mathbf{J}. \tag{2.4}$$

As we can see, they consist of coupled first-order partial differential equations, relating the components of the electric and magnetic fields. In order to solve them the most convenient way is by introducing potentials [92]. The purpose is to obtain a smaller number of second-order equations, that also satisfy Maxwell equations identically. Since we want Eq. (2.2) to hold, we can simply define the magnetic field $\mathbf{B}$ in terms of a vector potential

$$\mathbf{B} = \nabla \times \mathbf{A}. \tag{2.5}$$

Substituting this definition into Faraday's law, Eq. (2.3) gives

$$\nabla \times \left(\mathbf{E} + \frac{\partial \mathbf{A}}{\partial t} \right) = 0, \tag{2.6}$$

which implies that the quantity in brackets can be written as the gradient of some scalar function, as it is the case for any function with vanishing curl. Thus, we shall define the scalar potential Φ, such that the electric field can be written as

$$\mathbf{E} = -\nabla \Phi - \frac{\partial \mathbf{A}}{\partial t}. \tag{2.7}$$

These new definitions for $\mathbf{E}$ and $\mathbf{B}$ in terms of the potentials $\mathbf{A}$ and Φ satisfy identically the two homogeneous Maxwell equations. The dynamic behaviour of $\mathbf{A}$ and Φ will be determined by the two inhomogeneous Maxwell equations. Thus, if we write them in terms of such potentials, we can reduce the set of four Maxwell equations to only two equations, which are coupled. In order to uncouple them, we shall take advantage of the arbitrariness of the definition of the potentials. According to the definition of $\mathbf{B}$, Eq. (2.5), the vector potential is arbitrary to the extent that the gradient of some scalar function can be added. To preserve the other definitions, we need simultaneously to transform the scalar potential. Such transformations of the potentials are called gauge transformations. A gauge for the electromagnetic field is specified by some condition on the potentials $\mathbf{A}$ and Φ, which can be realised by a gauge transformation, in which the physically measurable fields, $\mathbf{E}$ and $\mathbf{B}$, do not depend on the choice of gauge. The

gauge that is particularly useful in quantum electrodynamics is the so-called Coulomb or transverse gauge. The name comes from the fact that transverse radiation fields are given by the vector potential alone. For our system, we choose to work in the generalised Coulomb gauge

$$\nabla \cdot [\varepsilon(z)\mathbf{A}(\mathbf{r})] = 0, \tag{2.8}$$

which is convenient because anywhere except right on the boundaries of the dielectric slab, it is equivalent to the Coulomb gauge $\nabla \cdot \mathbf{A} = 0$. This means that we shall only make sure that the physical fields satisfy the appropriate matching conditions at the boundary. Furthermore, since we are considering an overall neutral system, we can set the scalar potential $\Phi(\mathbf{r}, t) = 0$. By using this conditions, the inhomogeneous Maxwell equations (2.1) and (2.4), written in terms of the potentials, can be reduced to the wave equation for the vector potential

$$\nabla^2\mathbf{A} - \varepsilon(\mathbf{r})\frac{\partial^2\mathbf{A}}{\partial t^2} = 0, \tag{2.9}$$

which must satisfy appropriate conditions on the dielectric boundaries. The solutions of the Maxwell equations can be seen to be travelling waves, which represent the transport of energy. The simplest and most fundamental electromagnetic waves are transverse, plane waves. The general solution of Eq. (2.9) forms a set of modes; which in the classical case allow the expression of an arbitrary electromagnetic field, and in the quantum case give an expansion of the quantum electromagnetic field operators, after following a standard quantisation procedure. We can thus achieve quantisation by expanding the vector field $\mathbf{A}(\mathbf{r}, t)$ in terms of normal modes, in the same way that one can express the field in free space in terms of the free-space modes, e.g., the plane waves[1]. Thus,

$$\mathbf{A}(\mathbf{r}, t) = \sum_{\mathbf{k}\lambda} \frac{1}{\sqrt{2\omega}} \left[a_{\mathbf{k}\lambda} e^{-\mathrm{i}\omega t}\mathbf{f}_{\mathbf{k}\lambda}(\mathbf{r}) + a^\dagger_{\mathbf{k}\lambda} e^{\mathrm{i}\omega t}\mathbf{f}^*_{\mathbf{k}\lambda}(\mathbf{r}) \right]. \tag{2.10}$$

[1]The vector potential for the free electromagnetic field is given in Eq. (A.1).

Note that we have introduced the variable λ, in order to account for the two polarisation directions of the electromagnetic waves: TE and TM. Further details will be given in the following. Since we are requiring solutions with harmonic time dependence, the wave equation for the vector potential (2.9) can be reduced to the Helmholtz equation for the normal modes $\mathbf{f}_{\mathbf{k}\lambda}(\mathbf{r})$

$$\left[\varepsilon(z)\omega^2 + \nabla^2\right] \mathbf{f}_{\mathbf{k}\lambda}(\mathbf{r}) = 0, \tag{2.11}$$

that can also be written as an eigenvalue problem

$$\left[\frac{1}{\sqrt{\varepsilon}}\nabla^2\frac{1}{\sqrt{\varepsilon}}\right] \sqrt{\varepsilon}\mathbf{f}_{\mathbf{k}\lambda}(\mathbf{r}) = -\omega^2 \sqrt{\varepsilon}\mathbf{f}_{\mathbf{k}\lambda}(\mathbf{r}). \tag{2.12}$$

As the operator in the square brackets in Eq. (2.12) is Hermitian, it follows that its eigenfunctions $\sqrt{\varepsilon}\mathbf{f}_{\mathbf{k}\lambda}(\mathbf{r})$ must form an orthonormal and complete system. For travelling modes all components of $\mathbf{k}$ are continuous variables, so that the orthogonality relation is

$$\int \mathrm{d}^3\mathbf{r}\ \varepsilon(z)\mathbf{f}^*_{\mathbf{k}\lambda}(\mathbf{r}) \cdot \mathbf{f}_{\mathbf{k}'\lambda'}(\mathbf{r}) = \delta^{(3)}(\mathbf{k} - \mathbf{k}')\delta_{\lambda\lambda'}, \tag{2.13}$$

where $\delta_{\lambda\lambda'}$ is the Kronecker delta. For trapped modes the normal component k_z is a discrete variable, and thus the orthogonality relation is changed slightly to

$$\int \mathrm{d}^3\mathbf{r}\ \varepsilon(z)\mathbf{f}^*_{\mathbf{k},\lambda}(\mathbf{r}) \cdot \mathbf{f}_{\mathbf{k}'\lambda'}(\mathbf{r}) = \delta^{(2)}(\mathbf{k}_\parallel - \mathbf{k}'_\parallel)\delta_{k_z k'_z}\delta_{\lambda\lambda'}. \tag{2.14}$$

The completeness relation reads

$$\int \mathrm{d}^2\mathbf{k}_\parallel \sum_{k_z} \sqrt{\varepsilon}f^i_{\mathbf{k}\lambda}(\mathbf{r})\ \sqrt{\varepsilon}f^{*j}_{\mathbf{k}\lambda}(\mathbf{r}') = (\delta_{ij} - \Delta^{-1}\partial_i\partial_j)\delta^{(3)}(\mathbf{r} - \mathbf{r}'), \tag{2.15}$$

where the sum over all modes consists of an integral over the wave vector $\mathbf{k}_\parallel = (k_x, k_y)$ that lies parallel to the interface, and an integral and a sum over the normal component k_z for travelling and trapped modes, respectively, because travelling modes have a continuous spectrum but trapped modes occur only at certain discrete k_z. The transverse

delta function that appears on the right-hand side of the completeness relation reflects the fact that, away from the interface, the gauge condition (2.8) requires the vector field to be transverse. Concerning the transversality of the set, this can be achieved by introducing polarisation vectors, such that the mode functions can be written as

$$\mathbf{f}_{\mathbf{k}\lambda}(\mathbf{r}) = \hat{\mathbf{e}}_\lambda f_{\mathbf{k}\lambda}(\mathbf{r}). \tag{2.16}$$

Such vectors arise from the fact that the electromagnetic waves have two transverse polarisation directions, which we have denoted by λ. These can be chosen as the transverse electric polarisation (TE), for which the electric field vector lies perpendicular to the plane of incidence, and the transverse magnetic polarisation (TM), for which the magnetic field vector lies perpendicular to the plane of incidence. In the generalized Coulomb gauge the direction of the electromagnetic field can be described by the following choice of polarisation vectors:

$$\hat{\mathbf{e}}_{\mathrm{TE}}(\partial_r) = (-\Delta_\parallel)^{-1/2}(-i\partial_y, i\partial_x, 0) \tag{2.17}$$

$$\hat{\mathbf{e}}_{\mathrm{TM}}(\partial_r) = (\Delta\Delta_\parallel)^{-1/2}(-\partial_x\partial_z, -\partial_y\partial_z, \Delta_\parallel), \tag{2.18}$$

when acting on plane waves or parts thereof. Here $\Delta = \partial_x^2 + \partial_y^2 + \partial_z^2$ is the Laplacian in three dimensions and $\Delta_\parallel = \partial_x^2 + \partial_y^2$ the Laplacian in two dimensions parallel to the surface of the dielectric. Applying the polarisation vectors on a plane wave $e^{\mathrm{i}\mathbf{k}\cdot\mathbf{r}}$ propagating to the right (+), one can express these modes in terms of the wave vector components, i.e.,

$$\hat{\mathbf{e}}_{\mathrm{TE}}(\mathbf{k}^+) = \frac{1}{|\mathbf{k}_\parallel|}(k_y, -k_x, 0), \tag{2.19}$$

$$\hat{\mathbf{e}}_{\mathrm{TM}}(\mathbf{k}^+) = \frac{1}{|\mathbf{k}_\parallel||\mathbf{k}|}(k_x k_z, k_y k_z, -k_\parallel^2). \tag{2.20}$$

However, we must realise that the explicit representation in $\mathbf{k}$ space is different, and thus, the incident, reflected and transmitted parts have polarisation vectors that point out in different directions (more details below). For that reason and to avoid confusion,

we have found it quite useful to keep the first notation (Eqs. (2.17) and (2.18)), which describes them in a more general way. It is also important to emphasize that for travelling waves the polarisation vectors together with the wave vector form an orthonormal triplet. Thus, the set of polarisation vectors must satisfy the following relations

$$\hat{\mathbf{e}}_{\mathrm{TE}}(\mathbf{k}) \cdot \hat{\mathbf{e}}^*_{\mathrm{TE}}(\mathbf{k}) = 1, \qquad \hat{\mathbf{e}}_{\mathrm{TM}}(\mathbf{k}) \cdot \hat{\mathbf{e}}^*_{\mathrm{TM}}(\mathbf{k}) = 1, \tag{2.21}$$

$$\hat{\mathbf{e}}_{\mathrm{TE}}(\mathbf{k}) \cdot \hat{\mathbf{e}}^*_{\mathrm{TM}}(\mathbf{k}) = 0, \qquad \hat{\mathbf{e}}_{\mathrm{TM}}(\mathbf{k}) \cdot \hat{\mathbf{e}}^*_{\mathrm{TE}}(\mathbf{k}) = 0, \tag{2.22}$$

where the asterisk denotes complex conjugation, and obey the completeness relation

$$\sum_{\lambda} \hat{e}^i_{\lambda} \hat{e}^j_{\lambda} + \frac{k^i k^j}{|\mathbf{k}|^2} = \delta_{ij}. \tag{2.23}$$

The modes, defined as elementary solutions of the field equations satisfying proper boundary conditions on the vacuum-dielectric interfaces, are not unique. A particular set of modes is obtained by taking combinations of incident, reflected and refracted waves; and taking into account both left- and right-incident modes. The boundary conditions that these mode functions $\mathbf{f}_{\mathbf{k}\lambda}(\mathbf{r})$ must satisfy, can be derived from classical electrodynamics. From Eqs. (2.3), (2.1) and (2.4), respectively, we get the following conditions:

$$E_{\parallel}, \quad D_{\perp}, \quad \text{and} \quad \mathbf{B} \qquad \text{continuous} \tag{2.24}$$

across the interface between dielectric and vacuum. In order to distinguish waves propagating in the positive and negative z directions, we have adopted a notation very similar to the one used in Ref. [77], where $\mathbf{k}^{\pm}$ is the wave vector in vacuum

$$\mathbf{k}^{\pm} = (k_x, k_y, \pm k_z) = (\mathbf{k}_{\parallel}, \pm k_z), \tag{2.25}$$

adding the subscript d in order to refer to the corresponding wave vector inside the

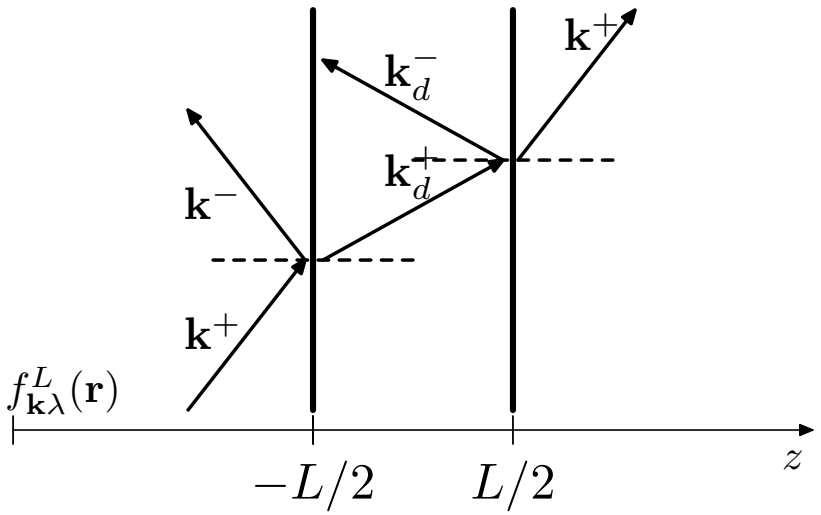

Figure 2.2: Geometrical details of the dielectric slab showing the wave vectors that appear in the left-incident travelling mode functions $f^L_{\mathbf{k}\lambda}(r)$. Note that inside the dielectric, there will be repeated internal reflections.

dielectric slab

$$\mathbf{k}_{\rm d}^{\pm} = (\mathbf{k}_{\parallel}, \pm k_{\rm zd}). \tag{2.26}$$

Thus the propagation direction of the wave in the z axis is specified by the superscripts $(+)$ and $(-)$. Fig. 2.2 shows the geometrical arrangement of the dielectric slab with the interfaces perpendicular to the z-axis. We have included some incoming waves to make the notation completely clear. We have only shown the x-z plane, as it is the only relevant plane. In the expressions above, $\mathbf{k}_{\parallel}$ is the wave vector component that is parallel to the interface, and its magnitude is given by $k_{\parallel} = \sqrt{k_x^2 + k_y^2}$. The continuity requirements from Maxwell's equation imply that both the parallel wave vector $\mathbf{k}_{\parallel}$ and the frequency are the same on both sides of the interface. Since the wavelength is $|\mathbf{k}| = k = \omega/c$ in free space, and $k_{\rm d} = n\omega/c$ inside the dielectric, one can immediately get from the definitions above a very useful expression that relates the z-components of the wave vectors in free-space and dielectric,

$$k_{\rm zd} = \sqrt{(n^2-1)k_{\parallel}^2 + n^2 k_z^2}, \tag{2.27}$$

and in reverse

$$k_z = \frac{1}{n}\sqrt{k_{\rm zd}^2 - (n^2-1)k_\parallel^2}, \tag{2.28}$$

which are always positive. The relation (2.28) shows again that we get two types of modes. If the argument of the square root is positive then k_z is real and the modes are travelling; if the argument turns out to be negative then k_z is purely imaginary and the modes are evanescent outside the dielectric, in the z-direction, and trapped inside the slab. Khosravi and Loundon [77] have named them travelling and trapped modes, though they can also be identified as radiation and waveguided modes, respectively. We will follow the former convention. A consequence of the discussion above becomes apparent when we write down a general z-dependence solution of the Helmholtz Eq. (2.11) outside the slab

$$f_{\mathbf{k}\lambda}(z) = Ae^{{\rm i}z\sqrt{\omega^2-k_\parallel^2}} + Be^{-{\rm i}z\sqrt{\omega^2-k_\parallel^2}}. \tag{2.29}$$

Thus the two types of modes will arise depending on the argument $\omega^2 - k_\parallel^2$ being either positive (travelling modes) or negative (evanescent modes).

2.2.1 Travelling modes

The most common choice for the travelling modes, which we will use through out this work, assumes the incident wave impinging on one side of the slab. To form a mode, the incident wave must be accompanied by two other waves (for each interface), the reflected and the transmitted one, and their wave vectors are related according to laws of wave transmission across the boundary.

For each set of wave vectors, and for each transverse polarisation λ, there are two distinct mode functions corresponding to plane waves incoming from the left and from the right towards the dielectric slab. We denote them as $f^L_{\mathbf{k}\lambda}(\mathbf{r})$ and $f^R_{\mathbf{k}\lambda}(\mathbf{r})$, respectively. We have sketched the left-incident travelling modes in Fig. 2.3. According to Eq.

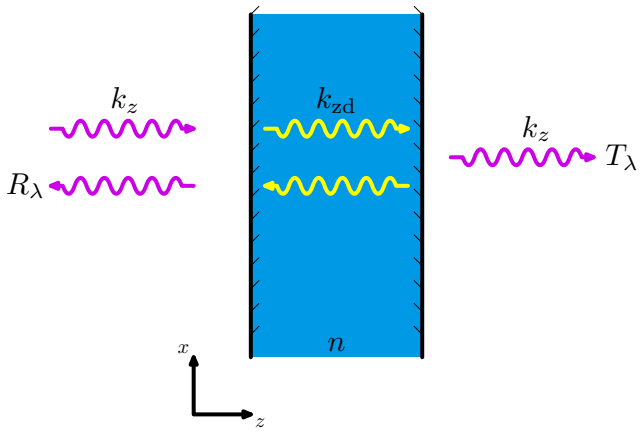

Figure 2.3: Left-incident travelling modes. Notice that to form a mode, the incident wave must be accompanied by a reflected and a transmitted wave, for each interface.

(2.16), the spatial dependence of the left-incident modes reads

$$f^L_{\mathbf{k}\lambda}(\mathbf{r}) = N \begin{cases} e^{i\mathbf{k}^+\cdot\mathbf{r}} + R_\lambda e^{i\mathbf{k}^-\cdot\mathbf{r}} & z \le -L/2 \\ I_\lambda e^{i\mathbf{k}_d^+\cdot\mathbf{r}} + J_\lambda e^{i\mathbf{k}_d^-\cdot\mathbf{r}} & |z| \le L/2 \\ T_\lambda e^{i\mathbf{k}^+\cdot\mathbf{r}} & z \ge L/2 \end{cases}$$

The right-incident modes can be obtained straightforwardly from the left-incident modes. Due to the symmetry of the system, it is possible to obtain them simply by inverting the z-axis, i.e. by letting $z \to -z$. Their spatial dependence is thus given by

$$f^R_{\mathbf{k}\lambda}(\mathbf{r}) = N \begin{cases} T_\lambda e^{i\mathbf{k}^-\cdot\mathbf{r}} & z \le -L/2 \\ I_\lambda e^{i\mathbf{k}_d^-\cdot\mathbf{r}} + J_\lambda e^{i\mathbf{k}_d^+\cdot\mathbf{r}} & |z| \le L/2 \\ e^{i\mathbf{k}^-\cdot\mathbf{r}} + R_\lambda e^{i\mathbf{k}^+\cdot\mathbf{r}} & z \ge L/2 \end{cases}$$

As we stated earlier, these modes must be orthonormal. Following the condition (2.13) we obtain the normalisation factor

$$N = \frac{1}{(2\pi)^{3/2}}, \tag{2.30}$$

which is independent of the polarisation and, due to the symmetry, the same for both left- and right-incident modes. The reflection and transmission coefficients R_λ and T_λ,

as well as the coefficients I_λ and J_λ are determined through the conditions of continuity of $E_\parallel$, $D_\perp$ and $\mathbf{B}$ that arise from Maxwell's equations. We will not give any further details on how to calculate these coefficients, since they have been correctly calculated before for the same system [77, 79], and more generally, for a three different materials system [80]. The reflection and transmission coefficients are given by

$$R_\lambda = r_\lambda \frac{1 - e^{2\mathrm{i}k_{\mathrm{zd}}L}}{1 - r_\lambda^2 e^{2\mathrm{i}k_{\mathrm{zd}}L}}\, e^{-\mathrm{i}k_z L} \qquad \text{and} \qquad T_\lambda = \frac{1 - r_\lambda^2}{1 - r_\lambda^2 e^{2\mathrm{i}k_{\mathrm{zd}}L}}\, e^{\mathrm{i}(k_{\mathrm{zd}} - k_z)L} \tag{2.31}$$

where

$$r_{\mathrm{TE}} = \frac{k_z - k_{\mathrm{zd}}}{k_z + k_{\mathrm{zd}}} \qquad \text{and} \qquad r_{\mathrm{TM}} = \frac{n^2 k_z - k_{\mathrm{zd}}}{n^2 k_z + k_{\mathrm{zd}}} \tag{2.32}$$

are the well-known Fresnel coefficients from basic geometrical optics, for a single interface, for the transverse electric and transverse magnetic polarisations, respectively. Notice that the coefficients (2.31) are the same for both left- and right-incident modes. This is clearly due to the symmetry of the system, and the symmetric choice of reference frame is reflected in the phase $e^{-\mathrm{i}k_z L}$ that appears in the reflection and transmission coefficients. Therefore, if we had chosen to work with a system where one of the slab interfaces is located at $z = 0$, the coefficients for the modes $f^L_{\mathbf{k}\lambda}(\mathbf{r})$ would differ from to those for $f^R_{\mathbf{k}\lambda}(\mathbf{r})$ only by a phase factor, in such a way that the relation

$$|R_\lambda|^2 + |T_\lambda|^2 = 1 \tag{2.33}$$

still holds, and thus the conservation of energy. We have stated in Eq. (2.13) that the travelling modes are orthogonal. More specifically, all of the modes incident from the right are orthogonal to all of the modes incident from the left. This reads

$$\int \mathrm{d}^3\mathbf{r}\; \varepsilon(z) \mathbf{f}^{L*}_{\mathbf{k}\lambda}(\mathbf{r}) \cdot \mathbf{f}^R_{\mathbf{k}\lambda}(\mathbf{r}) = 0, \tag{2.34}$$

and the relation

$$R_\lambda T^*_\lambda + R^*_\lambda T_\lambda = 0 \tag{2.35}$$

helps to ensure the orthogonality. The coefficients for the spatial modes inside the slab are calculated by using the continuity conditions (2.24). Hence,

$$I_\lambda = (r_\lambda + 1)\,\frac{e^{\mathrm{i}(k_{\mathrm{zd}}-k_z)L}}{1 - r_\lambda^2 e^{2\mathrm{i}k_{\mathrm{zd}}L}} \qquad \text{and} \qquad J_\lambda = -I_\lambda\, r_\lambda\, e^{\mathrm{i}k_{\mathrm{zd}}L}, \tag{2.36}$$

which satisfy the relation

$$k_{\mathrm{zd}}(|I_\lambda|^2 - |J_\lambda|^2) = k_z|T_\lambda|^2. \tag{2.37}$$

2.2.2 Trapped Modes

The slab forms a planar dielectric waveguide. The Maxwell's equations describing the electromagnetic field are exactly solvable for this simple system, and the solutions, particularly the waveguiding solutions, have been described in several books on dielectric waveguides or surface excitations [93, 94]. In order to explain how this class of modes is produced, I have considered it worth reviewing briefly what we know about it in basic geometrical optics[2]. The reason is simply because light rays have intuitive appeal since a narrow beam is a good approximation to the more complex concept of light rays. We shall first explain the phenomenon of total internal reflection [11]. The word internal implies that both incident and reflected waves are in a medium of index of refraction n_1, which is larger that the index n_2 of the medium in which the refracted wave propagates (see Fig. 2.4). When $n_1 > n_2$ is satisfied, the angle of refraction θ_r is larger than the angle of incidence θ_i, as it can be shown from Snell's law. If we want $\theta_r = \pi/2$, the incident wave should have an angle of incidence θ_c, as it is shown in Fig. 2.4. In this case, the refracted wave propagates parallel to the surface and there is no energy flow across the surface. This implies that at such an angle of incidence there must be total reflection (no light can emerge, so all of the light is completely reflected). θ_c is called the critical angle and is given by

$$\theta_c = \arcsin(n_2/n_1); \tag{2.38}$$

[2]See for instance Ref. [95]

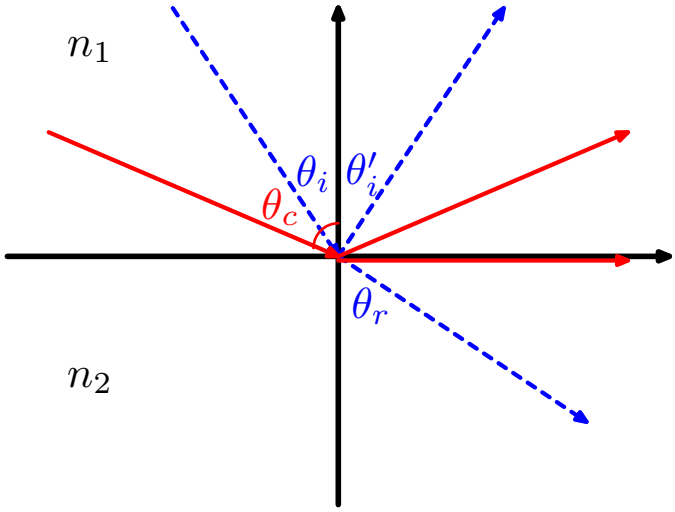

Figure 2.4: The rays depicted by the blue dashed lines show the incident and reflected waves in a medium with refractive index n_1, and the refracted wave in a medium with refractive index n_2, satisfying the condition $n_1 > n_2$, such that it permits total internal reflection for all angles greater than θ_c. The latter is shown in red rays.

which by convention is measured with respect to the normal to the surface, as it is shown in the Fig. 2.4. An interesting phenomenon occurs when $\theta_i > \theta_c$. The refracted wave is propagated only parallel to the surface and is attenuated exponentially beyond the interface, along the z-direction. This is known as an evanescent wave. Satisfying the same physics, trapped modes exist only when the internal modes reach the dielectric-vacuum interface with polar angles that are larger than the critical angle, producing total internal reflection. Because of the symmetry of the slab, once it happens at one interface it will then also happen on the opposite side, and so forth. This will cause the *light* to stay confined in the dielectric, and the system will form what is called a waveguide. Therefore, it is natural to expect standing waves inside the slab. Outside the slab, these modes have imaginary wave vector $z-$components,

$$k_z = \pm \mathrm{i}\kappa \qquad \text{with} \qquad \kappa = \frac{1}{n}\sqrt{(n^2-1)k_{\parallel}^2 - k_{\mathrm{zd}}^2}, \tag{2.39}$$

and the positive sign is chosen such that the amplitudes of the modes propagating parallel to the dielectric decay exponentially with distance from the surface of the slab,

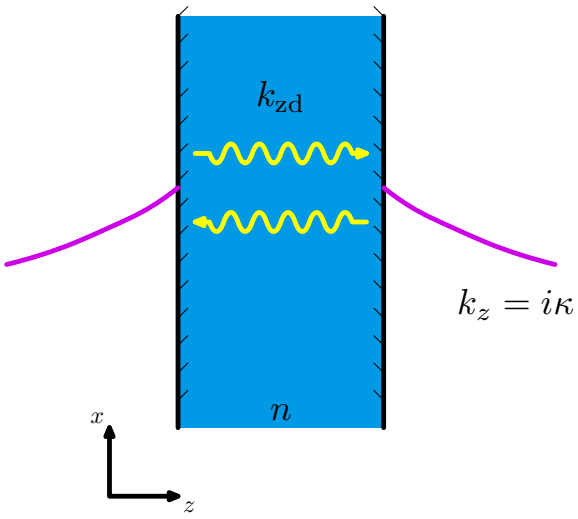

Figure 2.5: Illustration of the evanescent behaviour of the modes, as a result of the internal polar angles being $\theta > \arctan(1/n)$

along the z-direction, as shown in the Fig. 2.5. This evanescent behaviour characterizes the guided or trapped modes of the slab. From Snell's law, it can be concluded that the trapped modes have internal wave vectors that satisfy

$$k_{\mathrm{zd}} < \frac{\omega}{c}\sqrt{n^2 - 1}, \tag{2.40}$$

thus they only exist in certain region of the $(\omega, \mathbf{k})$ space, well defined.

Before introducing the expressions for the trapped modes, let us get back to the concept of spatial modes as solutions of the Helmholtz equation (2.29) for the specific case $\omega < |\mathbf{k}_{\parallel}|$, and emphasize that this implies that the solutions in free-space are decaying exponentials. One can show that it is not possible to have solutions with imaginary wave vector both inside and outside the dielectric slab, satisfying the boundary conditions (2.24). Therefore, we will have oscillating solutions of Eq. (2.11) inside the slab. As we are looking for the simplest solutions, we shall consider purely symmetric fields or purely antisymmetric fields, behaving, respectively as cosine or sine functions inside the dielectric. Adopting this designation by parity, we shall divide the trapped modes into symmetric and antisymmetric modes, and label them with the superscripts S and

A, respectively. They are given by

$$\mathbf{f}_{\mathbf{k}\lambda}^{S,A}(\mathbf{r}) = \hat{\mathbf{e}}_\lambda \begin{cases} P_\lambda^{S,A} e^{\mathrm{i}\mathbf{k}^- \cdot \mathbf{r}} & z \leq -L/2 \\ M_\lambda \left(e^{i\mathbf{k}_d^+ \cdot \mathbf{r}} \pm e^{i\mathbf{k}_d^- \cdot \mathbf{r}} \right) & |z| \leq L/2 \\ Q_\lambda^{S,A} e^{\mathrm{i}\mathbf{k}^+ \cdot \mathbf{r}} & z \geq L/2 \end{cases}$$

with $\mathbf{k}^\pm = (\mathbf{k}_\parallel, \pm \mathrm{i}\kappa)$. The calculation of the coefficients $P_\lambda^{S,A}$, $Q_\lambda^{S,A}$ and M_λ is done following the same procedure used for the travelling modes. However, we have decided to give more details in this case because there is an issue with how the polarisation vectors are chosen.

Let us commence with the treatment of the TE polarisation, in which the electric field is perpendicular to the plane of incidence. Since we want to use the continuity condition for the parallel component of the electric field $\mathbf{E}_\parallel$, we shall use the definition of the TE polarisation vector (Eq. (2.17)) in order to write the required component of the field. For simplicity and since only the z direction is relevant, we will reduce our expressions to that component. Then, from the continuity condition, it turns out that one can redefine the coefficients to $P_{TE}^{S,A} = \pm M_{TE} L_{TE}^{S,A}$ and $Q_{TE}^{S,A} = M_{TE} L_{TE}^{S,A}$ (and the same relations will hold for the TM polarisation). Thus, the spatial dependence of the electric field simply reads

$$E_\parallel(z) \sim M_{TE} \begin{cases} \pm L_{TE}^{S,A} e^{\kappa z} & z \leq -L/2 \\ e^{\mathrm{i}k_{\mathrm{zd}} z} \pm e^{-\mathrm{i}k_{\mathrm{zd}} z} & |z| \leq L/2 \\ L_{TE}^{S,A} e^{-\kappa z} & z \geq L/2 \end{cases}$$

with coefficients $L_{TE}^{S,A}$ given by

$$L_{TE}^{S} = 2\cos\left(\frac{k_{\mathrm{zd}} L}{2}\right) e^{\kappa L/2} \tag{2.41}$$

$$L_{TE}^{A} = 2i \sin\left(\frac{k_{\mathrm{zd}} L}{2}\right) e^{\kappa L/2} \tag{2.42}$$

Using Faraday's Eq. (2.3), we can also obtain the parallel component of the magnetic

field. Hence,

$$B_{\parallel}(z) \sim M_{TE} \begin{cases} \pm\kappa\, L_{TE}^{S,A} e^{\kappa z} & z \leq -L/2 \\ \mathrm{i}k_{\mathrm{zd}} \left(e^{\mathrm{i}k_{\mathrm{zd}}z} \mp e^{-\mathrm{i}k_{\mathrm{zd}}z}\right) & |z| \leq L/2 \\ -\kappa\, L_{TE}^{S,A} e^{-\kappa z} & z \geq L/2. \end{cases}$$

For a given value of the frequency ω, there are trapped modes only for a limited number of discrete values of k_{zd}, which depend on both the polarisation and the parity of the modes. The allowed values of k_{zd} are determined through the dispersion relations, which are obtained by using simultaneously the continuity conditions for the magnetic and electric field at the dielectric-vacuum interface. For instance, if we use the symmetric field, it must be satisfied at $z = L/2$ such that

$$\mathrm{i}k_{\mathrm{zd}} \left(e^{\mathrm{i}k_{\mathrm{zd}}L/2} - e^{-\mathrm{i}k_{\mathrm{zd}}L/2}\right) = -\kappa\, L_{TE}^{S}\, e^{-\kappa L/2} \tag{2.43}$$

$$e^{\mathrm{i}k_{\mathrm{zd}}L/2} + e^{-\mathrm{i}k_{\mathrm{zd}}L/2} = L_{TE}^{S}\, e^{-\kappa L/2} \tag{2.44}$$

Thus, by solving simultaneously these equations, we obtain the following dispersion relation

$$\kappa = k_{\mathrm{zd}} \tan\left(\frac{k_{\mathrm{zd}}L}{2}\right) \qquad \text{TE, S.} \tag{2.45}$$

In order to show the allowed values of k_{zd} for each frequency ω or, more conveniently, for each wave vector parallel component $k_{\parallel}$, we shall use Eq. (2.39) to express κ as a function of k_{zd} and $k_{\parallel}$. Thus, the dispersion relation above reads

$$k_{\parallel} = \frac{k_{\mathrm{zd}}}{\sqrt{n^2-1}} \sqrt{1 + n^2 \tan^2(k_{\mathrm{zd}}L/2)}. \tag{2.46}$$

We can rescale this equation in order to hide the L-dependence and plot for an arbitrary value of n. As shown in Fig. 2.6, for a particular value of $k_{\parallel}$, there exists only a few values of k_{zd}, limited by the condition (2.40). The same procedure follows for the

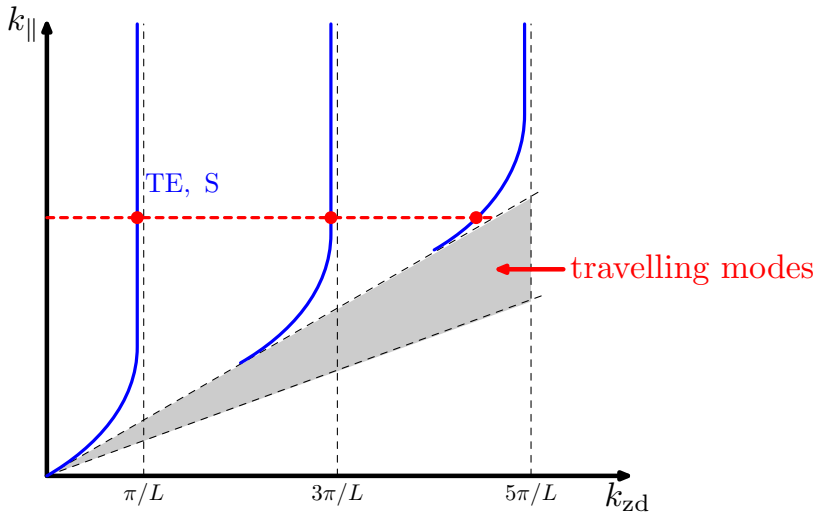

Figure 2.6: The region in gray shows the space where travelling modes exist. The blue branches represent the dispersion relation for the TE symmetric trapped modes: $\kappa = k_{\rm zd}\tan(k_{\rm zd}L/2)$

antisymmetric modes. At the interface, the continuity of $\mathbf{B}_{\parallel}$ implies that

$$\mathrm{i}k_{\rm zd}\left(e^{\mathrm{i}k_{\rm zd}L/2}+e^{-\mathrm{i}k_{\rm zd}L/2}\right)=-\kappa L_{TE}^{A}e^{-\kappa L/2}, \tag{2.47}$$

so we can simply substitute the coefficient L_{TE}^{A} given in Eq. (2.42) (which implies the continuity condition for $E_{\parallel}$ that must be satisfied simultaneously), and obtain the dispersion relation

$$-\kappa = k_{\rm zd}\cot\left(\frac{k_{\rm zd}L}{2}\right) \qquad \text{TE, A.} \tag{2.48}$$

Furthermore, we can obtain the normalisation constant M_{TE} by using condition (2.14). For this polarisation it was calculated correctly by Khosravi and Loudon [77]. We get,

$$M_{\rm TE}=\frac{1}{4\pi\sqrt{\frac{n^2L}{2}+\frac{1}{\kappa}\left(\frac{k_{\parallel}}{k}\right)^2}}. \tag{2.49}$$

A very similar procedure is needed for the TM polarisation, in which the electric field $\mathbf{E}$ lies parallel to the plane of incidence. Therefore, the magnetic field is given by expressions similar to those for the electric field in the TE polarisation. Thus, one could start from the magnetic field, and derive $\mathbf{E}$ through the Maxwell's equation.

Alternatively, by using the polarisation vector (2.18), we can write the z-component of the electric field, which is needed in order to apply the first continuity condition. We will only focus on what happens at the interface $z = L/2$, as it is easy to intuit, from the symmetry of the system, the behaviour of the field in the rest of the space. It reads

$$E_z(z) \sim M_{TM} \begin{cases} \frac{1}{k_d}\left(e^{\mathrm{i}k_{\mathrm{zd}}z} \pm e^{-\mathrm{i}k_{\mathrm{zd}}z}\right) & |z| \leq L/2 \\ \frac{1}{k} L_{TM}^{S,A} e^{-\kappa z} & z \geq L/2. \end{cases}$$

The coefficients shall be calculated by using the continuity of the electric displacement $z-$component, which can be written in terms of the electric field by using the relation $D(z) = \varepsilon(z)E(z)$. Thus,

$$L_{TM}^{S} = 2n \cos\left(\frac{k_{\mathrm{zd}}L}{2}\right) e^{\kappa L/2} \tag{2.50}$$

$$L_{TM}^{A} = 2n\mathrm{i}\ \sin\left(\frac{k_{\mathrm{zd}}L}{2}\right) e^{\kappa L/2}. \tag{2.51}$$

In order to calculate the dispersion relations, we shall employ the continuity condition of $E_{\parallel}$. By using the required component of the polarisation vector in the general expressions for the trapped modes, we get

$$E_{\parallel}(z) \sim \begin{cases} \frac{k_{\mathrm{zd}}}{k_d}\left(e^{ik_{\mathrm{zd}}z} \pm e^{-ik_{\mathrm{zd}}z}\right) & |z| \leq L/2 \\ \frac{i\kappa}{k} L_{TM}^{S,A} e^{-\kappa z} & z \geq L/2. \end{cases}$$

Using the symmetric electric field, the continuity condition at the interface $z = L/2$ reads

$$\frac{k_{\mathrm{zd}}}{k_d}\left(e^{ik_{\mathrm{zd}}L/2} + e^{-ik_{\mathrm{zd}}L/2}\right) = \frac{i\kappa}{k} L_{TM}^{S} e^{-\kappa L/2}, \tag{2.52}$$

and by substituting the coefficient (2.50), we obtain the following dispersion relation

$$n^2\kappa = k_{\mathrm{zd}} \tan\left(\frac{k_{\mathrm{zd}}L}{2}\right) \qquad \text{TM, S.} \tag{2.53}$$

For the antisymmetric modes we get

$$\frac{k_{\rm zd}}{k_d}\left(e^{ik_{\rm zd}L/2}-e^{-ik_{\rm zd}L/2}\right)=\frac{i\kappa}{k}L^A_{TM}e^{-\kappa L/2}, \tag{2.54}$$

and by substitution of Eq. (2.51), we obtain a fourth dispersion relation

$$-n^2\kappa=k_{\rm zd}\cot\left(\frac{k_{\rm zd}L}{2}\right) \qquad \text{TM, A} \tag{2.55}$$

The normalisation constant for the TM polarisation modes is also calculated by using the condition (2.14). After some algebraic manipulation it turns out to be

$$M_{\rm TM}=\frac{1}{4\pi n\sqrt{\frac{L}{2}+\frac{1}{\kappa}\frac{k_\parallel^2}{(k_\parallel^2+n^2\kappa^2)}}}, \tag{2.56}$$

in agreement with [79], reaffirming that it was calculated incorrectly in [77].

2.3 Quantisation

Once we have obtained the spatial modes, one can proceed with the quantisation of the electromagnetic field [96]. This is achieved by introducing for each mode the annihilation and creation operators denoted by

$$\hat{a}^{L\dagger}_{\mathbf{k}\lambda} \text{ and } \hat{a}^{L}_{\mathbf{k}\lambda} \text{ for the left-incident mode } \mathbf{f}^{L}_{\mathbf{k}\lambda}$$
$$\hat{a}^{R\dagger}_{\mathbf{k}\lambda} \text{ and } \hat{a}^{R}_{\mathbf{k}\lambda} \text{ for the right-incident mode } \mathbf{f}^{R}_{\mathbf{k}\lambda}$$

for the travelling modes, and

$$\hat{a}^{S\dagger}_{\mathbf{k}\lambda} \text{ and } \hat{a}^{S}_{\mathbf{k}\lambda} \text{ for the symmetric mode } \mathbf{f}^{S}_{\mathbf{k}\lambda}$$
$$\hat{a}^{A\dagger}_{\mathbf{k}\lambda} \text{ and } \hat{a}^{A}_{\mathbf{k}\lambda} \text{ for the antisymmetric mode } \mathbf{f}^{A}_{\mathbf{k}\lambda}$$

for the trapped modes. The traveling modes satisfy the following commutation relations,

$$\left[\hat{a}^{L}_{\mathbf{k}\lambda}, \hat{a}^{L\dagger}_{\mathbf{k}'\lambda'}\right] = \left[\hat{a}^{R}_{\mathbf{k}\lambda}, \hat{a}^{R\dagger}_{\mathbf{k}'\lambda'}\right] = \delta_{\lambda\lambda'}\delta^{(3)}(\mathbf{k}-\mathbf{k}') \tag{2.57}$$

$$\left[\hat{a}^{L}_{\mathbf{k}\lambda}, \hat{a}^{R\dagger}_{\mathbf{k}'\lambda'}\right] = \left[\hat{a}^{R}_{\mathbf{k}\lambda}, \hat{a}^{L\dagger}_{\mathbf{k}'\lambda'}\right] = 0, \tag{2.58}$$

and similarly, the discrete trapped modes satisfy,

$$\left[\hat{a}^{S}_{\mathbf{k}\lambda}, \hat{a}^{S\dagger}_{\mathbf{k}'\lambda'}\right] = \left[\hat{a}^{A}_{\mathbf{k}\lambda}, \hat{a}^{A\dagger}_{\mathbf{k}'\lambda'}\right] = \delta_{\lambda\lambda'}\delta_{k_z,k_{z'}}\delta^{(2)}(\mathbf{k}_{\parallel}-\mathbf{k}'_{\parallel}) \tag{2.59}$$

$$\left[\hat{a}^{S}_{\mathbf{k}\lambda}, \hat{a}^{A\dagger}_{\mathbf{k}'\lambda'}\right] = \left[\hat{a}^{A}_{\mathbf{k}\lambda}, \hat{a}^{S\dagger}_{\mathbf{k}'\lambda'}\right] = 0. \tag{2.60}$$

All the traveling modes operators commute with all the trapped mode operators.

$$\left[\hat{a}^{L,R}_{\mathbf{k}\lambda}, \hat{a}^{S,A\dagger}_{\mathbf{k}'\lambda'}\right] = \left[\hat{a}^{S,A}_{\mathbf{k}\lambda}, \hat{a}^{L,R\dagger}_{\mathbf{k}'\lambda'}\right] = 0. \tag{2.61}$$

Using such creation and annihilation operators one can express the field operator $\hat{\mathbf{E}}(\mathbf{r},t)$ in terms of the normal modes. The Heisenberg electric field operator is written as a sum of hemitian-conjugate creation and destruction operator parts as

$$\hat{\mathbf{E}}(\mathbf{r},t) = \hat{\mathbf{E}}^{-}(\mathbf{r},t) + \hat{\mathbf{E}}^{+}(\mathbf{r},t), \tag{2.62}$$

where

$$\begin{aligned}\hat{\mathbf{E}}^{+}(\mathbf{r},t) &= \mathrm{i}\sum_{\lambda}\int_{k_z>0}\mathrm{d}^3\mathbf{k}\left(\frac{\hbar\omega}{2\epsilon_o}\right)^{1/2}\left(\mathbf{f}^{L}_{\mathbf{k}\lambda}(\mathbf{r})\hat{a}^{L}_{\mathbf{k}\lambda}e^{-i\omega t} + \mathbf{f}^{R}_{\mathbf{k}\lambda}(\mathbf{r})\hat{a}^{R}_{\mathbf{k}\lambda}e^{-i\omega t}\right) \\ &+ \mathrm{i}\sum_{\lambda}\sum_{k_z}\int\mathrm{d}^2\mathbf{k}_{\parallel}\left(\frac{\hbar\omega}{2\epsilon_o}\right)^{1/2}\left(\mathbf{f}^{S}_{\mathbf{k}\lambda}(\mathbf{r})\hat{a}^{S}_{\mathbf{k}\lambda}e^{-i\omega t} + \mathbf{f}^{A}_{\mathbf{k}\lambda}(\mathbf{r})\hat{a}^{A}_{\mathbf{k}\lambda}e^{-i\omega t}\right),\end{aligned} \tag{2.63}$$

and $\hat{\mathbf{E}}^{-}(\mathbf{r},t)$ is given by the hermitian conjugate expression.

2.4 Completeness

2.4.1 Motivation: How to add all the modes?

We have derived the electromagnetic field modes by solving the Helmholtz equation and imposing boundary conditions at the dielectric-vacuum interface. Also, we have made sure that the orthonormality condition is satisfied for our set of normal modes. The other indispensable condition that we have only mentioned so far is the completeness of the solutions of Helmholtz equation. In previous papers [77, 79], it has been assumed to be satisfied, but not proven, possibly because it is a highly non-trivial exercise.

However, there is a deeper reason to our proof of completeness of the modes: to come up with an efficient way to sum over all field modes, as required in the energy shift calculation. We shall explain in detail in the next chapter how to obtain the latter, but in brief, it is achieved by using second-order perturbation-theory, and involves a product of mode functions and a sum over intermediate photon states. Due to the nature of the modes, the shift naturally splits into two contributions, so clearly, this sum consist of a sum over the discrete trapped modes and an integral over the continuous travelling modes,

$$\Delta E = \int \mathrm{d}^2\mathbf{k}_\parallel \left(\int \mathrm{d}k_z \text{ (Travelling modes)} + \sum_{k_z} \text{ (Trapped modes)} \right). \tag{2.64}$$

At first glance, we can intuitively think of analysing the two contributions separately, which we initially tried. The method we followed was very similar to the one applied in Wu and Eberlein's calculation [76], which is based on an asymptotic analysis of Fourier integrals [97]. The problem with calculating separately travelling and trapped modes is that they have parts that diverge if calculated separately. This appears in the calculation for the half-space, but by combining travelling and evanescent modes contributions into one single expression [75] it is possible to eliminate such divergences. In our case, we expected to find a similar way, but this exercise seemed impossible.

The vital idea on how to solve the problem of summing over the travelling and

trapped modes is to transform the integral over the continuous set into a sum over discrete modes, so the shift can be written as a single expression from the beginning

$$\Delta E = \int \mathrm{d}^2\mathbf{k}_\parallel \left(\int \mathrm{d}k_z + \sum_{k_z} \right) \rightarrow \int \mathrm{d}^2\mathbf{k}_\parallel \left(\sum_{\mathrm{trav}} + \sum_{\mathrm{trap}} \right) = \int \mathrm{d}^2\mathbf{k}_\parallel \sum_{\mathrm{all}} . \tag{2.65}$$

We shall bear in mind that the system is translation-invariant in the direction parallel to the slab interface, and hence, the parallel wave vector $\mathbf{k}_\parallel$ is not affected by any assumption that will be described in the following sections and remains always continuous. In order to obtain a whole discrete set of modes, we need to place our system in a quantisation volume. Then, since the completeness relation (2.15) involves the same sum that we need, checking that it is satisfied will lead us to the correct way of summing all modes without ambiguities. Furthermore, by taking the limit of an infinite quantisation limit we shall recover the modes as calculated in free space, and hence the right way to sum them, i.e. the correct relative weightings should come up. The rest of this section is organised as follows: In 2.4.2, we shall explain in detail the procedure to quantise the electromagnetic field in the presence of a slab, when it is placed in a quantisation box. In section 2.4.3, we shall present the proof of the completeness of the electromagnetic modes. Finally, in section 2.4.4, we shall derive the method that will allow us to add both travelling and trapped modes in a more convenient way. This will be done by introducing a new integration path in the complex k_z plane.

2.4.2 Quantisation box

With the purpose of obtaining a discrete sum over all the modes, as shown in (2.65), we shall make all the modes discrete. This can be achieved by placing our system into a large quantisation volume and imposing boundary conditions at the edges. We have chosen the quantisation box as it would help us to avoid ambiguities. Once we have obtained the modes inside the box, we will consider the limit of an infinite quantisation volume, and thus, we will be able to see in a natural way how the travelling modes emerge, transforming into an integral over continuous modes.

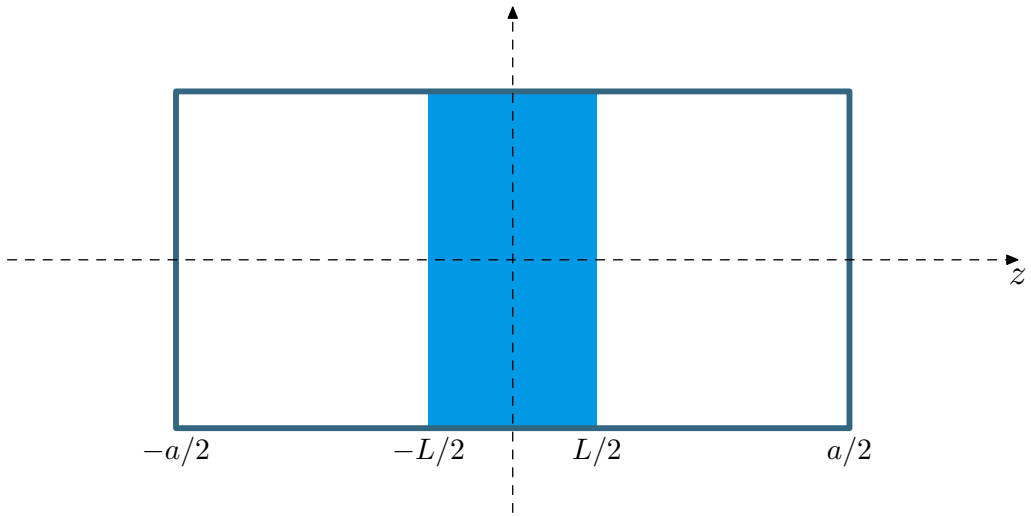

Figure 2.7: The quantisation box used, with edges at $z = \pm a/2$. The slab is centred so interfaces are located at $z = \pm L/2$.

We thus place our system inside a box of width a in the z direction, as it is drawn in Fig. 2.7. We follow a standard procedure: solve Helmholtz Eq. (2.12) in each region and apply the corresponding continuity conditions. But in this case, in addition to what we have done so far to obtain the spatial modes for this system, we have to include the boundary conditions imposed by the edges of the box. We shall apply Dirichlet boundary conditions

$$f_{\mathbf{k}\lambda}(z = \pm a/2) = 0. \tag{2.66}$$

However, the left- and right-incident modes that we introduced in the previous section, are incompatible with the vanishing conditions at the edge of the box. This is because by definition, the travelling modes represent running waves, contrary to the standing waves confined inside a quantisation box. Therefore, we shall form symmetric and antisymmetric combinations which corresponds to a rotation in the Hilbert space of these modes

$$f^{S,A}_{\mathbf{k}\lambda}(\mathbf{r}) = \frac{1}{\sqrt{2}} \left(f^{L}_{\mathbf{k}\lambda}(\mathbf{r}) \pm f^{R}_{\mathbf{k}\lambda}(\mathbf{r}) \right), \tag{2.67}$$

where the $+$ and $-$ signs are associated with the symmetric and antisymmetric mode functions. Thus, substituting in the right- and left-incident modes we get the travelling

modes inside a box

$$f^{S,A}_{\mathbf{k}\lambda}(\mathbf{r}) = \frac{\mathcal{N}_\lambda}{\sqrt{2}} \begin{cases} e^{i\mathbf{k}^+\cdot\mathbf{r}} + (R_\lambda \pm T_\lambda)\, e^{i\mathbf{k}^-\cdot\mathbf{r}} & z \le -L/2 \\ (I_\lambda \pm J_\lambda)\left(e^{i\mathbf{k}_d^+\cdot\mathbf{r}} \pm e^{i\mathbf{k}_d^-\cdot\mathbf{r}}\right) & |z| \le L/2 \\ e^{i\mathbf{k}^-\cdot\mathbf{r}} + (R_\lambda \pm T_\lambda)\, e^{i\mathbf{k}^+\cdot\mathbf{r}} & z \ge L/2 \end{cases}$$

where the coefficients R_λ, T_λ, I_λ J_λ are exactly the same as before, and $\mathcal{N}$ is the new normalisation constant. Since the travelling modes now form a discrete set, we shall calculate their dispersion relation. Thus, applying Dirichlet boundary conditions (2.66) and using relations (2.33) and (2.35) to simplify, we can obtain the general dispersion relation for the discrete modes. For any polarisation $\lambda = TE, TM$ we have

$$-e^{-\mathrm{i}k_z a} = R_\lambda \pm T_\lambda. \tag{2.68}$$

If we substitute the reflection and transmission coefficients (2.31) for the TE polarisation into the equation above, after some algebraic manipulation, we find an alternative way of writing the dispersion relations. Thus, for symmetric and antisymmetric modes, respectively, they read

$$k_{\mathrm{zd}} \tan\left(\frac{k_{\mathrm{zd}} L}{2}\right) = k_z \cot\left(\frac{k_z}{2}(a-L)\right) \qquad \text{TE, S} \tag{2.69}$$

$$-k_{\mathrm{zd}} \cot\left(\frac{k_{\mathrm{zd}} L}{2}\right) = k_z \cot\left(\frac{k_z}{2}(a-L)\right) \qquad \text{TE, A.} \tag{2.70}$$

One can also get the corresponding dispersion relations for the TM polarisation by using R_{TM} and T_{TM}.

Let us get back to the expressions for the symmetric travelling modes, as given on page 48. One can use the dispersion relation (2.68) to rewrite the reflection and transmission coefficients in terms of the width of the box a. Then, for any polarisation

λ, the modes are given by

$$f^{S,A}_{\mathbf{k}\lambda}(\mathbf{r}) = \sqrt{2}\mathcal{N}_\lambda\, e^{i\mathbf{k}_\parallel\cdot\mathbf{r}_\parallel} \times \begin{cases} \mathrm{i}\, e^{-ik_z a/2}\sin(k_z(a/2+z)) & z \le -L/2 \\ (I_\lambda \pm J_\lambda)\left(e^{\mathrm{i}k_{\mathrm{zd}}z} \pm e^{\mathrm{i}k_{\mathrm{zd}}z}\right)/2 & |z| \le L/2 \\ \pm\mathrm{i}\, e^{-ik_z a/2}\sin(k_z(a/2-z)) & z \ge L/2 \end{cases}$$

where the coefficients I_λ and J_λ are given by Eq. (2.36), and can also be written in terms of a by using the dispersion relations. In order to calculate the normalisation constant $\mathcal{N}_\lambda$, we shall use the normalisation condition (2.14), which is valid for discrete k_{zd} components. By substituting the modes (for any polarisation λ) in each region of space (vacuum-dielectric-vacuum) into Eq. (2.14), and then integrating over the whole of space, we obtain a lengthy expression for the normalisation constant. Nevertheless, what is important to note — as we are particularly interested in the limit of an infinite quantisation volume — is that only one term rises linearly and the rest vanish as $a \to \infty$. In such a limit, the normalisation constant is given by

$$|\mathcal{N}_\lambda|^2 \sim \frac{1}{(2\pi)^2}\,\frac{1}{a-L}. \tag{2.71}$$

In order to obtain the trapped modes that arise from the quantisation box, the procedure is the same. However, it is much easier in this case because it is more natural to think of them as a discrete set, and we have already classified them into symmetric and antisymmetric modes (page 39). To write a complete solution to the Helmholtz equation, we must add the exponentially rising solutions that we neglected in our previous analysis (with the purpose of obtaining well behaved functions, i.e., that vanish far away from the surface of the slab). For instance, to the right of the slab, where the solution was $\sim e^{-\kappa z}$, we have to add $e^{\kappa z}$. Therefore, we can express

the modes outside the slab in terms of hyperbolic functions, as follows

$$f^{S,A}_{\mathbf{k}\lambda}(\mathbf{r}) = \sqrt{2}\mathcal{N}_\lambda\, e^{i\mathbf{k}_\parallel\cdot\mathbf{r}_\parallel} \times \begin{cases} -e^{\kappa a/2}\sinh(\kappa(a/2+z)) & z \le -L/2 \\ (I_\lambda \pm J_\lambda)\left(e^{\mathrm{i}k_{\mathrm{zd}}z} \pm e^{\mathrm{i}k_{\mathrm{zd}}z}\right)/2 & |z| \le L/2 \\ \mp\, e^{\kappa a/2}\sinh(\kappa(a/2-z)) & z \ge L/2 \end{cases}$$

Note that they can alternatively be obtained from the expressions for the travelling modes, by replacing $k_z = \mathrm{i}\kappa$ (i.e., by analytic continuation). We can see that, introducing a quantisation volume only shifts the frequencies of the trapped modes by an amount that vanishes in the limit $a \to \infty$, recovering thus the modes given on page 39. If we apply the continuity conditions (2.24) at the dielectric-vacuum interface, we get the following dispersion relations

$$k_{\mathrm{zd}}\tan\left(\frac{k_{\mathrm{zd}}L}{2}\right) = \kappa\coth\left(\frac{\kappa}{2}(a-L)\right) \qquad \text{TE, S} \tag{2.72}$$

$$-k_{\mathrm{zd}}\cot\left(\frac{k_{\mathrm{zd}}L}{2}\right) = \kappa\coth\left(\frac{\kappa}{2}(a-L)\right) \qquad \text{TE, A.} \tag{2.73}$$

These equations look very similar to the dispersion relations for the travelling modes (Eqs. (2.69) and (2.70), respectively). We can recover them simply by replacing $k_z = \mathrm{i}\kappa$, which implies the analytic continuation that we mentioned previously. Furthermore, if we take the limit $a \to \infty$ (i.e. use $\lim_{x\to\infty}\coth(x) = 1$), we can recover the dispersion relations for free space, as given in Eqs. (2.45) and (2.48). Clearly, the same applies for the TM polarisation, and similiar equations are obtained. We can thus intuit another, more general way to write them. After some simple but extensive algebra we obtain a general formula for any polarisation or parity,

$$-e^{\kappa a} = (R_\lambda \pm T_\lambda)\,|_{k_z\,=\,\mathrm{i}\kappa}\,. \tag{2.74}$$

2.4.3 The proof of the completeness

So far, we have discretized the spatial modes of the system by using the quantisation box, and our goal is how to prove the completeness of the modes for the original system.

Thus, we shall calculate first the product $f_{\mathbf{k}\lambda}(z)f^*_{\mathbf{k}\lambda}(z')$, sum over all the modes as in (2.15) and then take the limit of an infinite quantisation volume. We shall concentrate in the region that is to the right of the slab, on $z, z' \geq L/2$. The calculation of the contribution to completeness from the trapped modes is obtained straightforwardly, as taking the limit does not cause any difficulty and one can easily recover the old expressions. Thus, the product of the trapped modes that exist to the right of the slab, inside the box, is given by

$$f^{S,A}_{\mathbf{k}\lambda}(z)f^{S,A*}_{\mathbf{k}\lambda}(z') = 2|\mathcal{N}_\lambda|^2 \sinh(\kappa(a/2-z))\sinh(\kappa(a/2-z'))e^{\kappa a} \tag{2.75}$$

$$\stackrel{a\to\infty}{\longrightarrow} |M_\lambda|^2 \left|L^{S,A}_\lambda\right|^2 e^{-\kappa(z+z')}. \tag{2.76}$$

The total contribution to completeness from the trapped modes is obtained by adding both polarisations

$$\int \mathrm{d}^2\mathbf{k}_\parallel \sum_{k_z,\lambda} \sqrt{\varepsilon} f^i_{\mathbf{k}\lambda}(\mathbf{r})\ \sqrt{\varepsilon} f^{*j}_{\mathbf{k}\lambda}(\mathbf{r}')\Big|_{\text{evan.}} = \sum_\lambda \hat{e}^i_\lambda(\partial_r)\hat{e}^j_\lambda(\partial_{r'}) \int \mathrm{d}^2\mathbf{k}_\parallel \sum_{k_z} |M_\lambda|^2 \left|L^{S,A}_\lambda\right|^2 e^{-\kappa(z+z')+\mathrm{i}\mathbf{k}_\parallel\cdot(\mathbf{r}_\parallel-\mathbf{r}'_\parallel)}. \tag{2.77}$$

Since the coefficients M_λ and $L^{S,A}_\lambda$ do not depend on the position $\mathbf{r}$, we can substitute their values from Eqs. (2.49), (2.41) and (2.42) for the TE polarisation and (2.56), (2.50) and (2.51) for the TM polarisation, to obtain a more explicit expression,

$$\begin{aligned}\int \mathrm{d}^2\mathbf{k}_\parallel \sum_{k_z,\lambda} \sqrt{\varepsilon} f^i_{\mathbf{k}\lambda}(\mathbf{r})\ \sqrt{\varepsilon} f^{*j}_{\mathbf{k}\lambda}(\mathbf{r}')\Big|_{\text{evan.}} &= \frac{\hat{e}^i_{TE}(\partial_r)\hat{e}^j_{TE}(\partial_{r'})}{(2\pi)^2(n^2-1)} \int \mathrm{d}^2\mathbf{k}_\parallel\, e^{\mathrm{i}\mathbf{k}_\parallel\cdot(\mathbf{r}_\parallel-\mathbf{r}'_\parallel)} \sum_{\kappa^{TE}} \frac{k^2_{\mathrm{zd}}\, e^{-\kappa(z+z'-L)}}{n^2\frac{L}{2}k^2+k^2_\parallel/\kappa} \\ &+ \frac{\hat{e}^i_{TM}(\partial_r)\hat{e}^j_{TM}(\partial_{r'})}{(2\pi)^2(n^2-1)} \int \mathrm{d}^2\mathbf{k}_\parallel\, e^{\mathrm{i}\mathbf{k}_\parallel\cdot(\mathbf{r}_\parallel-\mathbf{r}'_\parallel)} \sum_{\kappa^{TM}} \frac{k^2_{\mathrm{zd}}\, e^{-\kappa(z+z'-L)}}{\frac{L}{2}(k^2_\parallel+n^2\kappa^2)+k^2_\parallel/\kappa}.\end{aligned} \tag{2.78}$$

From Eqs. (2.41) and (2.42) we see that $\left|L^S_{TE}\right| = \left|L^A_{TE}\right|$ (and the same for the TM polarisation), and thus the expressions look the same regardless the parity. However,

the sum over κ includes both symmetric and antisymmetric modes, as they satisfy different dispersion relations.

The treatment for the travelling modes contribution is not so simple since it is not obvious what happens in the limit of an infinite quantisation volume, and thus we have to proceed with more insight. For instance, it is not evident what happens to the functions $\mathbf{f}_{\mathbf{k}\lambda}^{S,A}(\mathbf{r})$ or to the dispersion relations (2.69) and (2.70) in such a limit, where we get very rapid oscillatory functions containing information related to the density of modes. It is important to bear in mind that this formalism, in which we have classified travelling modes into symmetric and antisymmetric modes, is indeed equivalent to the one in terms of right- and left-incident modes. However, it is essential to express the modes in this way, in order to make them compatible with the boundary conditions at the edge of the box. Thus, we will be able to obtain the factor that correctly transforms a sum over the discrete modes into an integral, in the limit $a \to \infty$. This misleading factor, given in Ref. [78], was introducing divergences into our results when we were just basing our calculations on those published results.

The dispersion relations tell us the allowed values of k_z for each value of the frequency ω. This of course must be related to the density of modes, which describes the number of states at each energy level that are available to be occupied, as it is normally defined in solid state physics [98]. Furthermore, the density of modes is used to transform from a discrete summation over field modes to a continuous one.

To understand how to calculate such a density of states, let us consider first a much simpler system: the particle propagating freely in a zero or constant potential. In this case it would be difficult to deal with the normalisation of the momentum or energy eigenfunctions. This is why it is convenient to constrain the particle in a finite volume V, i.e., a cubic box of linear dimension a. In such a way, in the limit $V \to \infty$ we can recover the free moving particle, and moreover, before taking the limit we are allowed to do calculations using properly normalised states. What we have to do next is solve Schrödinger's equation, describing the particle by the wave function $\Psi(x, y, z)$. Its solutions are plane waves $\Psi(x, y, z) \sim e^{\mathrm{i}\mathbf{k}\cdot\mathbf{r}}$, and we shall apply appropriate periodic

boundary conditions which are the periodic conditions, i.e. $\Psi(x,y,z+\Delta z)=\Psi(x,y,z)$, and the same for the other coordinates. This implies that the components $\iota = x,y,z$ of the wave vector $\mathbf{k}$ must be of the form

$$k_\iota = \frac{2\pi n}{a} \qquad\qquad n = 1,2,3\ldots \tag{2.79}$$

Taking differentials of this expression, we find that the number of modes between k_z and $k_z+\Delta k_z$ is $\mathrm{d}n_z = \frac{a}{2\pi}\mathrm{d}k_z$. That means that the sum over modes can be transformed into an integral in the limit $a\to\infty$ by using

$$\sum_{n=0}^{\infty} \overset{a\to\infty}{\longrightarrow} \int_0^\infty \mathrm{d}n = \frac{a}{2\pi}\int_0^\infty \mathrm{d}k_z. \tag{2.80}$$

We want to do exactly the same for our system; and the relation analogous to (2.79) would be, for instance, the dispersion relation (2.69) for the TE symmetric modes. It is convenient to first rewrite it in terms of the two independent variables, k_z and $k_\parallel$. Eq. (2.69) becomes

$$\sqrt{(n^2-1)k_\parallel^2+n^2k_z^2}\,\tan\left(\frac{L}{2}\sqrt{(n^2-1)k_\parallel^2+n^2k_z^2}\right) = k_z\cot\left(\frac{k_z}{2}(a-L)\right). \tag{2.81}$$

Hence, in order to find its solutions, we can plot the left- and right-hand side functions, as shown in Fig. 2.8 in red and blue, respectively. Note that we have used L to rescale our variables and taken an arbitrary value of a. We have set a to be much bigger than the width of the slab L. Then, for a fixed $k_\parallel$, the solutions are the intersections of the blue and red plots.

It can be seen that the right-hand side function of Eq. (2.81), plotted in blue, oscillates very rapidly. Thus, increasing the argument by a factor of π implies

$$\frac{\Delta k_z}{2}(a-L)=\pi \qquad \Rightarrow \qquad \Delta k_z = \frac{2\pi}{a-L}, \tag{2.82}$$

which is a much shorter period than the one for the left-hand side function in Eq. (2.81),

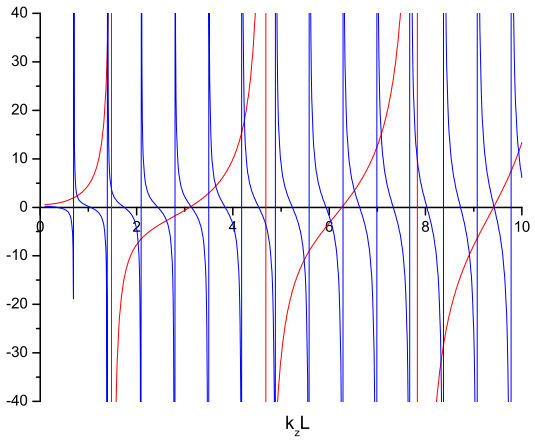

Figure 2.8: The intersections of the left- and right-hand side functions of Eq. (2.81), plotted in blue and red, respectively, show the solutions to the dispersion relation for the TE symmetric travelling modes.

and it vanishes in the limit $a \to \infty$. This illustrates the fact that the spacing between eigenvalues diminishes as the size of the boundary increases, until eventually k_z is a continuous variable and the summation over n becomes an integral in k_z. Therefore, if we number the solutions of the dispersion relations by m, and sum them in the limit $a \to \infty$, it should transform in the following way,

$$\sum_{m=1}^{\infty} \overset{a\to\infty}{\longrightarrow} \int_0^{\infty} \mathrm{d}m = \int_0^{\infty} \mathrm{d}k_z \left(\frac{\partial m}{\partial k_z}\right) = \int_0^{\infty} \mathrm{d}k_z \left(\frac{\partial k_z}{\partial m}\right)^{-1}. \tag{2.83}$$

From Eq. (2.81) we can define

$$F(k_z) \equiv \frac{\sqrt{(n^2-1)k_\parallel^2 + n^2 k_z^2}}{k_z} \tan\left(\frac{L}{2}\sqrt{(n^2-1)k_\parallel^2 + n^2 k_z^2}\right), \tag{2.84}$$

which is a slowly varying function. Let us suppose that we know the m^{th} solution to the dispersion relation (2.81). Thus we can write,

$$F(k_z^{(m)}) = \cot\left(\frac{k_z^{(m)}}{2}(a-L)\right). \tag{2.85}$$

From Eq. (2.82) we know that its next solution is given by

$$k_z^{(m+1)} = k_z^{(m)} + \Delta k_z \tag{2.86}$$

$$= k_z^{(m)} + \frac{2\pi}{a-L} + \delta k_z, \tag{2.87}$$

therefore one can write the function $F(k_z)$, as a Taylor expansion

$$F(k_z^{(m+1)}) \approx F(k_z^{(m)}) + \frac{\partial F}{\partial k_z}\Delta k_z, \tag{2.88}$$

and the same for the right-hand side of Eq. (2.85), round the phase δk_z

$$\cot\left(\frac{k_z^{(m+1)}}{2}(a-L)\right) = \cot\left(\frac{k_z^{(m)}}{2}(a-L)\right) - \frac{(a-L)\,\delta k_z}{2\sin^2\left(\frac{k_z^{(m)}}{2}(a-L)\right)}, \tag{2.89}$$

where the last term in the equation above is the derivative in k_z of the cotangent function times δk_z. Comparing the two equations above we can thus conclude that

$$\frac{\partial F}{\partial k_z}\left(\frac{2\pi}{(a-L)} + \delta k_z\right) = -\frac{(a-L)\,\delta k_z}{2\sin^2\left(\frac{k_z^{(m)}}{2}(a-L)\right)} \tag{2.90}$$

and simply obtain δk_z from this expression. Also, it can be seen from Eq. (2.87) how the solutions change

$$\frac{\partial k_z}{\partial m} = \frac{2\pi}{a-L} + \delta k_z, \tag{2.91}$$

so we can simply substitute the obtained value of δk_z and calculate the inverse of $\partial k_z/\partial m$, as required in Eq. (2.83). Hence the factor that transforms a sum into an integral in the limit $a \to \infty$ is given by

$$\sum_{m=1}^{\infty} \overset{a\to\infty}{\longrightarrow} \int_0^{\infty} \mathrm{d}k_z \left[\frac{a-L}{2\pi} + \frac{1}{\pi}\frac{\partial F}{\partial k_z}\sin^2\left(\frac{k_z}{2}(a-L)\right)\right], \tag{2.92}$$

where the derivative $\partial F/\partial k_z$ must come from Eq. (2.84). One can see that the second term inside the square brackets is finite for real k_z and thus it can be neglected.

For this derivation we have considered the dispersion relation (2.69) for TE sym-

metric modes, but the same result would be obtained for the other modes.

An alternative way of deriving the prescription of how to turn the sum over modes into an integral over k_z in the limit $a \to \infty$, would be to consider the relations between R_λ and T_λ given in Eqs. (2.33) and (2.35) to conclude that $|R_\lambda + T_\lambda| = 1$, which is equivalent to

$$R_\lambda + T_\lambda = e^{2\mathrm{i}\delta_s}, \tag{2.93}$$

with δ_s real. Note that this relation agrees with the dispersion relation obtained in Eq. (2.68). Replacing the expression above into the symmetric modes at $z > L/2$ we obtain,

$$f^S_{\mathbf{k}\lambda}(z \geq L/2) = \sqrt{2} N_\lambda e^{\mathrm{i}\mathbf{k}_\parallel \cdot \mathbf{r}_\parallel + \mathrm{i}\delta_s} \cos(k_z z + \delta_s). \tag{2.94}$$

It can be seen that the presence of the slab in the quantisation volume manifests itself as a phase shift δ_s of the modes calculated in the empty quantisation box. Applying the boundary condition (2.66) we get

$$\frac{k_z a}{2} + \delta_s = \left(m + \frac{1}{2}\right)\pi, \tag{2.95}$$

where m is an integer. This, together with the relation (2.93), is equivalent to the dispersion relation (2.68) obtained previously. As was explained, in the limit of a very large quantisation box, these discrete modes move closer and closer together, until we get a continuous distribution. Therefore, in order to transform the sum into an integral we shall simply calculate the derivative of the equation above, as needed in Eq. (2.83)

$$\sum_{m=1}^{\infty} \overset{a\to\infty}{\longrightarrow} \int_0^\infty \mathrm{d}k_z \left(\frac{a}{2\pi} + \frac{1}{\pi}\frac{\partial \delta_s}{\partial k_z}\right). \tag{2.96}$$

Since the derivative of the phase shift stays finite as $a \to \infty$, one can ignore the second term.

We can now proceed with the calculation of the contribution to completeness from the travelling modes. We shall first calculate the product $f_{\mathbf{k}\lambda}(z) f^*_{\mathbf{k}\lambda}(z')$, using the normal modes that we obtained through the quantisation box. For any polarisation λ

we have

$$\begin{aligned} f^{S,A}_{\mathbf{k}\lambda}(z) f^{S,A*}_{\mathbf{k}\lambda}(z') &= 2|\mathcal{N}_\lambda|^2 \sin(k_z(a/2-z)) \sin(k_z(a/2-z')) \\ &= \frac{1}{2}|\mathcal{N}_\lambda|^2 \left(e^{ik_z(z-z')} - e^{ik_z(z+z'-a)} + C.C \right). \end{aligned} \tag{2.97}$$

As we need to sum over symmetric and antisymmetric travelling modes, we find it convenient to substitute their respective dispersion relation (2.68) into Eq. (2.97), to *hide* the a-dependence before taking the limit. In that way, the expressions above do not contain explicitly the width of the box. Thus, the contribution to completeness from travelling modes reads

$$\sum_{k_z,\lambda} f_{\mathbf{k}\lambda}(z) f^*_{\mathbf{k}\lambda}(z') = \sum_{k_z,\lambda} \left(f^S_{\mathbf{k}\lambda}(z) f^{S*}_{\mathbf{k}\lambda}(z') + f^A_{\mathbf{k}\lambda}(z) f^{A*}_{\mathbf{k}\lambda}(z') \right) \tag{2.98}$$

$$= \sum_{k_z,\lambda} |\mathcal{N}_\lambda|^2 \left(e^{ik_z(z-z')} + R_\lambda e^{ik_z(z+z')} + C.C \right), \tag{2.99}$$

which can be transformed into an integral in k_z in the limit of an infinite quantisation volume, by using Eq. (2.92). Notice that the factor $a-L$ appearing in the normalisation constant, cancels with the $a-L$ that appears in the factor that transforms the sum into an integral. Thus, in the limit we can write

$$\begin{aligned} \sum_{k_z} f_{\mathbf{k}\lambda}(z) f^*_{\mathbf{k}\lambda}(z') &\overset{a\to\infty}{\longrightarrow} \frac{1}{(2\pi)^3} \int_0^\infty \mathrm{d}k_z \left(e^{ik_z(z-z')} + R_\lambda e^{ik_z(z+z')} + C.C \right) \\ &= \int_{-\infty}^\infty \mathrm{d}k_z \left(f^R_{\mathbf{k}\lambda}(z)\, f^{R*}_{\mathbf{k}\lambda}(z') + f^L_{\mathbf{k}\lambda}(z)\, f^{L*}_{\mathbf{k}\lambda}(z') \right), \end{aligned} \tag{2.100}$$

and adding the integral in $\mathbf{k}_\parallel$ and the sum over polarisations we get,

$$\begin{aligned} \int \mathrm{d}^2\mathbf{k}_\parallel \sum\!\!\!\!\!\!\int_{k_z,\lambda} \sqrt{\varepsilon} f^i_{\mathbf{k}\lambda}(\mathbf{r})\, \sqrt{\varepsilon} f^{*j}_{\mathbf{k}\lambda}(\mathbf{r}') \Big|_{\text{trav.}} &= (\delta_{ij} - \Delta^{-1}\partial_i\partial_j)\delta^{(3)}(\mathbf{r}-\mathbf{r}') \\ + \frac{1}{(2\pi)^3} \sum_\lambda \hat{e}^i_\lambda(\partial_r) \hat{e}^j_\lambda(\partial_{r'}) \int \mathrm{d}^2\mathbf{k}_\parallel \int_{-\infty}^\infty \mathrm{d}k_z\, R_\lambda(k_z, \mathbf{k}_\parallel)\, e^{\mathrm{i}k_z(z+z') + \mathrm{i}\mathbf{k}_\parallel \cdot (\mathbf{r}_\parallel - \mathbf{r}'_\parallel)}. \end{aligned} \tag{2.101}$$

2.4.4 New integration path

Since we want to prove the completeness relation (2.15), we need to sum over the travelling and trapped modes. We have utilised a finite quantisation volume to obtain the field modes, and hence there is no ambiguity in how to carry out such a sum, because all modes are discrete. We have obtained so far that, in the limit of an infinite quantisation volume, that the contribution to completeness coming from travelling modes is given by Eq. (2.101) and from trapped modes by Eq. (2.77). Adding both contributions

$$\begin{aligned}\int \mathrm{d}^2\mathbf{k}_\parallel \sum\!\!\!\!\!\!\int_{k_z,\lambda} \sqrt{\varepsilon} f^i_{\mathbf{k}\lambda}(\mathbf{r})\, \sqrt{\varepsilon} f^{*j}_{\mathbf{k}\lambda}(\mathbf{r}') \Bigg|_{\text{all}} \\ = \quad (\delta_{ij} - \Delta^{-1}\partial_i\partial_j)\delta^{(3)}(\mathbf{r}-\mathbf{r}') \; + \sum_\lambda \hat{e}^i_\lambda(\partial_r)\hat{e}^{j*}_\lambda(\partial_{r'}) \int \mathrm{d}^2\mathbf{k}_\parallel e^{\mathrm{i}\mathbf{k}_\parallel\cdot(\mathbf{r}_\parallel-\mathbf{r}'_\parallel)} \\ \times \quad \left(\frac{1}{(2\pi)^3}\int_{-\infty}^{\infty} \mathrm{d}k_z\; R_\lambda(k_z,\mathbf{k}_\parallel)\; e^{\mathrm{i}k_z(z+z')} + \sum_{k_z} |M_\lambda|^2 \left|L^{S,A}_\lambda\right|^2 \; e^{-\kappa(z+z')} \right).\end{aligned} \tag{2.102}$$

We have realised that this expression is the same that we would have originally obtained by simply using the modes obtained in sections 2.2.1 and 2.2.2, without any quantisation box. In that case the sum over modes comprises an integral over travelling modes and a discrete sum over trapped modes, with travelling modes normalised as in the plane-wave case. This means that travelling and trapped modes should be added together without any additional weighting factor, in contrast to the suggestion made by Khosravi and Loudon in Eq. (4.13) of Ref. [77], that a factor $2\pi/L$ should be used in front of the trapped modes. They do not give any arguments or explanation on how to derive it, and we shall stress that it is not very clear from their paper to which part of the calculation that factor was applied.

One can see from Eq. (2.102), that the first term in this expression is already the transverse delta function that we require. However we still have to prove that the terms inside the round brackets cancel out each other. Finding out the right way to do it will

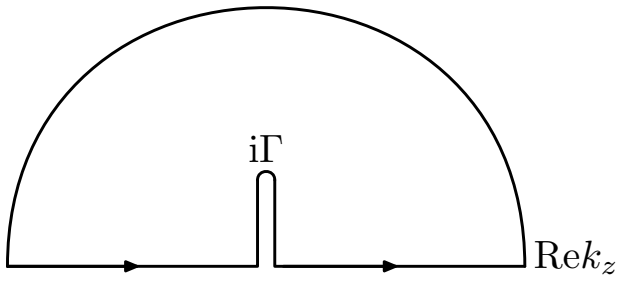

Figure 2.9: Integration contour in the k_z plane. The branch cut is due to the square root of k_z, thus $\Gamma = \sqrt{n^2 - 1}k_{\parallel}/n$

be crucial to figure out the most convenient way to add discrete and continuous modes.

For the simpler system of a semi-infinite dielectric half-space the quantisation was first achieved by Carniglia and Mandel [99], although they left unsolved the proof of the completeness of the electromagnetic field modes, which was shown later on in a paper by Bialynicki-Birula and Brojan [100]. In their calculation, Bialynicki-Birula and Brojan manage to combine the contribution from travelling modes (in the form of an integral in the real k_z-axis) and the one from evanescent modes (which is an integral in the imaginary k_z-axis), into one single expression: a contour integral in the complex k_z plane. This contour, as illustrated in Fig 2.9, consists of two halves of the real axis and part of the imaginary axis up to the branch point of the function (2.28). Their calculation has inspired us to do something similar, especially as we have learned, from frustrating attempts at calculating the travelling and trapped modes contributions separately, about the importance of having a single equation. Choosing the right integration path, one analogous to Fig. 2.9, will make a meaningful difference, guiding us to possibly the easiest method of tackling the problem of adding travelling and trapped modes in an unambiguous way.

The chief problem will be solving the integral in k_z contained in Eq. (2.102). Since the TE and TM polarisations are independent, and the procedure followed for each one is very similar, we will provide a more detailed description of the procedure only for

the TE modes. We are thus interested in the calculation of the integral

$$\int_{-\infty}^{\infty} \mathrm{d}k_z \; R_{TE}(k_z, \mathbf{k}_{\parallel}) \; e^{\mathrm{i}k_z(z+z')}, \tag{2.103}$$

where R_{TE} is the reflection coefficient (2.31). One can work out this integral in k_z by using complex analysis and closing the contour in the complex plane. As the argument of the exponential in the integrand is $z + z' - L > 0$ (where we have taken into account the phase that comes up from R_λ), and we are only looking at the case $z, z' \geq L/2$, we must close the contour in the upper half-plane. In order to proceed with the evaluation of the integral (2.103) we have to understand its analytic properties. These will become more evident if we substitute the Fresnel coefficient (2.32) into the reflection coefficient (2.31), obtaining

$$R_{TE} = \frac{(k_z^2 - k_{\mathrm{zd}}^2) \; e^{-\mathrm{i}k_z L}}{[k_z - \mathrm{i}k_{\mathrm{zd}} \tan(k_{\mathrm{zd}} L/2)] \, [k_z + \mathrm{i}k_{\mathrm{zd}} \cot(k_{\mathrm{zd}} L/2)]}. \tag{2.104}$$

In such a way, it can be seen that the reflection coefficient has poles in the upper half-plane, at $k_z = \mathrm{i}\kappa$ given by Eqs. (2.45) and (2.48), where the trapped modes occur. In other words, the poles correspond to the location of the bound states [101], which are solutions of the dispersion relations. One might find it surprising the fact that the bound states are mathematically related to the reflection coefficients this way. However, this is a well know fact [102]. Also, it was shown by Wylie and Sipe [89] in a paper about the quantum electrodynamics near an interface, that the surface effects depend only on the appropriate Fresnel coefficient. More specifically, contributions of surface excitations can be easily investigated because they are indicated by poles in those coefficients. We can hence generalise this idea for our case.

As shown in Fig (2.10), these poles are located on the complex k_z-axis, at $\kappa^S = k_{\mathrm{zd}} \tan(k_{\mathrm{zd}} L/2)$ and $\kappa^A = -k_{\mathrm{zd}} \cot(k_{\mathrm{zd}} L/2)$, appearing, periodically, one symmetric solution κ^S after an antisymmetric solution κ^A, up to $k_z = \mathrm{i}\sqrt{n^2 - 1}k_{\parallel}/n$. Thus, by closing the contour in the upper half-plane, we pick up residues from those poles.

It is well-known from complex variable techniques that a set of isolated singularities

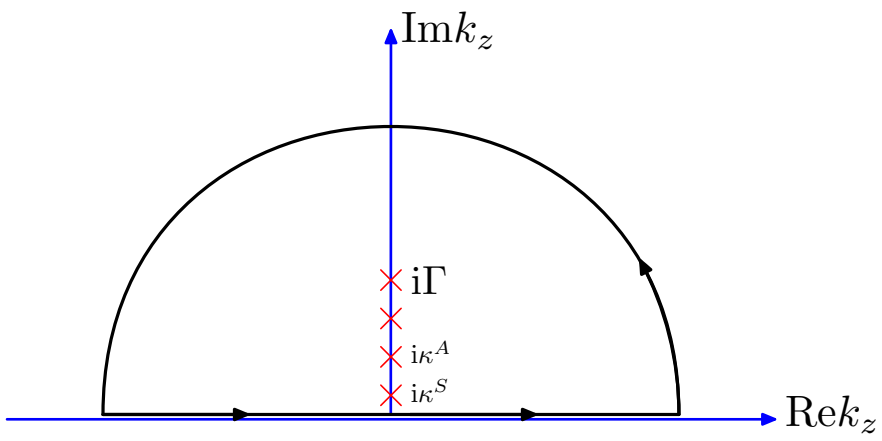

Figure 2.10: Integration contour for the travelling modes contribution. The figure shows the location of the poles of R_λ on the posive complex k_z plane, which are located up to $k_z = \mathrm{i}\Gamma = \mathrm{i}\sqrt{n^2-1}k_\parallel/n$. Thus, by closing the contour in the upper half-plane, we pick up residues from these poles.

can be handled very nicely by deforming the contour. From the residue theorem [103], we know that the circular integral around a simple pole is given by,

$$\oint f(z)\mathrm{d}z = 2\pi\mathrm{i}a_{-1} \tag{2.105}$$

where a_{-1} is the residue and the contour integral is taken in the clockwise direction. Since we have closed the contour in the upper-half plane, and the integral is otherwise analytic, one can thus deform this contour, enclosing each pole $\kappa_n = \kappa^A, \kappa^S$ in small circles. Therefore, the problem of evaluating one contour integral is replaced by the algebraic problem of computing residues at the enclosed singular points.

The procedure to calculate these residues is a standard one, bearing in mind that k_z and $k_\parallel$ are independent variables, and that k_{zd} is a function of them, as shown in Eq. (2.28). Thus, to calculate the residue of the nth pole of R_{TE} at $k_z = \mathrm{i}\kappa_n$ that corresponds, for instance, to a symmetric trapped mode, we shall write Eq. (2.104) more conveniently as a product of the denominator that has the pole and some function $H(k_z, \mathbf{k}_\parallel)$,

$$R_{TE} = \frac{H(k_z, \mathbf{k}_\parallel)}{k_z - \mathrm{i}k_{\mathrm{zd}}\tan(k_{\mathrm{zd}}L/2)}. \tag{2.106}$$

As the residues are typically obtained using

$$\mathrm{Res}[R_\lambda(k_z,\mathbf{k}_\parallel)]_{k_z=\mathrm{i}\kappa_n}=\lim_{k_z\to\mathrm{i}\kappa_n}(k_z-\mathrm{i}\kappa_o)R_\lambda(k_z,\mathbf{k}_\parallel), \tag{2.107}$$

we can use L'Hospital's rule [104] to take the limit when calculating the residue,

$$\begin{aligned}\mathrm{Res}[R_{TE}(k_z,\mathbf{k}_\parallel)]_{k_z=\mathrm{i}\kappa_n} &= \lim_{k_z\to\mathrm{i}\kappa_n}\frac{H(k_z,\mathbf{k}_\parallel)}{k_z-\mathrm{i}k_{\mathrm{zd}}\tan(k_{\mathrm{zd}}L/2)}(k_z-\mathrm{i}\kappa_n) &(2.108)\\ &= \lim_{k_z\to\mathrm{i}\kappa_n}\frac{H(k_z,\mathbf{k}_\parallel)}{1-\mathrm{i}\frac{\partial}{\partial k_z}[k_{\mathrm{zd}}\tan(k_{\mathrm{zd}}L/2)]}. &(2.109)\end{aligned}$$

We can calculate the residues around the second set of poles, the corresponding to the antisymmetric trapped modes. Thus, in total for the TE polarisation we get

$$\begin{aligned}\int_{-\infty}^{\infty}\mathrm{d}k_z\;R_{TE}(k_z,\mathbf{k}_\parallel)\;e^{\mathrm{i}k_z(z+z')} &= 2\pi\mathrm{i}\;\mathrm{Res}\left[R_{TE}(k_z,\mathbf{k}_\parallel)\;e^{\mathrm{i}k_z(z+z')}\right] &(2.110)\\ &= -\frac{2\pi}{n^2-1}\sum_\kappa\frac{k_{\mathrm{zd}}^2\;e^{-\kappa(z+z'-L)}}{n^2\frac{L}{2}k^2+k_\parallel^2/\kappa}, &(2.111)\end{aligned}$$

where the sum runs over the location of the poles.

In order to calculate the integral (2.103), for the TM polarisation, we shall rewrite the reflection coefficient as

$$R_{TM}=\frac{(n^4k_z^2-k_{\mathrm{zd}}^2)\;e^{-\mathrm{i}k_zL}}{[n^2k_z-\mathrm{i}k_{\mathrm{zd}}\tan(k_{\mathrm{zd}}L/2)]\,[n^2k_z+\mathrm{i}k_{\mathrm{zd}}\cot(k_{\mathrm{zd}}L/2)]}, \tag{2.112}$$

in such a way that it has the same form as (2.106) and the residues can be calculated by using the same procedure. In this case, the poles correspond to the solutions of the dispersion relations (2.53) and (2.55). Taking into account both sets of poles, for the symmetric and antisymmetric modes, the integral finally reads

$$\begin{aligned}\int_{-\infty}^{\infty}\mathrm{d}k_z\;R_{TM}(k_z,\mathbf{k}_\parallel)\;e^{\mathrm{i}k_z(z+z')} &= 2\pi\mathrm{i}\;\mathrm{Res}\left[R_{TM}(k_z,\mathbf{k}_\parallel)\;e^{\mathrm{i}k_z(z+z')}\right] &(2.113)\\ &= -\frac{2\pi}{n^2-1}\sum_\kappa\frac{k_{\mathrm{zd}}^2\;e^{-\kappa(z+z'-L)}}{\frac{L}{2}(k_\parallel^2+n^2\kappa^2)+k_\parallel^2/\kappa_o}, &(2.114)\end{aligned}$$

where the sum runs over the location of the poles, as shown in Fig. 2.10. It can be seen that the integrals (2.111) and (2.114), times the factor $1/(2\pi)^3$, are equal to the contribution from the evanescent modes (2.78), but with opposite signs,

$$\frac{1}{(2\pi)^3}\int_{-\infty}^{\infty} \mathrm{d}k_z \; R_\lambda(k_z, \mathbf{k}_\parallel)\, e^{\mathrm{i}k_z(z+z')} = -\sum_{k_z} |M_\lambda|^2 \left|L_\lambda^{S,A}\right|^2 \; e^{-\kappa(z+z')}. \tag{2.115}$$

Therefore, the term in round brackets in Eq. (2.102) is zero for each polarisation, leaving only the desired transverse delta function, as required in Eq. (2.15) to prove the completeness of the field modes.

2.5 Discussion

In this chapter we have quantised the electromagnetic field in the presence of a finite width dielectric slab. We have derived the modes and checked their orthonormality and completeness. Even though this system has been studied previously, the completeness of the modes was not proven, probably because, as it was shown, the procedure is not trivial. Clearly, this is due to the fact that the spectrum of modes includes a set of continuous travelling modes and a set of discrete trapped modes, and thus it is difficult to know *a priori* how to add them with the correct relative weightings. Therefore we introduced a quantisation box. Since all modes become discrete in a quantisation box, one can add them in an unambiguous way. By taking the limit of an infinite quantisation volume, we can recover our original modes, as obtained in free space, and hence a correct way to sum them.

Although the proof of the completeness relation (2.15) is very important in order to demonstrate that we are working with the correct set of modes (and not missing any of them), we shall remember that the original reason that we had, to embark on the completeness calculation, was to understand how to add all modes. This is because a typical second-order perturbative calculation in quantum electrodynamics, like the one of the Casimir-Polder force between an atom an a dielectric slab, involves a product of mode functions and a sum over intermediate photon states. Clearly, this sum

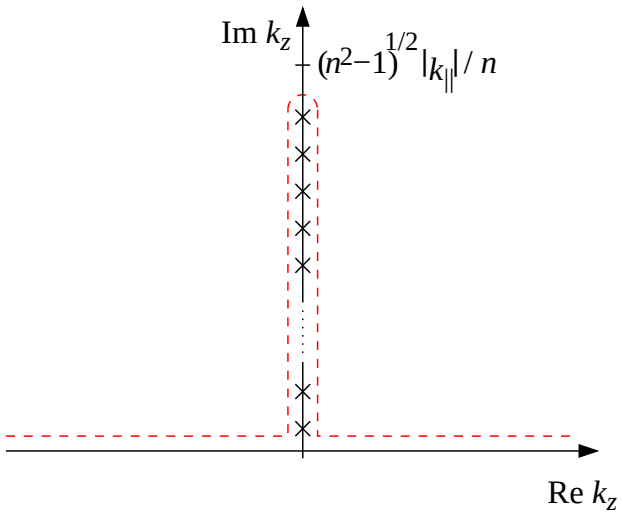

Figure 2.11: The red dotted line shows the new integration path in the complex k_z-plane. The sum over trapped modes can be transformed into a contour integral that goes round the poles on the imaginary axis.

consists of a continuous and a discrete part, corresponding to the travelling and trapped modes, respectively, and that is why the results obtained are of vital importance. Thus, following in reverse the procedure described in section (2.4.4), one can transform the sum over trapped modes into a contour integral in the complex k_z plane and then combine it with the integration path for the travelling modes (along the real k_z axis), obtaining one single integration path, as shown in Fig. 2.11. These results have been presented recently in [105].

In general, for any function $Q(k_z, \mathbf{k}_\parallel)$ in the integrand, assuming that such a function is analytic in the vicinity of the poles of the reflection coefficients R_{TE} and R_{TM} on the positive imaginary k_z axis, one can calculate the sum over all modes by writing it in the following way,

$$\int \mathrm{d}^2\mathbf{k}_\parallel \sum\!\!\!\!\!\!\int_{k_z\lambda} Q(k_z,\mathbf{k}_\parallel)\,\sqrt{\varepsilon} f^i_{\mathbf{k}\lambda}(\mathbf{r})\,\sqrt{\varepsilon} f^{*j}_{\mathbf{k}\lambda}(\mathbf{r}')\Big|_{\text{all modes}} = \frac{1}{(2\pi)^3}\int \mathrm{d}^3\mathbf{k}\, Q(k_z,\mathbf{k}_\parallel)\, e^{\mathrm{i}\mathbf{k}\cdot(\mathbf{r}-\mathbf{r}')} + \frac{1}{(2\pi)^3}\sum_\lambda \int \mathrm{d}^2\mathbf{k}_\parallel \int_{\mathcal{C}} \mathrm{d}k_z\, Q(k_z,\mathbf{k}_\parallel)\, R_\lambda(k_z,\mathbf{k}_\parallel)\, e^{\mathrm{i}k_z(z+z')+\mathrm{i}\mathbf{k}_\parallel\cdot(\mathbf{r}_\parallel-\mathbf{r}'_\parallel)}. \quad (2.116)$$

The resulting integral can be evaluated by using complex variable techniques, by de-

forming the integration path $\mathcal{C}$, shown in Fig. (2.11), in the most convenient way. As can be seen, it encloses all poles of R_λ. Note that in the equation above, the first term on the right-hand side corresponds to the free-space contribution and thus it will be eliminated in the energy-level shift calculation through renormalisation. More details will follow in the next chapter, where we will apply our main result (as given in Eq. (2.116)) to the calculation of the Casimir-Polder force on an atom near a dielectric slab.

Chapter 3

Energy-level shift of an atom in front of a dielectric slab

Though the calculation of the energy-level shift of an atom near a dielectric slab may seem to be a basic problem, its solution has not yet been obtained in an exact way. In fact, only a few systems of high symmetry have been studied by means of an explicit mode expansion of the electromagnetic field, which is the procedure that would facilitate obtaining analytical formulae. Nevertheless, if one wishes to consider more complex systems, e.g., atoms near absorbing boundaries, it will require other methods to study quantum electrodynamics [7]. However, applying such results[1] to a particular case might require extensive numerical calculations. Using those formalisms, the energy-level shift of atoms due to the presence of conducting or permeable media has been calculated for several systems, including spheres, cylinders, and dielectric half-spaces [86].

As we have emphasized, we are interested in a calculation based on the explicit mode expansion of the electromagnetic field, which should lead us to a very simple and practical result. The field quantisation for this system has been achieved in chapter 2. A much simpler calculation of another quantum effect that arises from the atom-field interaction that also necessitates such a quantisation, is the one for the radiative decay

[1] Generally in terms of Green functions.

rate of the atom. The standard way to calculate it is through the Fermi's Golden Rule[2], though it can also be obtained based on the nonlocal treatment of optical response. A brief explanation of the latter is presented in Ref. [107], where some graphs for the radiative decay of the atom as a function of its distance from the surface of the slab are given. It is shown that the contribution due to the wave guide modes is very large when the atom is placed inside and just outside the slab. Also, as expected, the effect of the slab vanishes at large atom-surface separations.

We have given in the introduction, in section 1.2.2, a review on the work done to date to calculate the spontaneous emission (i.e., the radiative rate) for the same system. Several researchers have attempted this calculation. Nevertheless, the problem that they encounter is to figure out the proper way to sum over all photon states, as arises from perturbation theory. Of course, the same problem emerges for the calculation of the energy-level shift. As people have not found the most convenient way to perform such summation, a complete analytical calculation has not been successful. We have explained in the previous chapter that the complication arises from having to sum over a discrete set of trapped modes and a continuous spectrum of travelling modes. Now, we have came up with the correct way to sum over all modes. We have shown that the sum over discrete trapped modes can be seen as a sum of residues of an integral in the complex k_z plane, where such residues are located on the imaginary axis. Thus, by combining this with the integral in k_z that arises from the travelling modes contribution, one can obtain an integration path in the complex k_z plane that facilitates the sum over all modes. This trick is summarised in Eq. (2.116), and it is not difficult to apply it to the energy-shift calculation. Such a procedure will be shown is section 3.5. Then, we can use complex-variable techniques and deform the integration contour in order to calculate the integral in a more efficient and suitable way.

In chapter 1 we introduced the concept of retardation, and its importance depends on how appreciably the atoms evolve during the time-scale of the interaction. It is clear then, that only two regimes matter in this problem. The most interesting one is the

[2]See for instance Ref. [106].

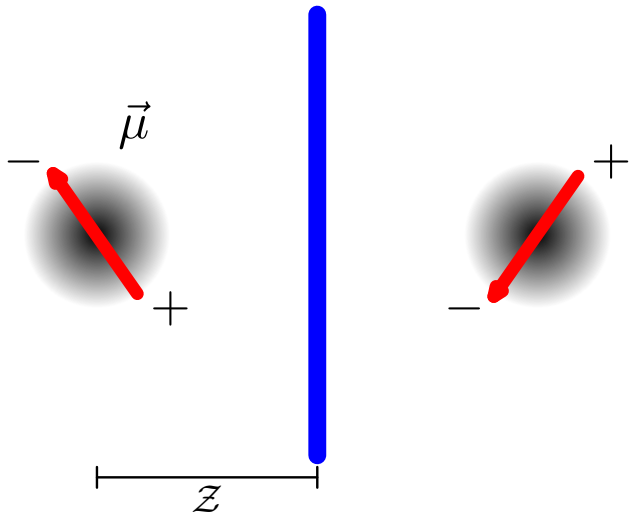

Figure 3.1: Atomic dipole and its image in the other side of the interface of a perfect conductor.

retarded regime, in which we take into account the coupling of the atom to the fluctuating electromagnetic field. On the other hand, we know that when the atom is close to the surface we can neglect the fluctuations of the field and thus the dispersion forces are dominated by the Coulomb interaction between the fluctuating dipole moment of this atom and the solid dielectric. This is called the *non-retarded* regime. In this chapter we shall demonstrate how to obtain a general formula that describes the shift as a function of the atom-surface separation $\mathcal{Z}$ and the thickness of the slab L. Then, we shall proceed with an asymptotic analysis for both the retarded and non-retarded regimes. In such a way, we can obtain explicit expressions for the energy-shift in terms of the thickness, and thus make apparent the variation of the Casimir-Polder due to the thickness of the slab. More details on the criteria for retardation and how to perform this analysis will be given in section 3.6.

Alternatively, we can calculate the non-retarded or electrostatic interaction by using an electrostatic treatment. As it was shown by Lennard-Jones [108] for an atom in front of a conducting plate, this interaction can be calculated by using the image method, considering the dipole-dipole interaction of this atom with its image on the other side of the interface (see Fig. 3.1). The resulting energy reads

$$\Delta E = -\frac{1}{64\pi\epsilon_o \mathcal{Z}^3}(|\mu_{\parallel}^2| + 2|\mu_{\perp}^2|), \tag{3.1}$$

where $\mu_{\parallel}$ and $\mu_{\perp}$ are the parallel and perpendicular components of the electric-dipole moment operator, respectively. Later on McLachlan [14] showed that the image method can be extended for the interaction of an atom with a solid dielectric. The interaction energy is given by

$$\Delta E = -\frac{\varepsilon - 1}{\varepsilon + 1}\frac{1}{64\pi\epsilon_o \mathcal{Z}^3}(|\mu_{\parallel}^2| + 2|\mu_{\perp}^2|), \tag{3.2}$$

where ε is the dielectric permittivity. A detailed explanation on the calculation of the electrostatic interaction will be given in section 3.6.2.

First of all, in section 3.1, we shall describe the model utilised in the present work. In section 3.2, a description of the interaction hamiltonian that we have adopted will be provided. Then, the application of second-order perturbation theory will follow in order to obtain the energy-level shift of the atom. Contributions from travelling and trapped modes will be initially treated separately, until section 3.5, where the trick that we derived (Eq. (2.116)) will be necessary in order to achieve the final result. In the last section of this chapter we shall calculate the double-integral that arises from the calculation, but only for certain interesting limits in both the retarded and the non-retarded regimes.

3.1 The model

We consider only a neutral atom in its ground state. We use the electric dipole approximation [109, 110], which is adequate because, for the relevant modes, the electromagnetic field varies slowly over the size of the atom. We assume that the atom's centre is fixed at the position $\mathbf{r}_o = (0, 0, z_o)$, which is a distance $\mathcal{Z} = z_o - L/2$ from the surface of the dielectric slab as shown in Fig. 3.2. The slab's interfaces are located at $z = \pm L/2$, and its properties are as described in the previous chapter.

In this work we have only considered the system at zero temperature though one can relatively easily extend this calculation to a system at finite temperature, as was

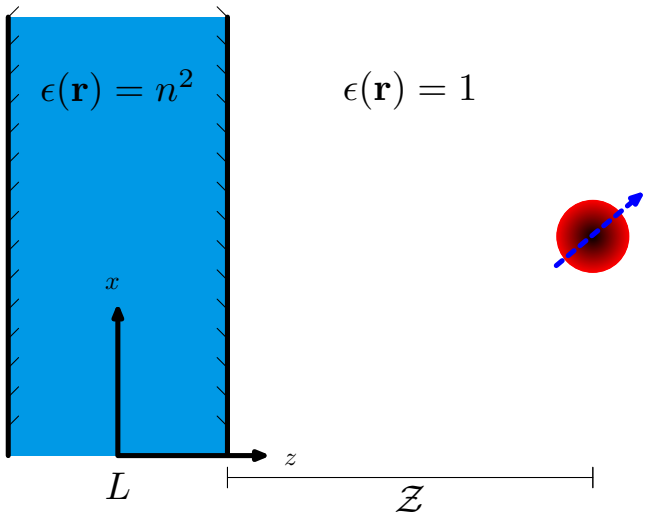

Figure 3.2: Single-electron atom in front of a dielectric slab

done for the simpler system of a semi-infinite dielectric half-space [111].

Furthermore, the model assumes that the interaction between the atom and the surface is purely electromagnetic, i.e. that the overlap of the surface with the wave function of the atomic electron is negligible. One is allowed to make this assumption because the distance $\mathcal{Z}$ is much greater than the size of the atom. In fact, if we do not consider this assumption, we have to take into account the interaction of the atom with the solid-state of the surface potential. The latter has been done in [112], for the calculation of the van der Waals interaction between an atom and a planar surface. In this work, they employed the retarded surface response function to describe the metal, which allowed them to obtain the binding energies of helium on simple metal surfaces.

We are only concerned by the energy-level shift of an atom located in free-space. The problem of an atom embedded in a material medium is far more complicated to deal with. Nevertheless, some theoretical work can be found in the literature [80], especially motivated by experiments that were performed previously [82]. When one considers an atom inside a dielectric, a microscopic theory might be required to calculate the polarisability of the atom. This gives the response of the atom to the effective or local field. The value of such a local field that acts at the site of an atom is significantly

different from the value of the macroscopic electric field. A classical treatment of the local-field corrections can be obtained by using the Clausius-Mossotti model [98]. In this model, the local electric field is written in terms of the macroscopic electric field and the commonly used induced polarisation field. However, it was proven in a paper by Scheel *et al* [113] that the polarisation fluctuations in the local field can dramatically change the spontaneous decay rate, compared with the familiar result obtained from the classical local-field correction. In order to avoid such complications, we shall restrict ourselves to the study of the effects of an atom located in free space.

3.2 The Hamiltonian

Quantum electrodynamics deals with the interaction of radiation and charges. The Hamiltonian can be obtained from the Lagrangian, like in classical mechanics, as the Hamiltonian corresponds to the Legendre transform of the Lagrangian[114]. Then, for a quantum mechanical treatment, we shall replace the classical variables with the quantum operators. The Hamiltonian of an atom coupled to any quantised electromagnetic field has three main components: $H^{\rm rad} + H_o^{\rm atom} + H^{\rm int}$. The first one refers to the free electromagnetic radiation field, and it is given by

$$H^{\rm rad} = \int {\rm d}\tau (\mathbf{E}^2 + \mathbf{B}^2). \tag{3.3}$$

Note that in the gauge in that we are working it is sufficient to quantise only the transverse electromagnetic field. The longitudinal field energy is replaced by instantaneous Coulomb interactions among particles [3]. The remaining terms refer to the atomic hamiltonian

$$H = H_o^{\rm atom} + H^{\rm int} = \frac{(\mathbf{p} - e\mathbf{A})^2}{2m} + V_{\rm Coul}(\mathbf{r}) + V_{\rm es}(\mathbf{r}). \tag{3.4}$$

In this expression, the first term includes the coupling of the atom to the electromagnetic field; $V_{\rm Coul}(\mathbf{r})$ refers to the non-retarded electron-nucleus potential, i.e. the

Coulomb interaction between the ion core and the electron within the atom, given by

$$V_{\text{Coul}}(\mathbf{r}) = \frac{\alpha}{|\mathbf{r} - \mathbf{r}_o|}, \tag{3.5}$$

where α is the fine structure constant. Note that we set $c = 1 = \hbar$ and use Heaviside-Lorentz units for electromagnetic quantities $\epsilon_o = 1 = \mu_o$. Thus the free structure constant is $\alpha = e^2/4\pi\epsilon_o\hbar c = e^2/4\pi \simeq 1/137$. In the eq. above, V_{es} is the electrostatic interaction between the atomic dipole and its image charges due to the presence of the dielectric. This interaction can normally be obtained by using the image method [11]. However, for this system the calculation turns out to be more complicated, since we have to deal with two interfaces.

As was explained in chapter 2, we have chosen to work in the generalised Coulomb gauge. Since the dielectric function $\varepsilon(\mathbf{r})$ is constant over the whole of space, with a discontinuity at the interface, this gauge is equivalent to the Coulomb gauge $\nabla \cdot \mathbf{A} = 0$. We shall only make sure that the physical fields satisfy the appropriate matching conditions at the boundary. The advantage is that one could simplify the atomic Hamiltonian above

$$H = \frac{\mathbf{p}^2}{2m} + V_{\text{Coul}}(\mathbf{r}) - \frac{e}{m}(\mathbf{A} \cdot \mathbf{p}) + \frac{e^2\mathbf{A}^2}{2m} + V_{\text{es}}(\mathbf{r}), \tag{3.6}$$

and identify from that expression the unperturbed Hamiltonian, which corresponds to the Hamiltonian of a free atom (without field)

$$H_o^{\text{atom}} = \frac{\mathbf{p}^2}{2m} + V_{\text{Coul}}(\mathbf{r}). \tag{3.7}$$

Hence, we can also recognise the remaining terms as the interaction Hamiltonian

$$H^{\text{int}} = -\frac{e}{m}(\mathbf{A} \cdot \mathbf{p}) + \frac{e^2\mathbf{A}^2}{2m} + V_{\text{es}}(\mathbf{r}), \tag{3.8}$$

and thus apply perturbation theory in order to calculate the effects of the interaction

of the atom with the dielectric slab.

An extensive calculation for the half-space case was done in [76] by applying first and second-order perturbation to the the minimal coupling Hamiltonian of Eq. (3.8). However, it is possible to transform the conventional interaction Hamiltonian (3.8) to

$$H_I = -\boldsymbol{\mu} \cdot \mathbf{E}(\mathbf{r}, t). \tag{3.9}$$

Such a procedure is achieved through the Power-Zienau-Wooley transformation [115] and an explanation in detail is given in Appendix B. This is the lowest-order in the multipole Hamiltonian and corresponds to the electric-dipole interaction [114, 116]. In this equation, $\boldsymbol{\mu} = e(\mathbf{r} - \mathbf{r}_o)$ is the electric-dipole moment operator and $\mathbf{E}(\mathbf{r}, t)$ the transverse electric field.

As an example of the use of the alternative interaction Hamiltonian (3.9) we can cite Barton's paper [28], in which he calculated the force between an atom and a wall, obtaining the same result as the one using the minimal-coupling Hamiltonian. A complete proof of the equivalence of these Hamiltonians was first done by Göpper and Mayer and then generalised by Power and Zienau [115]. They showed that a canonical transformation on the minimal-coupling Hamiltonian (for an atom with radiation confined in a cavity) leads to a new Hamiltonian, which is written in a multipolar form.

The advantage of working with this new Hamiltonian is that it does not contain explicitly either the interatomic potential or the electrostatic interaction between the atomic dipole and its image charges inside the dielectric. The generator that gives us this transformation eliminates them, leaving only the intra-atomic electrostatic binding energies [117]. Therefore the calculations are usually much easier.

The problem of an atom in front of a dielectric half-space was analysed by Wu and Eberlein in [76] and revisited in [75] by using the electric-dipole interaction (3.9) instead. In the latter, they reduced considerably the amount of calculation involved, though I shall emphasize that an even more ingenious procedure was required. From that experience and motivated by such a work, we are interested in the calculation of

the energy-shift of an atom in front of a dielectric slab. We shall thus apply second-order perturbation theory to the alternative interaction Hamiltonian (3.9). We assume that the system is initially in the composite state $|i;0\rangle$, with the atom in state $|i\rangle$ and zero-point electromagnetic field in the vacuum state $|0\rangle$ (no photons).

3.3 Perturbative calculation

In the theory of quantum electrodynamics, the atom-photon interactions are treated perturbatively. In stationary perturbation theory, H_I causes shifts of the eigenvalues of the unperturbed Hamiltonian H_o^{atom} described above, given as a series expansion in H_I. Thus, the shift of energy in the initial state $|i;0\rangle$ of H_o^{atom} is given by

$$\Delta E = \langle i;0|\, H_I\, |i;0\rangle + \sum_{j\neq i}\sum_{\nu} \frac{\langle i;0|\, H_I\, |j;\nu\rangle\, \langle j;\nu|\, H_I\, |i;0\rangle}{E_i - (E_j + \omega_\nu)} + \dots \tag{3.10}$$

where $|j;\nu\rangle$ is the composite state for an atom in the excited state $|j\rangle$ and the electromagnetic field carrying one photon of energy ω_ν. The initial state $|i\rangle$ has been excluded in the sum over intermediate states $|j\rangle$. In order to simplify our notation, we have introduced the variable $\nu = (\mathbf{k}, \lambda)$ which comprises the wave vector $\mathbf{k}$ and the polarisation λ.

Since the interaction Hamiltonian (3.9) is linear in the electron charge e, we must calculate the shift up to the second order of perturbation theory if we want to obtain it to first order in the fine-structure constant α. To calculate the first-order energy shift we utilise the first term of Eq. (3.10). This contribution vanishes because being linear in the electric field, H_I creates or annihilates one photon from the state it operates on. Hence, only the second-order shift survives and the total shift is given by

$$\Delta E = -\sum_{j\neq i}\sum_{\nu} \frac{\left|\left\langle j;\nu|\boldsymbol{\mu}\cdot\hat{\mathbf{E}}(\mathbf{r},t)|i;0\right\rangle\right|^2}{E_j - E_i + \omega_\nu}, \tag{3.11}$$

where $\hat{\mathbf{E}}(\mathbf{r},t)$ is given by Eq. (2.62) on page 44. If we now apply the creation $\hat{a}^\dagger_{\mathbf{k}\lambda}$ and

annihilation operators $\hat{a}_{\mathbf{k}\lambda}$ onto the field states, one can see that only the creation part ($\hat{\mathbf{E}}^{-}(\mathbf{r},t)$ of Eq. (2.62)) contributes. Thus the shift can be simplified

$$\Delta E = -\sum_{j\neq i}\sum_{\nu}\frac{\left|\left\langle j;\nu|\boldsymbol{\mu}\cdot\hat{\mathbf{E}}^{-}(\mathbf{r},t)|i;0\right\rangle\right|^{2}}{E_j - E_i + \omega_\nu} \tag{3.12}$$

where

$$\begin{aligned}\hat{\mathbf{E}}^{-}(\mathbf{r},t) &= \mathrm{i}\sum_{\lambda}\int_{k_z>0}\mathrm{d}^3\mathbf{k}\left(\frac{\hbar\omega}{2\epsilon_o}\right)^{1/2}\left(\mathbf{f}^{L*}_{\mathbf{k}\lambda}(\mathbf{r})\hat{a}^{L\dagger}_{\mathbf{k}\lambda}e^{i\omega t}+\mathbf{f}^{R*}_{\mathbf{k}\lambda}(\mathbf{r})\hat{a}^{R\dagger}_{\mathbf{k}\lambda}e^{i\omega t}\right)\\ &+ \mathrm{i}\sum_{\lambda}\sum_{k_z}\int\mathrm{d}^2\mathbf{k}_{\parallel}\left(\frac{\hbar\omega}{2\epsilon_o}\right)^{1/2}\left(\mathbf{f}^{S*}_{\mathbf{k}\lambda}(\mathbf{r})\hat{a}^{S\dagger}_{\mathbf{k}\lambda}e^{i\omega t}+\mathbf{f}^{A*}_{\mathbf{k}\lambda}(\mathbf{r})\hat{a}^{A\dagger}_{\mathbf{k}\lambda}e^{i\omega t}\right),\end{aligned} \tag{3.13}$$

and the expressions for the travelling modes $\mathbf{f}^{L,R}_{\mathbf{k}\lambda}(\mathbf{r})$ and the trapped modes $\mathbf{f}^{S,A}_{\mathbf{k}\lambda}(\mathbf{r})$ are given in the previous chapter, on pages 34 and 39, respectively. As we mentioned before, we are working within the electric dipole approximation. That means that we can assume that the electric field at the electron position is roughly the same as it is in the centre of the atom, and write

$$\langle j|\mathbf{f}(\mathbf{r})\cdot\boldsymbol{\mu}|i\rangle \simeq \mathbf{f}(\mathbf{r}_o)\cdot\langle j|\boldsymbol{\mu}|i\rangle\,, \tag{3.14}$$

where $\mathbf{r}_o$ is the position of the centre of the atom. Thus the shift is given by

$$\Delta E = -\sum_{j\neq i}\sum_{\nu}\frac{\hbar\omega_\nu}{2\epsilon_o}\frac{\left|\mathbf{f}^{*}_{\nu}(\mathbf{r}_o)\cdot\langle j|\boldsymbol{\mu}|i\rangle\right|^{2}}{E_{ji}+\omega_\nu} \tag{3.15}$$

$$= -\sum_{j\neq i}\sum_{\nu}\sum_{\iota=x,y,z}\frac{\hbar\omega_\nu}{2\epsilon_o}\frac{f^{*}_{\nu\iota}(\mathbf{r}_o)f_{\nu\iota}(\mathbf{r}_o)}{E_{ji}+\omega_\nu}\left|\mu_\iota\right|^{2}, \tag{3.16}$$

since the crossed terms $f^{*}_{\alpha}f_{\beta}\ \langle i|\mu_\alpha|j\rangle\langle j|\mu_\beta|i\rangle$ are zero for $\alpha\neq\beta$. We have defined $E_{ji} = E_j - E_i$ and abbreviated the moduli squares of the matrix elements of the dipole-moment operator between the ground state i and the excited states j by

$$|\mu_\iota|^2 \equiv |\langle j|\mu_\iota|i\rangle|^2 \qquad \text{with} \qquad \iota = x,y,z. \tag{3.17}$$

We have also introduced the parallel and perpendicular parts of $\boldsymbol{\mu}$ as they will be very useful in the following sections,

$$|\mu_{||}|^2 \equiv |\langle j|\mu_x|i\rangle|^2 + |\langle j|\mu_y|i\rangle|^2 \qquad \text{and} \qquad |\mu_{\perp}|^2 \equiv |\langle j|\mu_z|i\rangle|^2. \tag{3.18}$$

Let us get back to Eq. (3.15). By substituting the electric field $\mathbf{E}^{-}(\mathbf{r}, t)$ into Eq. (3.15), we can obtain a more explicit expression for the energy-level shift of an atom in front of a dielectric slab. Since the form of the quantised electric field depends on the boundary conditions, one can see clearly that the shift depends on how the electromagnetic fluctuations are constrained by the presence of any media.

In the previous chapter it became evident that solving the Helmholtz equation outside the slab will give us two different kind of solutions, i.e. spacial modes. The consequence is that the energy-level shift naturally splits into two contributions: one that comes from the continuous spectrum of travelling modes, and one arising from the discrete spectrum of trapped modes. As a first attempt, one could think of analysing them separately. We tried this, but we realised that this procedure was not the most convenient.

It is quite useful to first write the contributions from the travelling and from the trapped modes separately, although what we are actually aiming for is to obtain one single expression for the total energy-shift, as was done in [75]. This will be achieved by using Eq. (2.116). This expression will allow us to change the sum over trapped modes into an integration path in the complex plane. The procedure will be shown in detail in the following sections. Let us start with the contribution from travelling modes.

3.3.1 Contribution from travelling modes

We can proceed with the calculation of the shift by substituting the first part of Eq. (3.13), which corresponds to the travelling modes, into Eq. (3.15). Thus, the energy-

level shift is given by

$$\Delta E^{\text{trav}} = -\sum_{\iota}\sum_{j\neq i}\sum_{\lambda}\int \mathrm{d}^3\mathbf{k}\frac{\hbar\omega}{2\epsilon_o}\left\{|\mathbf{f}^L_{\nu\iota}(\mathbf{r}_o)|^2 + |\mathbf{f}^R_{\nu\iota}(\mathbf{r}_o)|^2\right\}\frac{|\langle j|\mu_\iota|i\rangle|^2}{E_{ji}+\omega}, \tag{3.19}$$

where the sum over ι runs over the x, y and z components of the electric field, and the subscript $\nu = (\lambda, \mathbf{k})$ includes both the polarisation λ and the corresponding wave vector $\mathbf{k}$. This expression can be put into a more explicit form by substitution of the left- and right-incident mode functions given in section (2.2.1). Since we are interested in the energy-shift of an atom located in front of the dielectric slab, at $z > L/2$, we shall only substitute the spatial modes for that region. Thus,

$$\begin{aligned}\Delta E^{\text{trav}} = &-\frac{\hbar}{2(2\pi)^3\epsilon_o}\sum_{j\neq i}\sum_{\lambda,\,\iota}\int \mathrm{d}^3\mathbf{k}\,\frac{\omega}{E_{ji}+\omega}\,|\langle j|\mu_\iota|i\rangle|^2\\ &\times\Big\{\hat{e}^\iota_\lambda(\mathbf{k}^-)\hat{e}^{\iota*}_\lambda(\mathbf{k}^-) + \left(|R|^2+|T|^2\right)\hat{e}^\iota_\lambda(\mathbf{k}^+)\hat{e}^{\iota*}_\lambda(\mathbf{k}^+) +\\ &\hat{e}^\iota_\lambda(\mathbf{k}^+)\hat{e}^{\iota*}_\lambda(\mathbf{k}^-)R_\lambda(k_z,\mathbf{k}_\parallel)\,e^{2\mathrm{i}k_z z_o} + \hat{e}^\iota_\lambda(\mathbf{k}^-)\hat{e}^{\iota*}_\lambda(\mathbf{k}^+)R^*_\lambda(k_z,\mathbf{k}_\parallel)\,e^{-2\mathrm{i}k_z z_o}\Big\}.\end{aligned} \tag{3.20}$$

Note that we have used a notation for the polarisation vectors as given in Eqs. (2.19) and (2.20) for $\hat{\mathbf{e}}_{\text{TE}}(\mathbf{k}^+)$ and $\hat{\mathbf{e}}_{\text{TM}}(\mathbf{k}^+)$, respectively. The notation $\hat{e}_\lambda(\partial_r)$ is no longer useful as we had to apply the vectors into the plane waves first, and then evaluate the result at the position of the atom $\mathbf{r}_o = (0, 0, z_o)$. In Eq. (3.20), $\hat{\mathbf{e}}_\lambda(\mathbf{k}^-)$ is the polarisation vector for a wave moving to the left, and thus, it is obtained by changing $k_z \to -k_z$ in Eqs. (2.19) and (2.20). Moreover, it can be proven that $\hat{e}^\iota_\lambda(\mathbf{k}^-)\hat{e}^{\iota*}_\lambda(\mathbf{k}^-) = \hat{e}^\iota_\lambda(\mathbf{k}^+)\hat{e}^{\iota*}_\lambda(\mathbf{k}^+)$ and $\hat{e}^\iota_\lambda(\mathbf{k}^+)\hat{e}^{\iota*}_\lambda(\mathbf{k}^-) = \hat{e}^\iota_\lambda(\mathbf{k}^-)\hat{e}^{\iota*}_\lambda(\mathbf{k}^+)$. Also, by using the relation (2.33), one can make further simplifications to Eq. (3.20). Finally, the contribution from travelling modes is given by,

$$\begin{aligned}\Delta E^{\text{trav}} = &-\frac{\hbar}{2(2\pi)^3\epsilon_o}\sum_{j\neq i}\sum_{\lambda,\,\iota}\int \mathrm{d}^3\mathbf{k}\,\frac{\omega}{E_{ji}+\omega}\Big\{2\hat{e}^\iota_\lambda(\mathbf{k}^+)\hat{e}^{\iota*}_\lambda(\mathbf{k}^+) +\\ &\hat{e}^\iota_\lambda(\mathbf{k}^+)\hat{e}^{\iota*}_\lambda(\mathbf{k}^-)\left[R_\lambda(k_z,\mathbf{k}_\parallel)\,e^{2\mathrm{i}k_z z_o} + R^*_\lambda(k_z,\mathbf{k}_\parallel)\,e^{-2\mathrm{i}k_z z_o}\right]\Big\}|\langle j|\mu_\iota|i\rangle|^2.\end{aligned} \tag{3.21}$$

3.3.2 Contribution from Trapped Modes

In the same way we can calculate the contribution to the energy-level shift due to the trapped modes. They correspond to the second part of Eq. (3.13). Substituting into Eq. (3.15), we can get the energy-shift

$$\Delta E^{\text{trap}} = -\sum_{\iota}\sum_{j\neq i}\sum_{\lambda}\int \mathrm{d}^2\mathbf{k}_{\parallel}\,\frac{\hbar\omega}{2\epsilon_o}\left\{|\mathbf{f}^{S}_{\nu\iota}(\mathbf{r}_o)|^2+|\mathbf{f}^{A}_{\nu\iota}(\mathbf{r}_o)|^2\right\}\frac{|\langle j|\mu_\iota|i\rangle|^2}{E_{ji}+\omega}, \tag{3.22}$$

which can be written in a more explicit form by substituting the trapped modes to the right of the slab,

$$\Delta E^{\text{trap}} = -\frac{\hbar}{2\epsilon_o}\sum_{j,\,\iota}\sum_{k_z\,\lambda}\int \mathrm{d}^2\mathbf{k}_{\parallel}\,\frac{\omega}{E_{ji}+\omega}\,\hat{e}^{\iota}_{\lambda}(\mathbf{k}^{+})\hat{e}^{\iota *}_{\lambda}(\mathbf{k}^{-})\,|M_\lambda|^2\left|L^{S,A}_{\lambda}\right|^2 e^{-2\kappa z_o}\,|\mu_\iota|^2\,, \tag{3.23}$$

where the definition (3.17) has been used. We have followed the same convention for the polarisation vectors as described below Eq. (3.20). However, we shall bear in mind that in this case the z-component of the wave vector is purely imaginary, and thus we must substitute $k_z = \mathrm{i}\kappa$ into Eqs. (2.19) and (2.20) in order to obtain the polarisation vectors for the waves decaying in the positive z direction. We shall remark that these vectors are no longer unit vectors.

Unlike the travelling modes contribution, Eq. (3.23) contains a sum over the z-component of the wave vector, with a maximum allowed value of k_z given by Eq. (2.40). Since the total shift is obtained by adding the contributions from both travelling and trapped modes, Eqs. (3.21) and (3.23), and they have a completely different nature, we first thought of analysing them separately. However, we will instead use a more ingenious procedure, that was developed in the previous chapter, in which we derived the convenient way to sum a continuous and a discrete set of modes, as required.

In order to calculate the integral in $\mathbf{k}_{\parallel}$ of Eq. (3.23), it is convenient to use polar coordinates; thus, we shall express the integrand in terms of the appropriate variables. First of all, it is useful to sum over the two polarisation directions, writing explicitly all the components $\iota = x, y, z$ of the field. For this, we shall substitute the polarisation

vectors components in terms of k_x, k_y and k_z. We get,

$$\Delta E^{\text{trap}} - \frac{\hbar}{2\epsilon_o}\sum_j \int \mathrm{d}^2\mathbf{k}_\parallel \sum_{k_z} \frac{\omega}{E_{ji}+\omega}\left\{\frac{k_\parallel^2}{k^2}\,|M_{\text{TM}}|^2\left|L_{\text{TM}}^{S,A}\right|^2\,|\mu_z|^2\,e^{-2\kappa z_o}\right.$$
$$+\,|M_{\text{TE}}|^2\left|L_{\text{TE}}^{S,A}\right|^2\left(k_y^2|\mu_x|^2+k_x^2|\mu_y|^2\right)\frac{1}{k_\parallel^2}\,e^{-2\kappa z_o}$$
$$\left.+\,|M_{\text{TM}}|^2\left|L_{\text{TM}}^{S,A}\right|^2\,\left(k_x^2|\mu_x|^2+k_y^2|\mu_y|^2\right)\frac{\kappa^2}{k_\parallel^2 k^2}\,e^{-2\kappa z_o}\right\}. \tag{3.24}$$

The integral in $\mathbf{k}_\parallel$ is transformed by using

$$\int \mathrm{d}^2\mathbf{k}_\parallel \to \int_0^\infty \mathrm{d}k_\parallel\; k_\parallel \int_0^{2\pi}\mathrm{d}\phi, \tag{3.25}$$

where $k_x = k_\parallel\cos\phi$ and $k_y = k_\parallel\sin\phi$. Substituting these into Eq. (3.24) and using Eq. (A.2), it is possible to carry out the integration in the azimuthal angle ϕ. Hence,

$$\Delta E^{\text{trap}} = -\frac{\pi\hbar}{\epsilon_o}\sum_j \int_0^\infty \mathrm{d}k_\parallel \sum_{k_z}\frac{k_\parallel\omega}{E_{ji}+\omega}\left\{\frac{k_\parallel^2}{k^2}\,|M_{TM}|^2\left|L_{TM}^{S,A}\right|^2|\mu_\perp|^2\,e^{-2\kappa z_o}\right.$$
$$\left.+\frac{1}{2}\left(|M_{TE}|^2\left|L_{TE}^{S,A}\right|^2\,e^{-2\kappa z_o}+|M_{TM}|^2\left|L_{TM}^{S,A}\right|^2\frac{\kappa^2}{k^2}\,e^{-2\kappa z_o}\right)|\mu_\parallel|^2\right\}, \tag{3.26}$$

where we have used the definitions (3.18).

3.4 Renormalisation

Before any other attempt on evaluating the expressions for the energy-shift, we shall first remove all contributions due to the interaction of the atom and the electromagnetic field in general (Lamb Shift). We must do this in order to obtain the change in the energy levels of the atom due solely to the presence of the dielectric slab, which is the correction that we are interested in. At the same time, this procedure removes all divergences from the formulas [76]. One way to proceed is by subtracting the contribution for a transparent slab ($n = 1$). An equivalent way to renormalise is by subtracting the extremely far-field limit ($\mathcal{Z} \to \infty$). The only surviving terms at this limit are the $\mathcal{Z}$-independent terms, which are the free-space contributions. We shall

follow the former.

For the travelling modes contribution, it is evident that the reflection coefficients R_λ will vanish at the limit $n = 1$. Thus, the energy-shift due merely to the presence of the dielectric slab is given by

$$\begin{aligned}\delta E^{\rm trav} &\equiv \Delta E^{\rm trav} - \Delta E^{\rm trav}(n=1)\\ &= -\frac{\hbar}{16\pi^3\epsilon_o}\sum_j\sum_\iota\sum_\lambda\int_{k_z>0}\mathrm{d}^3\mathbf{k}\,\frac{\omega}{E_{ji}+\omega}\,\hat{e}^\iota_\lambda(\mathbf{k}^+)\hat{e}^{\iota *}_\lambda(\mathbf{k}^-)\left(R_\lambda e^{2ik_z z_o}+R^*_\lambda e^{-2ik_z z_o}\right)|\mu_\iota|^2\,.\end{aligned} \tag{3.27}$$

For the trapped modes this renormalisation procedure is meaningless, and this is simply because they only exist when the dielectric slab is present, so there is nothing to subtract. Thus

$$\delta E^{\rm trap} = \Delta E^{\rm trap}. \tag{3.28}$$

The total shift is then given by $\delta E = \delta E^{\rm trav} + \delta E^{\rm trap}$.

The following is simply more algebraic manipulation for Eq. (3.27), in order to obtain an expression analogous to (3.26). Firstly, by summing over the two polarisations and writing the polarisation vectors in terms of k_z and $k_\parallel$ we get,

$$\begin{aligned}\delta E^{\rm trav} = -\frac{\hbar}{16\pi^3\epsilon_o}\sum_j\int_0^\infty\mathrm{d}^2\mathbf{k}_\parallel\int_0^\infty\mathrm{d}k_z\,\frac{\omega}{E_{ji}+\omega}\,\Big\{\\ \left(R_{TE}(k_z,\mathbf{k}_\parallel)\,e^{2\mathrm{i}k_z z_o}+R^*_{TE}(k_z,\mathbf{k}_\parallel)\,e^{-2\mathrm{i}k_z z_o}\right)\left(k_y^2|\mu_x|^2+k_x^2|\mu_y|^2\right)\frac{1}{k_\parallel^2}\\ -\left(R_{TM}(k_z,\mathbf{k}_\parallel)\,e^{2\mathrm{i}k_z z_o}+R^*_{TM}(k_z,\mathbf{k}_\parallel)\,e^{-2\mathrm{i}k_z z_o}\right)\left(k_x^2|\mu_x|^2+k_y^2|\mu_y|^2\right)\frac{k_z^2}{k_\parallel^2 k^2}\\ +\left(R_{TM}(k_z,\mathbf{k}_\parallel)\,e^{2\mathrm{i}k_z z_o}+R^*_{TM}(k_z,\mathbf{k}_\parallel)\,e^{-2\mathrm{i}k_z z_o}\right)\frac{k_\parallel^2}{k^2}|\mu_z|^2\,\Big\}.\end{aligned} \tag{3.29}$$

Note that we have split up the three-dimensional integral in $\mathbf{k}$ into its parallel and perpendicular components, $\mathbf{k}_\parallel$ and k_z, This has the purpose of obtaining a common factor with the contribution from the trapped modes, i.e. the integral in $\mathbf{k}_\parallel$. Thereafter, one can utilise the transformation (2.116) to add the integral and the sum in k_z. As the

reflection coefficients R_λ do not depend on the azimuthal angle, we can easily perform the integral in ϕ. In that way, we are able to regroup the x and y components of μ. Finally the energy-shift reads,

$$\delta E^{\text{trav}} = -\frac{\hbar}{8\pi^2\epsilon_o}\sum_j \int_0^\infty \mathrm{d}k_\parallel\, k_\parallel \int_0^\infty \mathrm{d}k_z\, \frac{\omega}{E_{ji}+\omega}\left\{|\mu_\perp|^2 R_{TM}(k_z,\mathbf{k}_\parallel)\frac{k_\parallel^2}{k^2}\, e^{2\mathrm{i}k_z z_o}\right.$$
$$\left. +\frac{1}{2}|\mu_\parallel|^2\left(R_{TE}(k_z,\mathbf{k}_\parallel)\, e^{2\mathrm{i}k_z z_o} - R_{TM}(k_z,\mathbf{k}_\parallel)\frac{k_z^2}{k^2}\, e^{2\mathrm{i}k_z z_o}\right) + \text{C.C.}\right\}, \qquad (3.30)$$

where C.C. corresponds to the complex conjugate of the function within curly brackets.

3.5 Adding travelling and trapped modes

So far we have managed to obtain expressions for the energy-level shift, calculating separately the contributions from travelling and trapped modes (Eqs. (3.30) and (3.26), respectively). As it can be seen, they have in common the integral in $k_\parallel$, so we can write a single expression for the shift by factorizing the integral in $k_\parallel$, followed by $\int \mathrm{d}k_z \ldots + \sum_{k_z} \ldots$, in such a way that it looks similar to Eq. (2.102)

$$\delta E = -\frac{\pi\hbar}{\epsilon_o}\sum_{j\neq i}\int_0^\infty \mathrm{d}k_\parallel\, k_\parallel \left\{|\mu_\perp|^2\right.$$
$$\times\left(\int_{-\infty}^\infty \mathrm{d}k_z\, \frac{\omega}{E_{ji}+\omega}\,\frac{R_{TM}}{(2\pi)^3}\frac{k_\parallel^2}{k^2}\, e^{2\mathrm{i}k_z z_o} + \sum_{k_z}\frac{\omega}{E_{ji}+\omega}\,\frac{k_\parallel^2}{k^2}\,|M_{TM}|^2\left|L_{TM}^{S,A}\right|^2\, e^{-2\kappa z_o}\right)$$
$$+\frac{1}{2}|\mu_\parallel|^2\left\{\frac{1}{(2\pi)^3}\int_{-\infty}^\infty \mathrm{d}k_z\,\frac{\omega}{E_{ji}+\omega}\left(R_{TE}\, e^{2\mathrm{i}k_z z_o} - R_{TM}\frac{k_z^2}{k^2}\, e^{2\mathrm{i}k_z z_o}\right) + \right.$$
$$\left.\left.\sum_{k_z}\frac{\omega}{E_{ji}+\omega}\left(|M_{TE}|^2\left|L_{TE}^{S,A}\right|^2\, e^{-2\kappa z_o} + |M_{TM}|^2\left|L_{TM}^{S,A}\right|^2\frac{\kappa^2}{k^2}\, e^{-2\kappa z_o}\right)\right\}\right\}. \qquad (3.31)$$

Note that the limits of integration in k_z in Eq. (3.30) are from 0 to $k_z = \infty$. However, as $R_\lambda(k_z) = R_\lambda^*(-k_z)$, we have conveniently changed these limits to calculate the integral from $k_z = -\infty$ to ∞ instead.

We shall bear in mind that in Eq. (2.102) for the proof of the completeness (see page 58), the sum of the terms inside the round brackets turned out to be zero, and

therefore we could draw the conclusion shown in Eq. (2.116). This means that it is possible to transform the sum over trapped modes in Eq. (3.31), into a contour integral in the complex plane, as shown in Fig 2.11 on page 64. Then, by adding the integration in k_z that corresponds to the travelling modes, we obtain the path $\mathcal{C}$ that we described previously (Fig. 2.11). Thus, the energy-shift (3.31) can be written in a very much simplified form and reads,

$$\delta E = -\frac{\hbar}{2\pi^2\epsilon_o}\sum_{j\neq i}\sum_{\sigma=\parallel,\perp} E_{ji}^3 S_\sigma \left|\langle j|\boldsymbol{\mu}_\sigma|i\rangle\right|^2, \tag{3.32}$$

with parallel $S_\parallel$ and perpendicular contributions $S_\perp$ given by

$$S_\parallel \equiv \frac{1}{8E_{ji}^3}\int_0^\infty \mathrm{d}k_\parallel\; k_\parallel I_\parallel \qquad \text{and} \qquad S_\perp \equiv \frac{1}{4E_{ji}^3}\int_0^\infty \mathrm{d}k_\parallel\; k_\parallel I_\perp, \tag{3.33}$$

where the integrals in k_z are included in the following functions

$$I_\parallel = \int_{\mathcal{C}} \mathrm{d}k_z \frac{\omega}{E_{ji}+\omega}\; R_{TE}(k_z,\mathbf{k}_\parallel)\; e^{2\mathrm{i}k_z z_o} - \int_{\mathcal{C}} \mathrm{d}k_z \frac{\omega}{E_{ji}+\omega}\;\frac{k_z^2}{k^2}\; R_{TM}(k_z,\mathbf{k}_\parallel)\; e^{2\mathrm{i}k_z z_o} \tag{3.34}$$

$$I_\perp = \int_{\mathcal{C}} \mathrm{d}k_z \frac{\omega}{E_{ji}+\omega}\;\frac{k_\parallel^2}{k^2}\; R_{TM}(k_z,\mathbf{k}_\parallel)\; e^{2\mathrm{i}k_z z_o}. \tag{3.35}$$

A similar procedure was followed by Robaschik and Eberlein [118] in the calculation of the Wightman functions for a field quantised in the presence of a dielectric half-space. They included the contribution from evanescent waves in two different ways: first as a separate integral in k and then as part of an integration path in the complex plane, which is similar to ours. The solutions to those integrals however follow a different method.

In a completely different way, Eberlein and Wu [75] managed to join into one single integral the contribution from travelling and evanescent modes for the same system. They showed that this way to express the energy-level shift is particularly helpful only in the retarded regime. Fortunately, that will not be the case for our system, and we will be able to analyse the shift in both the retarded and the non-retarded regime from

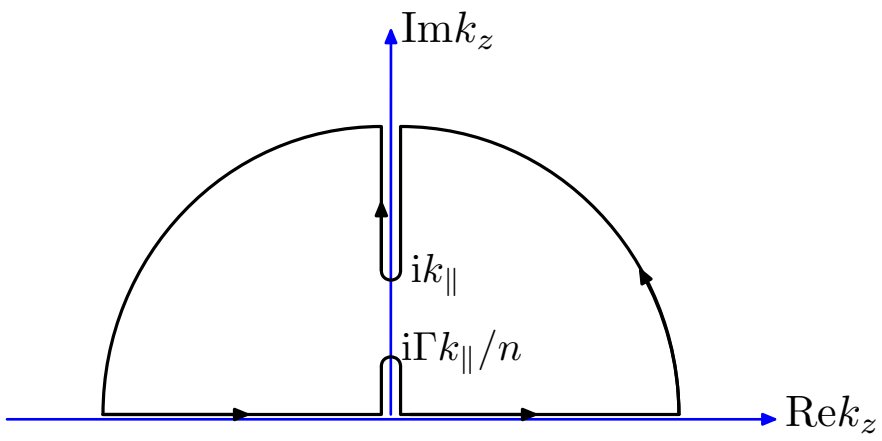

Figure 3.3: Closing the contour allows us to choose a more suitable integration path. In the figure, $\Gamma = \sqrt{n^2-1}$

Eq. (3.32).

In the following we will explain in detail how to deal with the integration path $\mathcal{C}$, that is used to calculate the integrals $I_\parallel$ and $I_\perp$. Let us start with the first integral in Eq. (3.34). Note that Eqs. (3.34) and (3.35) are in terms of the position z_o of the atom, measured from the centre of the slab. Nevertheless, it would be more useful to express our equations in terms of the variable $\mathcal{Z}$, which is the surface-atom distance. We shall thus define

$$\tilde{R}_\lambda = r_\lambda \frac{1 - e^{2ik_{zd}L}}{1 - r_\lambda^2 e^{2ik_{zd}L}}, \tag{3.36}$$

in such a way that we are now interested in the calculation of

$$\int_{\mathcal{C}} \mathrm{d}k_z \frac{\omega}{E_{ji} + \omega}\, \tilde{R}_{TE}\, e^{2ik_z \mathcal{Z}}, \tag{3.37}$$

where $\mathcal{Z} = z_o - L/2$. As it can be seen in Eq. (3.32), apart from the integral in k_z, we shall also perform an integration in $k_\parallel$. Therefore, we shall rewrite Eq. (3.37) in terms of these two variables. Since the frequency is given by $\omega = \sqrt{k_\parallel^2 + k_z^2}$, one can identify a branch point in the integrand at $k_z = \pm ik_\parallel$. We choose to place the cuts from $k_z = ik_\parallel$ to $i\infty$ and from $k_z = -ik_\parallel$ to $-i\infty$. Since the integral is convergent in the upper half-plane (due to the rapidly decaying exponential in the limit $k_z \to \infty$),

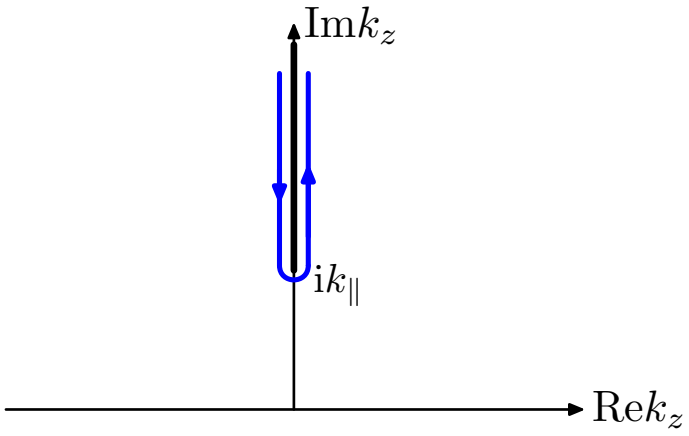

Figure 3.4: Final contour.

we close the contour as shown in Fig 3.3.

This will give us a more convenient path to calculate the integral in k_z. The region enclosed in Fig. 3.3 does not contain singularities and hence, from Cauchy theorem[3], we know that the integral along the closed contour must be zero. Since the integral vanishes along the big semicircle, the integration along the original path $\mathcal{C}$ is equivalent to integrating along the path that goes round the cut, as shown in Fig 3.4.

In order to calculate the integral (3.37) along such a path, it is necessary to treat separately the contour that goes down to the left of the cut and the one that goes up from i$k_\parallel$ to i∞ around the right of the cut. Due to earlier definitions for k_z (Eq. (2.28)), the choice of branch is taken in such a way that, on the real axis for $k_z > 0$ we have $\omega > 0$, and then, going along that branch to $k_z < 0$, we get $\omega > 0$. The integration

[3] A review in this subject can be found in Chapter 4 of Ref. [119].

around the branch cut can be decomposed as

$$\int_{\mathcal{C}} \mathrm{d}k_z \frac{\sqrt{k_\parallel^2+k_z^2}}{E_{ji}+\sqrt{k_\parallel^2+k_z^2}}\,\tilde{R}_{TE}\,e^{2\mathrm{i}k_z\mathcal{Z}} \tag{3.38}$$

$$= \int_{\mathrm{i}k_\parallel}^{\mathrm{i}\infty} \mathrm{d}k_z \frac{\sqrt{k_\parallel^2+k_z^2}}{E_{ji}+\sqrt{k_\parallel^2+k_z^2}}\,\tilde{R}_{TE}\,e^{2\mathrm{i}k_z\mathcal{Z}} - \int_{\mathrm{i}\infty}^{\mathrm{i}k_\parallel} \mathrm{d}k_z \frac{\sqrt{k_\parallel^2+k_z^2}}{E_{ji}-\sqrt{k_\parallel^2+k_z^2}}\,\tilde{R}_{TE}\,e^{2\mathrm{i}k_z\mathcal{Z}} \tag{3.39}$$

$$= 2E_{ji}\int_{\mathrm{i}k_\parallel}^{\mathrm{i}\infty} \mathrm{d}k_z \frac{\sqrt{k_\parallel^2+k_z^2}}{E_{ji}^2-(k_\parallel^2+k_z^2)}\,\tilde{R}_{TE}\,e^{2\mathrm{i}k_z\mathcal{Z}}. \tag{3.40}$$

The final integral can be solved by performing a $\pi/2$ rotation in the complex plane, such that $k_z = \mathrm{i}q$

$$= -2E_{ji}\int_{k_\parallel}^{\infty} \mathrm{d}q \frac{\sqrt{q^2-k_\parallel^2}}{E_{ji}^2-k_\parallel^2+q^2}\,\tilde{R}_{TE}\,e^{-2q\mathcal{Z}}. \tag{3.41}$$

Note that we have chosen the branch of the frequency $\omega = \sqrt{k_\parallel^2+k_z^2} = +\mathrm{i}\sqrt{q^2-k_\parallel^2}$ in such a way that it satisfies the conditions given above. In order to get an expression which is easier to deal with, we have decided to make a second change of variable. Defining $u^2 = q^2 - k_\parallel^2$ and calculating the corresponding Jacobian to get $\mathrm{d}q = \frac{u}{\sqrt{u^2+k_\parallel^2}}\,\mathrm{d}u$, one can write Eq. (3.37) as

$$= -2E_{ji}\int_0^{\infty} \mathrm{d}u \frac{1}{\sqrt{u^2+k_\parallel^2}}\frac{u^2}{E_{ji}^2+u^2}\,\tilde{R}_{TE}\,e^{-2\mathcal{Z}\sqrt{u^2+k_\parallel^2}}. \tag{3.42}$$

With the purpose of making our work easier to compare with previous results, we have followed the notation used in [75]. Thus, the definition of the parameter

$$\xi = 2\mathcal{Z}E_{ji} \tag{3.43}$$

is required. This parameter is the time that a photon takes in travelling to the dielectric surface and back, times the inverse of the frequency of an atomic transition. It will characterize the retardation of the system, as we will explain in detail in section 3.6. For now, we are only concerned about obtaining an expression that is mathematically

the simplest. Therefore, we shall scale our variables with the transition energy E_{ji}, defining the *normalised* variables thus

$$s \equiv \frac{u}{E_{ji}} \qquad \text{and} \qquad v \equiv \frac{k_\parallel}{E_{ji}} \tag{3.44}$$

to get finally that Eq. (3.37) reads

$$= -2E_{ji} \int_0^\infty \mathrm{d}s \, \frac{1}{\sqrt{s^2+v^2}} \, \frac{s^2}{1+s^2} \, \tilde{R}_{TE} \, e^{-\xi\sqrt{s^2+v^2}}, \tag{3.45}$$

and the reflection coefficients can be obtained in terms of s and v by substituting the wave vector z-components $k_z = \mathrm{i}E_{ji}\sqrt{s^2+v^2}$ and $k_{\mathrm{zd}} = \mathrm{i}E_{ji}\sqrt{n^2s^2+v^2}$, thus

$$\tilde{R}_{TE} = \frac{-(n^2-1)s^2}{(n^2+1)s^2 + 2v^2 + 2\sqrt{(s^2+v^2)(n^2s^2+v^2)}\coth(LE_{ji}\sqrt{n^2s^2+v^2})} \tag{3.46}$$

$$\tilde{R}_{TM} = \frac{(n^2-1)\left[n^2s^2+(n^2+1)v^2\right]}{(n^2+1)n^2s^2 + (n^4+1)v^2 + 2n^2\sqrt{(s^2+v^2)(n^2s^2+v^2)}\coth(LE_{ji}\sqrt{n^2s^2+v^2})}. \tag{3.47}$$

In order to write $S_\parallel$, we shall follow the same procedure for the second integral in Eq. (3.34). We finally obtain,

$$S_\parallel = \frac{1}{4}\int_0^\infty \mathrm{d}v \int_0^\infty \mathrm{d}s \, \frac{v}{\sqrt{s^2+v^2}} \frac{1}{1+s^2} \left[(s^2+v^2)\tilde{R}_{TM} - s^2\tilde{R}_{TE}\right] \, e^{-\xi\sqrt{s^2+v^2}}. \tag{3.48}$$

The same procedure works for the perpendicular contribution of the shift. After making the same change of variables we obtain,

$$S_\perp = \frac{1}{4E_{ji}^3}\int_0^\infty \mathrm{d}k_\parallel \, k_\parallel \int_{\mathcal{C}} \mathrm{d}k_z \frac{\sqrt{k_\parallel^2+k_z^2}}{E_{ji}+\sqrt{k_\parallel^2+k_z^2}} \, \frac{k_\parallel^2}{k_z^2+k_\parallel^2} \tilde{R}_{TM} \, e^{2\mathrm{i}k_z\mathcal{Z}} \tag{3.49}$$

$$= \frac{1}{2}\int_0^\infty \mathrm{d}v \int_0^\infty \mathrm{d}s \, \frac{v^3}{\sqrt{s^2+v^2}} \, \frac{1}{1+s^2} \, \tilde{R}_{TM} \, e^{-\xi\sqrt{s^2+v^2}}. \tag{3.50}$$

It is surprising to realise that these expressions have exactly the same form as those given in Eberlein and Wu's paper for the dielectric half-space problem (Eqs. (2.22) and

(2.23) in Ref. [75]); the only difference lies on the reflection coefficients $\tilde{R}_\lambda$, Eqs. (3.46) and Eqs. (3.47), which replace the Fresnel coefficients r_λ^F that arise in the case of one single interface.

As $\lim_{x\to\infty} \coth x = 1$, in the limit $L \to \infty$ one can recover the Fresnel reflection coefficients for a single interface. Hence, it can be seen straightforwardly how we recover the expressions that allowed Eberlein and Wu [75] to calculate the energy-shift of an atom in front of a dielectric half-space.

Since we want to obtain expressions that easily recover results for the half-space as given in [75], it might also be useful to convert the matrix elements of the dipole-moment operator of Eq. (3.32) into those of the momentum operator. We can perform this transformation by considering first the identity

$$[z, H_o] = \frac{1}{2m}[z, p_z^2] = \frac{1}{2m}\left([z, p_z]p_z + p_z[z, p_z]\right) = \frac{\mathrm{i}\hbar}{m}p_z, \tag{3.51}$$

where H_o is the Hamiltonian (3.7). Hence,

$$\langle j|p_z|i\rangle = \frac{m}{\mathrm{i}\hbar}\langle j|[z, H_o]|i\rangle = -\frac{\mathrm{i}m}{e\hbar}\langle j|[\mu_z, H_o]|i\rangle\,, \tag{3.52}$$

where we have used the electric dipole moment operator $\boldsymbol{\mu} \equiv e\mathbf{r}$, previously defined. Then, applying H_o into the atomic states we get

$$\langle j|p_z|i\rangle = -\frac{\mathrm{i}m}{e\hbar}\left(\langle j|\mu_z H_o|i\rangle - \langle j|H_o\mu_z|i\rangle\right) = \frac{\mathrm{i}m}{e\hbar}E_{ji}\langle j|\mu_z|i\rangle\,. \tag{3.53}$$

The same procedure is valid for the other components of $\boldsymbol{\mu}$ and thus we can generalise the expression above as

$$|\langle j|\boldsymbol{\mu}_\sigma|i\rangle|^2 = \frac{4\pi\alpha}{m^2E_{ji}^2}|\langle j|\mathbf{p}_\sigma|i\rangle|^2\,, \tag{3.54}$$

in terms of the fine structure constant $\alpha = e^2/4\pi$. In this way, the energy-shift is thus

given by

$$\delta E = -\frac{2\alpha}{\pi m^2} \sum_{j \neq i} \sum_{\sigma=\parallel,\perp} E_{ji} S_\sigma |p_\sigma|^2, \tag{3.55}$$

with $S_\parallel$ and $S_\perp$ as given in Eqs. (3.48) and (3.50), and the reflection coefficients by Eqs. (3.46) and (3.47).

3.6 Asymptotics

We have obtained so far a general expression that describes the energy-shift of an atom in front of a dielectric slab. The nature of the interaction of the atom with the slab depends on the separation between them, and this is because the electromagnetic interaction can be retarded or non-retarded.

We have explained that if the atom is very close to the surface, the interaction is much faster than the internal evolution of the atom, and we can assume that it occurs instantaneously. In this case the interaction is non-retarded and thus it will be dominated by electrostatics, i.e. the Coulomb force between the atomic dipole and its image charges on the other side of the surface. On the other hand, if the atom is placed further away from the surface, the retardation plays an important role and we must take it into account [2, 15]. The reason is that the state of the atom evolves appreciably during the time-scale of the interaction.

In order to analyse our system, it is necessary to define a measurement for the retardation. Hence, we shall first identify the characteristic time-scales. We can compare the time a photon takes to travel from the atom to the interface and back $t_{\rm ph} = 2\mathcal{Z}$ with the time-scale of the atomic evolution $t_{\rm at}$. The latter will be defined by the inverse of the average level spacing, $1/\langle |E_{ji}| \rangle$, weighted by the strength of the transition. Therefore the ratio $t_{\rm ph}/t_{\rm at} = 2\mathcal{Z}E_{ji}$ gives a suitable criterion for characterizing these regimes. Note that this is exactly the dimensionless variable ξ defined earlier, in Eq. (3.43).

In summary, the retarded regime will be characterised by a very large ξ and the non-retarded regime by a very small ξ. In order to understand the behaviour of the

atom near a slab, it is essential to study these two regimes. Hence, we shall concentrate on the asymptotic analysis of the integrals in Eq. (3.32) in the large or small-ξ limit.

3.6.1 Retarded regime

In the non-retarded regime, the interaction between the atom and the dielectric slab is purely Coulombic, and a simple electrostatic treatment will suffice to obtain it. Therefore, we shall start by studying the retarded regime $\xi \gg 1$, which clearly will come up with more interesting results. The fact that we have combined both travelling and trapped modes into one single expression facilitates the asymptotic analysis of δE, as concluded in Ref. [75]. Also, we do not have to deal with the divergences that would come up the alternative way[4]. As we are taking into account the finite width of the dielectric, we shall need to consider the thickness L of the slab into the asymptotic analysis, as a third characteristic length scale of the system.

We note that it is possible to distinguish three asymptotic limits, depending on the relative size of L in comparison with the other relevant length scales of the system: $2\mathcal{Z}$ and E_{ji}. Thus, it seems more natural to re-define L as $\tilde{L} = LE_{ji}$, so we can just compare $\tilde{L}$ with ξ and unity. The three asymptotic cases are:

$$\text{Thin slab:} \quad \xi \gg 1 \gg \tilde{L} \quad \text{or} \quad 2\mathcal{Z} \gg \bar{\lambda}_{ji} \gg L \tag{3.56}$$

$$\text{Thick slab:} \quad \xi \gg \tilde{L} \gg 1 \quad \text{or} \quad 2\mathcal{Z} \gg L \gg \bar{\lambda}_{ji} \tag{3.57}$$

$$\text{Half-space:} \quad \tilde{L} \gg \xi \gg 1 \quad \text{or} \quad L \gg 2\mathcal{Z} \gg \bar{\lambda}_{ji} \tag{3.58}$$

Note that we have introduced another measurable quantity, which is the wavelength of an atomic transition

$$\bar{\lambda}_{ji} = \frac{\lambda_{ji}}{2\pi} = \frac{\hbar c}{E_{ji}}. \tag{3.59}$$

In this section we shall obtain the energy-level shift of an atom in front of a thin or thick slab, using the limits (3.56) and (3.57), respectively. In chapter 4 — as an important proof of the validity of our results — we will recover important known limits,

[4]Note that such divergences disappear by combining all of the contributions [76].

such as the dielectric half-space (by using the asymptotic limit (3.58)) and the perfect conductor case.

Finite slab

We are particularly interested in the correction due to a finite thickness of the dielectric, not only due to the application that it would have in recent experiments, but also from the theoretical point of view. We intend to show that some papers about the interaction of a charge with a thin plasma sheet, by Michael Bordag [120, 121], are using inappropriate arguments and giving a misleading result for the interaction of a charge with a thin plasma sheet. In [121], Bordag claimed that different boundary conditions must be applied to a thin and a thick conductor while quantising the electromagnetic field. His reason is, apparently, the fact that the boundary conditions $\mathcal{E}_{\parallel} = 0 = B_{\perp}$ allow for a freedom in the normal component of the electric field on the surface of the conductor. For a *thick* conductor this is fulfilled by applying Gauss'law. Nevertheless, for a *thin* conductor (whose surface is assumed to be mathematically thin, i.e., purely two dimensional) no additional condition on $\mathcal{E}_{\perp}$ is assumed. What Bordag states, is that for thin conductors there is an interaction of classical charges across the surface which is absent for thick conductors. This would of course have measurable consequences. Thus, in order to show them, he calculates the interaction of the electromagnetic field with a thin plasma sheet, which represents the pi-electrons of a carbon nanotube or a C_{60} molecule. He finds that the Casimir-Polder force for a thin conductor is about 13% smaller than for a thick one, and he believes that the result agreess with the experiments. However, that difference could correspond to the 13% of uncertainty in those experiments [39]. A disagreement with these arguments has been shown by Gabriel Barton, who comes up with a different conclusion for the Casimir-Polder force acting between an atom and a flat plasma sheet [122, 123].

Even though we have defined two different cases in order to consider the width of the slab: an extremely thin sheet (3.56) and thick slab (3.57), it is not possible to distinguish mathematically between them at the beginning of the calculation. We could

thus expect that as it corresponds to a second-order correction. Therefore, we shall study both cases in one go, without any initial distinction, and try to find the limit afterwards.

In order to calculate the energy-shift, it is convenient to transform the expressions (3.48) and (3.50) into polar coordinates $s = r\cos\phi$ and $v = r\sin\phi$. Then, we shall perform a second change of variable by defining $t = \cos\phi$. Finally, the parallel contribution to the energy-shift can be written as

$$S_{\parallel} = \frac{1}{4}\int_0^{\infty} \mathrm{d}r \int_0^1 \mathrm{d}t \, \frac{r^3}{r^2t^2+1}\left(\tilde{R}_{TM} - t^2\tilde{R}_{TE}\right) e^{-\xi r}, \tag{3.60}$$

with reflection coefficients given by

$$\tilde{R}_{TE} = \frac{-(n^2-1)t^2}{2+(n^2-1)t^2+2\sqrt{1+(n^2-1)t^2}\coth(\tilde{L}r\sqrt{1+(n^2-1)t^2})}, \tag{3.61}$$

$$\tilde{R}_{TM} = \frac{n^4-1-(n^2-1)t^2}{n^4+1+(n^2-1)t^2+2n^2\sqrt{1+(n^2-1)t^2}\coth(\tilde{L}r\sqrt{1+(n^2-1)t^2})}. \tag{3.62}$$

Another convenient way of writing Eq. (3.60) is in terms of the physical variables $\mathcal{Z}$ and L. Thus, by introducing the variable $y = rE_{ji}$ and performing a second change of variable $t \to \tau = \sqrt{1+(n^2-1)t^2}$ with $\mathrm{d}t = \mathrm{d}\tau\ \tau/(\sqrt{\tau^2-1}\sqrt{n^2-1})$, the integrand reads

$$S_{\parallel} = \frac{1}{4E_{ji}^2\sqrt{n^2-1}}\int_0^{\infty}\mathrm{d}y\int_1^n \mathrm{d}\tau\, \frac{y^3}{(n^2-1)E_{ji}^2+y^2(\tau^2-1)}\frac{\tau}{\sqrt{\tau^2-1}} \times\left(\frac{(n^2-1)(n^4-\tau^2)}{n^4+\tau^2+2n^2\tau\coth(Ly\tau)}+\frac{(\tau^2-1)^2}{\tau^2+1+2\tau\coth(Ly\tau)}\right)e^{-2\mathcal{Z}y}. \tag{3.63}$$

In this way, we can see more clearly that for $2\mathcal{Z} \gg L$ the term $e^{-2\mathcal{Z}y}$ damps the integral long before $\coth(Ly\tau)$ varies appreciably. Therefore, we can approximate the reflection coefficients for the small argument for coth, by using [124]

$$\coth(z) \simeq \frac{1}{z}+\frac{z}{3}-\frac{z^3}{45}+... \tag{3.64}$$

The integrand can thus be approximated as

$$\begin{aligned} S_{\parallel} &= \frac{1}{4}(n^2-1)\int_0^\infty \mathrm{d}r \int_0^1 \mathrm{d}t\, \frac{r^3}{r^2t^2+1} \\ &\times \left(\frac{n^2+1-t^2}{n^4+1+(n^2-1)t^2+2n^2/\tilde{L}r} + \frac{t^4}{2+(n^2-1)t^2+2/\tilde{L}r} \right) e^{-\xi r}. \end{aligned} \tag{3.65}$$

This expression is again in terms of the original variables, as τ would make the integral more complicated. The previous equation was helpful to decide how to proceed with the analysis of the integral, and it will be useful in order to study other limits. Fortunately, the integral in t in Eq. (3.65) turns out to be elementary, and it is possible to solve it analytically. However, the result is not a simple expression and so, in order to perform the integral in r we shall consider the fact that we are analysing the limit $\xi \to \infty$. Thus, $e^{-\xi r}$ will strongly suppress the integrand, and the only significant contributions to the integral will come from small r. Note that this limit in Eqs. (3.61) and (3.62) would also lead to $\coth z \simeq 1/z$, provided $\tilde{L}$ is not infinite. Therefore, we can expand the remaining integrand around $r = 0$

$$S_{\parallel} \approx \frac{\tilde{L}}{4n^2}(n^2-1)(5+9n^2)\int_0^\infty \mathrm{d}r\, r^4 e^{-\xi r}, \tag{3.66}$$

and solve the simple integral in r that we get from such a series expansion, to obtain the parallel part of the shift in terms of L and $\mathcal{Z}$

$$S_{\parallel} \approx \frac{(n^2-1)(5+9n^2)}{80n^2E_{ji}^4}\frac{L}{\mathcal{Z}^5}. \tag{3.67}$$

The same procedure works for the perpendicular part, which in polar coordinates can be written as

$$S_{\perp} = \frac{1}{2}\int_0^\infty \mathrm{d}r \int_0^1 \mathrm{d}t\, \frac{r^3(1-t^2)}{r^2t^2+1}\, \tilde{R}_{TM}\, e^{-\xi r}. \tag{3.68}$$

Analogous to the parallel contribution, it can be expressed in terms of the variables $\mathcal{Z}$ and L, and we can apply the same arguments as used above for $S_{\parallel}$ in the limit $\mathcal{Z} \gg L$.

The integrand can thus be approximated to

$$S_\perp \approx \frac{1}{2}(n^2-1)\int_0^\infty \mathrm{d}r \int_0^1 \mathrm{d}t\, \frac{r^3}{r^2t^2+1}\, \frac{(1-t^2)(n^2+1-t^2)}{n^4+1+(n^2-1)t^2+2n^2/\tilde{L}r}\, e^{-\xi r}, \quad (3.69)$$

where the integration in t can be carried out analytically. As before, we shall perform a series expansion around $r=0$ and then calculate the integral in r. We get that the perpendicular part of the shift is given by

$$S_\perp \approx \frac{\tilde{L}}{15n^2}(n^2-1)(4+5n^2)\int_0^\infty \mathrm{d}r\, r^4 e^{-\xi r} = \frac{(n^2-1)(4+5n^2)}{40n^2E_{ji}^4}\frac{L}{\mathcal{Z}^5}. \quad (3.70)$$

We have obtained the coefficients $S_\parallel$ and $S_\perp$, and in order to draw the final conclusion, we shall plug them into the expression for the energy-level shift (3.55). The interaction reads

$$\delta E = -\frac{(n^2-1)\alpha L}{40\pi m^2 n^2 \mathcal{Z}^5}\sum_{j\neq i}\frac{(5+9n^2)|p_\parallel|^2+2(4+5n^2)|p_\perp|^2}{E_{ji}^3}. \quad (3.71)$$

What is interesting to note is that if one calculates analytically the integral in t in Eqs. (3.65) and (3.69) (exactly as we did), and then expand for $r\to 0$ and $L\to 0$, regardless which limit we consider first, we would obtain the same result for the energy-shift (3.71). This proves that the result for the retarded Casimir-Polder force is the same regardless how thick the slab is, provided $2\mathcal{Z}\gg L$.

3.6.2 Non-retarded regime

The non-retarded Casimir-Polder interaction arises when the atom is very close, in comparison with a wavelength of an atomic transition, to the surface of the object under consideration. For instance, for two neutral molecules located very close to each other, the interaction is purely due to the Coulomb force between the fluctuating electric dipole moments. As first shown by London and Eisenschitz [12, 125], it gives an energy proportional to $1/R^6$, where R is the distance between them. This interaction energy was given in Eq. (1.1), on page 4.

In order to calculate the non-retarded interaction between an atom and a dielectric slab, we can analyse asymptotically the general formula (Eq. (3.55)), as we did for the retarded regime. Unfortunately, the calculation is not straightforward since expressions (3.48) and (3.50) contained in Eq. (3.55) make difficult an asymptotic analysis for the parameter ξ, as it followed quite directly in the retarded regime. Actually, the same problem was encountered in the half-space calculation [75], when the same route was intended to be taken. As it was pointed out in Ref. [75], no matter how they rescaled their corresponding integral, it was not possible to take the limit $\xi \to 0$ because that would lead to divergences. Since our expression for the shift has the same form, it is obvious that the same argument applies and hence Eqs. (3.48) and (3.50) will be not useful in the specific way that they are written.

Motivated by what was suggested in Ref. [75], we should consider the expression of the energy-shift before it is transformed into one single expression. In [75], that meant taking travelling and trapped modes contributions separately, for which the asymptotic analysis for small ξ was very simple. In our case, it would not be convenient to go that far back, because the treatment of discrete trapped modes would make the calculation far more complicated. What we actually want in order to avoid those divergences, is an integrand with a higher order in the integration variable. It can be seen that expression (3.39) is a good candidate to get what we need (note that in the following step the denominator changes due to the addition of the two integrals). Mathematically, what we would be doing is simply integrating over the path in Fig. 2.11 on page 64, but separately over the branch that goes from $\mathrm{i}k_{\parallel}$ to $\mathrm{i}\infty$ (along right to the cut) and then over the remaining branch, performing the same change of variables that we have done so far. This will automatically lead us to an asymptotic analysis for ξ small.

Alternatively, one can start from the final expressions, where $S_{\parallel}$ and $S_{\perp}$ are given by Eqs. (3.60) and (3.68), respectively (but rescaling r with E_{ji}). Thus, we would only need to use complex-variables to rewrite the denominator as follows,

$$-\frac{2E_{ji}\mathrm{i}}{y^2t^2+E_{ji}^2}=\frac{1}{yt+\mathrm{i}E_{ji}}-\frac{1}{yt-\mathrm{i}E_{ji}}. \tag{3.72}$$

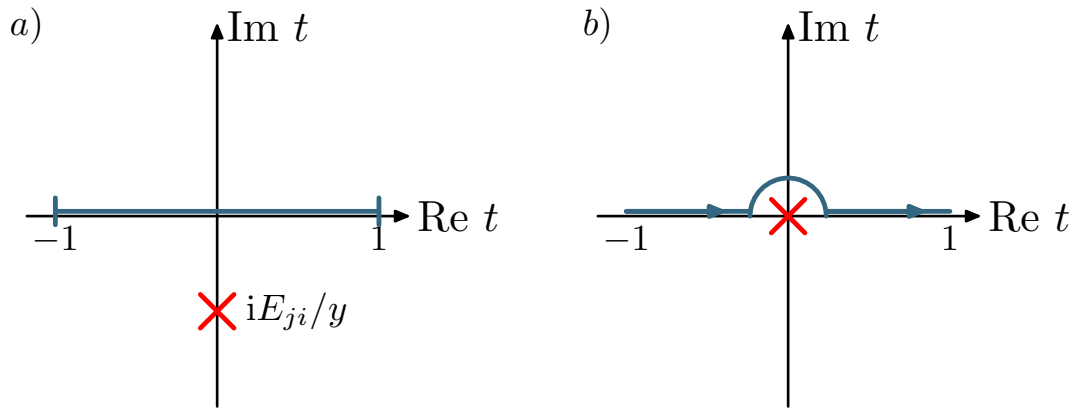

Figure 3.5: The part a) of this illustration shows the pole in the t integration. In the non-retarded regime $E_{ji} \to 0$ one can shift the pole to the origin an work with the path shown in b). The contribution along the negative real axis cancels out with the positive side.

Therefore, the perpendicular contribution of the shift becomes

$$S_\perp = \frac{\mathrm{i}}{4E_{ji}^3} \int_0^\infty \mathrm{d}y\, y^3 \int_0^1 \mathrm{d}t\, (1-t^2) \left(\frac{1}{yt + \mathrm{i}E_{ji}} - \frac{1}{yt - \mathrm{i}E_{ji}} \right) \tilde{R}_{TM} e^{-2\mathcal{Z}y}. \tag{3.73}$$

For a further simplification of this integral, one can note that the reflection coefficients (Eqs. (3.61) and (3.62)) do not depend linearly on t but on t^2, which suggests to us to perform the change of variable $t \to -t$ in the second term. In that way, we add both terms inside the round brackets by changing the integration limits,

$$S_\perp = \frac{\mathrm{i}}{4E_{ji}^3} \int_0^\infty \mathrm{d}y\, y^2 \int_{-1}^1 \mathrm{d}t\, \frac{1-t^2}{t + \mathrm{i}E_{ji}/y}\, \tilde{R}_{TM}\, e^{-2\mathcal{Z}y}. \tag{3.74}$$

It seems convenient to begin with the integral in t. We can identify one pole at $t = -\mathrm{i}E_{ji}/y$. The integration path is shown in Fig. 3.5. Since we are interested in the non-retarded regime, which is given by the limit $E_{ji} \to 0$, we can simplify the integration by shifting the pole to the origin of the complex plane. Thus, in order to perform the integral in t that goes from -1 to 1 on the real axis, we shall deform the contour going round the pole, as it is shown in Fig. 3.5. Therefore we can easily calculate the integral by calculating the residue at that pole. We shall be careful about the direction of the integration path and the sign conventions. Since it only goes half a circle, the integral

would be $-\mathrm{i}\pi$ times the residue around the origin, which is

$$\begin{aligned} S_\perp &= \frac{\pi}{4E_{ji}^3}\int_0^\infty \mathrm{d}y\, y^2\, \mathrm{Res}[\tilde{R}_{TM}]\, e^{-2\mathcal{Z}y} \\ &= \frac{\pi}{4E_{ji}^3}\,\frac{n^2-1}{n^2+1}\int_0^\infty \mathrm{d}y\, \frac{(n^2+1)^2y^2}{n^4+1+2n^2\coth(yL)}\, e^{-2\mathcal{Z}y}. \end{aligned} \tag{3.75}$$

We proceed by rewriting the hyperbolic cotangent in the integrand in terms of exponential functions, to get a more useful expression that can be interpreted in terms of the reflection coefficient for a single interface r defined previously. The perpendicular contribution of the shift reads

$$S_\perp = \frac{\pi}{4E_{ji}^3}\,\frac{n^2-1}{n^2+1}\int_0^\infty \mathrm{d}y\, y^2\, \frac{1-e^{-2yL}}{1-\left(\frac{n^2-1}{n^2+1}\right)^2 e^{-2yL}}\, e^{-2\mathcal{Z}y}. \tag{3.76}$$

It can be seen straightforwardly that the same procedure works for $S_\parallel$, given in Eq. (3.60). Using the transformation given in Eq. (3.72), and then joining both terms into a single integral we get

$$S_\parallel = \frac{\mathrm{i}}{8E_{ji}^3}\int_0^\infty \mathrm{d}y\, y^2 \int_{-1}^1 \mathrm{d}t\, \frac{(\tilde{R}_{TM}-t^2\tilde{R}_{TE})}{t+\mathrm{i}E_{ji}/y}\, e^{-2\mathcal{Z}y} \tag{3.77}$$

in which the integral in t can be solved using the integration path shown in Fig. 3.5 and rearranged in a similar way as before. Thus,

$$S_\parallel = \frac{\pi}{8E_{ji}^3}\,\frac{n^2-1}{n^2+1}\int_0^\infty \mathrm{d}y\, y^2\, \frac{1-e^{-2yL}}{1-\left(\frac{n^2-1}{n^2+1}\right)^2 e^{-2yL}}\, e^{-2\mathcal{Z}y}. \tag{3.78}$$

To recover the electrostatic shift, we substitute plug the expressions for $S_\perp$ and $S_\parallel$ that we just obtained into our general equation for the energy-shift (3.55). One finally gets

$$\delta E_{\mathrm{es}} = -\frac{\alpha}{m^2}\,\frac{n^2-1}{n^2+1}\int_0^\infty \mathrm{d}y\, y^2\, \frac{1-e^{-2yL}}{1-\left(\frac{n^2-1}{n^2+1}\right)^2 e^{-2yL}}\, e^{-2\mathcal{Z}y} \sum_j \frac{2|p_\perp|^2+|p_\parallel|^2}{E_{ji}^2}. \tag{3.79}$$

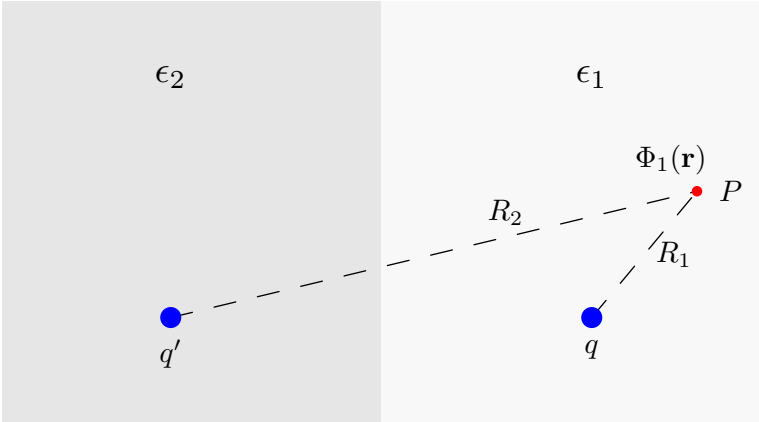

Figure 3.6: The diagram shows the three regions of the system. The atom is located in region III, at a distance $\mathcal{Z}$ from the interface.

Electrostatic calculation

We have mentioned in chapter 1, that the non-retarded Casimir-Polder force between an atom and a plate is given by the Coulombic interaction between the electric dipole and its image on the other side of the interface, in reference to the well-known image method from electrostatics. As the method works fine for very simple systems, it has been used to calculate the non-retarded Casimir-Polder force on an atom in front of a perfect conductor [108] and near a dielectric [14].

The method of images [11] is concerned with the problem of one or more point charges in the presence of boundary surfaces, and consists of replacing such boundaries by charges of the appropriate magnitude that can simulate the required boundary conditions. This is sometimes possible to infer from the geometry of the problem. One can illustrate in a few steps the image method for dielectrics if we consider a point charge q embedded in a semi-infinite medium of dielectric permittivity ϵ_1, located in front of a second medium with dielectric permittivity ϵ_2, as shown is Fig.3.6. From classical electrodynamics, we know that the system must satisfy the Poisson equation

$$\boldsymbol{\nabla}^2\Phi = -\frac{\rho}{\epsilon} \tag{3.80}$$

and the boundary conditions (2.24) at the interface. In this equation, ρ is the charge

density distribution and ϵ is the permittivity of the medium. Then, by solving Eq. (3.80), one can obtain the electric potential Φ in each medium. We can use the image method to obtain the potential Φ_1 in the medium 1, as we can intuit that, in order to replace the interface, there should be an image charge $q\prime$ inside the medium 2, in a symmetric position. Thus, the potential at any point P within the first region is given by

$$\Phi_1(\mathbf{r}) = \frac{1}{4\pi\epsilon_1}\left(\frac{q}{R_1} + \frac{q'}{R_2}\right), \tag{3.81}$$

where R_1 and R_2 are the distances from q and $q\prime$, respectively, to the point P. One could also obtain the potential at any point inside the dielectric medium 2. Since we do not have any charges, we shall solve Laplace equation $\boldsymbol{\nabla}^2\Phi = 0$. We obtain that the electric potential $\Phi_2(\mathbf{r})$ in region 2 is equivalent to the potential produced by a charge $q\prime\prime$ at the same position of q. Thus,

$$\Phi_2(\mathbf{r}) = \frac{1}{4\pi\epsilon_2}\frac{q\prime\prime}{R_1}. \tag{3.82}$$

Finally, in order to get the value of the images charges, we shall apply the continuity conditions (2.24),

$$q\prime = -\left(\frac{\epsilon_2 - \epsilon_1}{\epsilon_2 + \epsilon_1}\right) q \qquad \text{and} \qquad q\prime\prime = \frac{2\epsilon_2}{\epsilon_2 + \epsilon_1} q. \tag{3.83}$$

For our system it is not possible to use the method of images. In principle, it would just turn out more complicated to guess where the images should be located, as we have to consider the two dielectric-vacuum interfaces (two mirrors) and hence, we have to take into account the images of the image charges. However, the difficulty arises when we seem to require images on the side where the atom is located. This is because the method does not allow images in the region for which one is calculating the potential.

We are interested in an electrostatic calculation for the interaction between an atom and a dielectric slab. The result will serve as a good check for the validity of our general formula for the energy-shift, which lead us to the non-retarded interaction (3.79).

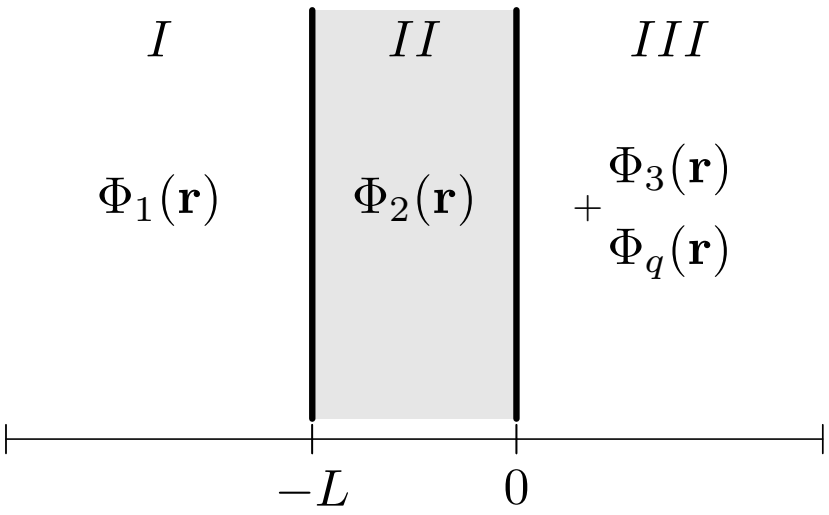

Figure 3.7: The diagram shows the three regions of the system. The atom is located in region III, at a distance $\mathcal{Z}$ from the interface.

Thus, by solving the Laplace equation in each region (vacuum-dielectric-vacuum) and imposing the corresponding boundary conditions (2.24), we shall obtain the electric potential in region III, as shown in Fig. 3.7. Note that in this diagram we have shifted the reference system used before; though we have kept the same notation so that the atom is placed at a distance $\mathcal{Z}$ from the slab of thickness L. Having the interfaces at $z = 0$ and $z = -L$ will be slightly more convenient at the moment of applying the boundary conditions.

We need to find the harmonic functions Φ_1, Φ_2 and Φ_3, which are the electric potential in regions I (vacuum), II (dielectric slab), and III (vacuum), respectively, as shown in Fig. 3.7. They are solutions to the three-dimensional Laplace equation, which in Cartesian coordinates reads

$$\frac{\partial^2\Phi}{\partial^2 x^2} + \frac{\partial^2\Phi}{\partial^2 y^2} + \frac{\partial^2\Phi}{\partial^2 z^2} = 0. \tag{3.84}$$

A detailed explanation on how to deal with this differential equation can be found in Ref. [119]. It can be conveniently solved by the method called *separation of variables*[5], which consists on solving this partial differential equation in terms of three ordinary

[5]See for instance Chapter 5.1 in [119].

differential equations, because the potential Φ can be expressed by a product of three independent functions, one for each coordinate: $\Phi(x,y,z) = X(x)Y(y)Z(z)$. After substitution of this into Eq. (3.84) one can split up the equation into

$$\frac{1}{X}\frac{\mathrm{d}^2X}{\mathrm{d}x^2} = -k_x^2, \qquad \frac{1}{Y}\frac{\mathrm{d}^2Y}{\mathrm{d}y^2} = -k_y^2 \qquad \text{and} \qquad \frac{1}{Z}\frac{\mathrm{d}^2Z}{\mathrm{d}z^2} = k^2, \tag{3.85}$$

with $k^2 = k_x^2 + k_y^2$. These simple equations have well known solutions, and hence it comes straightforward to conclude that the electric potential can thus be built up from the product solutions

$$\Phi(x,y,z) = e^{\mathrm{i}k_x x} e^{\mathrm{i}k_y y} e^{\pm kz}. \tag{3.86}$$

At this stage, the variables k_x and k_y are completely arbitrary and hence Φ, given above, represents a complete system of solutions of Laplace equation. In order to obtain a unique solution, we shall apply the continuity conditions (2.24) and also require that the solutions vanish at infinity. Thus, we can write more specifically for each region the electric potential as follows

$$\Phi_1(x,y,z) = \int_{-\infty}^{\infty}\mathrm{d}k_x \int_{-\infty}^{\infty}\mathrm{d}k_y\, f_1(k_x,k_y) e^{\mathrm{i}k_x x + \mathrm{i}k_y y + kz}, \tag{3.87}$$

$$\Phi_2(x,y,z) = \int_{-\infty}^{\infty}\mathrm{d}k_x \int_{-\infty}^{\infty}\mathrm{d}k_y \left[a_2(k_x,k_y) e^{\mathrm{i}k_x x + \mathrm{i}k_y y + kz} + b_2(k_x,k_y) e^{\mathrm{i}k_x x + \mathrm{i}k_y y - kz}\right], \tag{3.88}$$

$$\Phi_3(x,y,z) = \int_{-\infty}^{\infty}\mathrm{d}k_x \int_{-\infty}^{\infty}\mathrm{d}k_y\, c_3(k_x,k_y) e^{\mathrm{i}k_x x + \mathrm{i}k_y y - kz}. \tag{3.89}$$

which have the form of Fourier integrals (see page 453 in Ref. [119]). The sign for k is chosen so that $\Phi_1(z \to -\infty)$ and $\Phi_3(z \to \infty)$ are well behaved. In order to obtain the electric potential in region III, we shall add to $\Phi_3(x,y,z)$ the Coulombic potential generated by the point charge at $(0,0,\mathcal{Z})$

$$\Phi_q = \frac{1}{4\pi\epsilon_o}\frac{q}{\sqrt{x^2+y^2+(z-\mathcal{Z})^2}}. \tag{3.90}$$

The coefficients f_1, a_2, b_2 and c_3 can be calculated by applying the continuity condition

for the potential at the interface $z = 0$,

$$\Phi_2(x, y, 0) = \Phi_3(x, y, 0) + \frac{1}{4\pi\epsilon_o} \frac{q}{\sqrt{x^2 + y^2 + \mathcal{Z}^2}}. \tag{3.91}$$

One can thus substitute Eqs. (3.88) and (3.89) to get

$$\int_{-\infty}^{\infty} \mathrm{d}k_x \int_{-\infty}^{\infty} \mathrm{d}k_y (c_3 - a_2 - b_2) e^{\mathrm{i}k_x x + \mathrm{i}k_y y} = -\frac{1}{4\pi\epsilon_o} \frac{q}{\sqrt{x^2 + y^2 + \mathcal{Z}^2}}. \tag{3.92}$$

Note that the left hand-side term represents the inverse Fourier transform of those coefficients and hence we could apply the Fourier integral in order to obtain them

$$c_3 - a_2 - b_2 = -\frac{q}{4\pi\epsilon_o} \frac{1}{(2\pi)^2} \int_{-\infty}^{\infty} \mathrm{d}x \int_{-\infty}^{\infty} \mathrm{d}y \frac{e^{-\mathrm{i}k_x x - \mathrm{i}k_y y}}{\sqrt{x^2 + y^2 + \mathcal{Z}^2}}. \tag{3.93}$$

Applying to the same boundary the continuity condition of the normal dielectric displacement we have

$$\epsilon \frac{\partial \Phi_2}{\partial z}(x, y, 0) = \frac{\partial \Phi_3}{\partial z}(x, y, 0) + \frac{q}{4\pi\epsilon_o} \frac{\mathcal{Z}}{(x^2 + y^2 + \mathcal{Z}^2)^{3/2}}, \tag{3.94}$$

and again, by substitution of Eqs. (3.88) and (3.89) for the potentials Φ_2 and Φ_3, and using the Fourier integral as we did before we get

$$k(c_3 + \epsilon a_2 - \epsilon b_2) = \frac{q}{4\pi\epsilon_o} \frac{\mathcal{Z}}{(2\pi)^2} \int_{-\infty}^{\infty} \mathrm{d}x \int_{-\infty}^{\infty} \mathrm{d}y \frac{e^{-\mathrm{i}k_x x - \mathrm{i}k_y y}}{(x^2 + y^2 + \mathcal{Z}^2)^{3/2}}. \tag{3.95}$$

It is obvious that these two equations are not enough to obtain the four constants. Therefore we must utilise the same continuity conditions through the other interface, at $z = -L$, in order to get two more equations. The continuity condition for the electric potential at such an interface reads

$$\Phi_1(x, y, -L) = \Phi_2(x, y, -L) \tag{3.96}$$

$$f_1 e^{-kL} = a_2 e^{-kL} + b_2 e^{kL}. \tag{3.97}$$

Using the continuity of the normal dielectric displacement at $z = -L$ we obtain

$$\frac{\partial \Phi_1}{\partial z}(x, y, -L) = \epsilon \frac{\partial \Phi_2}{\partial z}(x, y, -L) \tag{3.98}$$

$$k f_1 e^{-kL} = \epsilon k \left(a_2 e^{-kL} - b_2 e^{kL} \right). \tag{3.99}$$

Finally, in order to obtain the coefficients, we shall use Eqs. (3.93), (3.95), 3.97) and (3.99). Let us start with the equations that came from the boundary at $z = -L$. Multiplying Eq. (3.97) by k_z and then subtracting the result from Eq. (3.99), we derive the coefficient b_2

$$b_2 = \frac{\epsilon - 1}{\epsilon + 1}\, a_2\, e^{-2kL}. \tag{3.100}$$

One can thus substitute it into Eq. (3.93) in order to obtain a_2, which will still appear in terms of c_3

$$a_2 = \frac{1}{1 + \frac{\epsilon-1}{\epsilon+1} e^{-2kL}} \left(c_3 + \frac{q}{16\pi^3 \epsilon_o} \int \mathrm{d}^2\rho \frac{e^{-\mathrm{i}\mathbf{k}\cdot\rho}}{\sqrt{\rho^2 + \mathcal{Z}^2}} \right). \tag{3.101}$$

Similarly to $\mathbf{k}$, we have introduced the two-dimensional spatial variable $\rho^2 = x^2 + y^2$ in order to simplify our notation. And finally, to obtain explicitly the coefficient c_3 we shall utilise Eq. (3.95), which came up from the continuity condition at $z = 0$. Using Eqs. (3.100) and (3.101) for the coefficients b_2 and a_2, we get

$$c_3 = \frac{q}{16\pi^3 \epsilon_o} \frac{1}{1 + \epsilon \frac{1 - \frac{\epsilon-1}{\epsilon+1}\, e^{-2kL}}{1 + \frac{\epsilon-1}{\epsilon+1}\, e^{-2kL}}} \left(\frac{\mathcal{Z}}{k_z} \int \mathrm{d}^2\rho \frac{e^{-\mathrm{i}\mathbf{k}\cdot\rho}}{(\rho^2 + \mathcal{Z}^2)^{3/2}} - \epsilon \frac{1 - \frac{\epsilon-1}{\epsilon+1}\, e^{-2kL}}{1 + \frac{\epsilon-1}{\epsilon+1}\, e^{-2kL}} \int \mathrm{d}^2\rho \frac{e^{-\mathrm{i}\mathbf{k}\cdot\rho}}{\sqrt{\rho^2 + \mathcal{Z}^2}} \right) \tag{3.102}$$

Since we are looking particularly for the electric potential in region III, this is the only coefficient that we need to calculate. Apart from some simple algebra simplification, we still have to solve the double integral in ρ. In order to do so, it is quite convenient

to transform into polar coordinates,

$$\begin{aligned}\int \mathrm{d}^2\rho \frac{e^{-\mathrm{i}\mathbf{k}\cdot\rho}}{\sqrt{\rho^2+\mathcal{Z}^2}} &= \int_0^\infty \mathrm{d}\rho \frac{\rho}{\sqrt{\rho^2+\mathcal{Z}^2}} \int_0^{2\pi} \mathrm{d}\phi\, e^{-\mathrm{i}k\rho\cos\phi} \\ &= 2\pi \int_0^\infty \mathrm{d}\rho\, \rho \frac{J_o(k\rho)}{\sqrt{\rho^2+\mathcal{Z}^2}} = \frac{2\pi}{k} e^{-k\mathcal{Z}}, \end{aligned} \tag{3.103}$$

where we have first calculated the integral in ϕ in terms of Bessel functions and then used the tabulated integral (C.1) in order to obtain the remaining integral.

For the other integral in Eq. (3.102) it is convenient to rewrite the integrand in the form of a derivative in $\mathcal{Z}$, in such a way we only need to know the integral calculated above, as it is shown

$$\int \mathrm{d}^2\rho\, e^{-\mathrm{i}\mathbf{k}\cdot\rho} \frac{\mathcal{Z}}{(\rho^2+\mathcal{Z}^2)^{3/2}} = -\frac{\partial}{\partial\mathcal{Z}} \int \mathrm{d}^2\rho\, \frac{e^{-\mathrm{i}\mathbf{k}\cdot\rho}}{\sqrt{\rho^2+\mathcal{Z}^2}} = 2\pi e^{-k\mathcal{Z}}. \tag{3.104}$$

The final expression for the coefficient c_3 can be obtained after substitution of these results,

$$c_3 = \frac{q}{8\pi^2\epsilon_o k} \left(\frac{1-\epsilon}{1+\epsilon}\right) \frac{1-e^{-2kL}}{1-\left(\frac{\epsilon-1}{\epsilon+1}\right)^2 e^{-2kL}}\, e^{-k\mathcal{Z}}, \tag{3.105}$$

which must be plugged into the expression for the electric potential Φ_3, felt in region III (Eq. (3.89)),

$$\Phi_3(x,y,z) = \frac{q}{8\pi^2\epsilon_o} \left(\frac{1-\epsilon}{1+\epsilon}\right) \int_{-\infty}^\infty \mathrm{d}k_x \int_{-\infty}^\infty \mathrm{d}k_y \frac{(1-e^{-2kL})\, e^{-k(z+\mathcal{Z})}}{1-\left(\frac{\epsilon-1}{\epsilon+1}\right)^2 e^{-2kL}} \frac{e^{\mathrm{i}k_x x+\mathrm{i}k_y y}}{k} \tag{3.106}$$

We can transform it into polar coordinates, and solve the integral in ϕ first to obtain

$$\begin{aligned}\Phi_3(x,y,z) &= -\frac{q}{8\pi^2\epsilon_o}\frac{\epsilon-1}{\epsilon+1} \int_0^\infty \mathrm{d}k\, \frac{1-e^{-2kL}}{1-(\frac{\epsilon-1}{\epsilon+1})^2 e^{-2kL}}\, e^{-k(z+\mathcal{Z})} \int_0^{2\pi} \mathrm{d}\phi\, e^{-\mathrm{i}k\rho\cos\phi} \\ &= -\frac{q}{4\pi\epsilon_o}\frac{\epsilon-1}{\epsilon+1} \int_0^\infty \mathrm{d}k\, J_o(k\rho)\, \frac{1-e^{-2kL}}{1-(\frac{\epsilon-1}{\epsilon+1})^2 e^{-2kL}}\, e^{-k(z+\mathcal{Z})}. \end{aligned} \tag{3.107}$$

As a verification of our result, we shall try to recover well-known results. In this case, we know what the potential is for an atom in front of a dielectric half-space (as

in the example given above, taking $\epsilon_2 = 1$). Then, if we take the limit $L \to \infty$, all the exponentials vanish and the only term that remains in the integrand can be calculated exactly,

$$\int_0^\infty \mathrm{d}k\; J_o(k\rho)\; e^{-kz'} = \frac{1}{\sqrt{\rho^2 + z'^2}}. \tag{3.108}$$

Therefore, if we substitute this result into Eq. (3.107), it is clear that it corresponds to the potential due to one image charge of dimension $q(\epsilon - 1)/(\epsilon + 1)$ located at $z = -\mathcal{Z}$, as we expected.

Now, it could be convenient to rewrite Eq. (3.107) in terms of a sum, as we can identify in the integrand the geometric series (Eq. 0.112 in [126]), and thus re-express the term in the integrand as

$$\frac{1}{1 - (\frac{\epsilon-1}{\epsilon+1})^2 e^{-2kL}} = \sum_{n=0}^{\infty} \left[\left(\frac{\epsilon - 1}{\epsilon + 1} \right)^2 e^{-2kL} \right]^n. \tag{3.109}$$

In this way, it could refer to the potential produced by individual charges. The electric potential in region III reads,

$$\Phi_3(x, y, z) = -\frac{q}{4\pi\epsilon_o} \frac{\epsilon - 1}{\epsilon + 1} \int_0^\infty \mathrm{d}k\; J_o(k\rho) e^{-k(z+\mathcal{Z})} \sum_{n=0}^{\infty} \left(\frac{\epsilon - 1}{\epsilon + 1} \right)^{2n} \left(e^{-2nkL} - e^{-2(n+1)kL} \right). \tag{3.110}$$

A more convenient way to write this potential can be obtained after playing around with the first term in the sum (m=0) and rearranging it (e.g. shifting the summation index to $n + 1$ in the first sum). The potential is hence given by

$$\begin{aligned} \Phi_3(x, y, z) = -\frac{q}{4\pi\epsilon_o} \frac{\epsilon - 1}{\epsilon + 1} \int_0^\infty \mathrm{d}k\; J_o(k\rho) e^{-k(z+\mathcal{Z})} \\ \times \left\{ 1 - \frac{4\epsilon}{(\epsilon + 1)^2} \sum_{n=0}^{\infty} \left(\frac{\epsilon - 1}{\epsilon + 1} \right)^{2n} e^{-2(n+1)kL} \right\}. \end{aligned} \tag{3.111}$$

The first term in the brackets refers to the image due to the first interface that the charge sees. The first term of the sum ($n = 0$) gives us the image due to the reflection in the second interface, as we guessed. The rest of the *images* are located consecutively

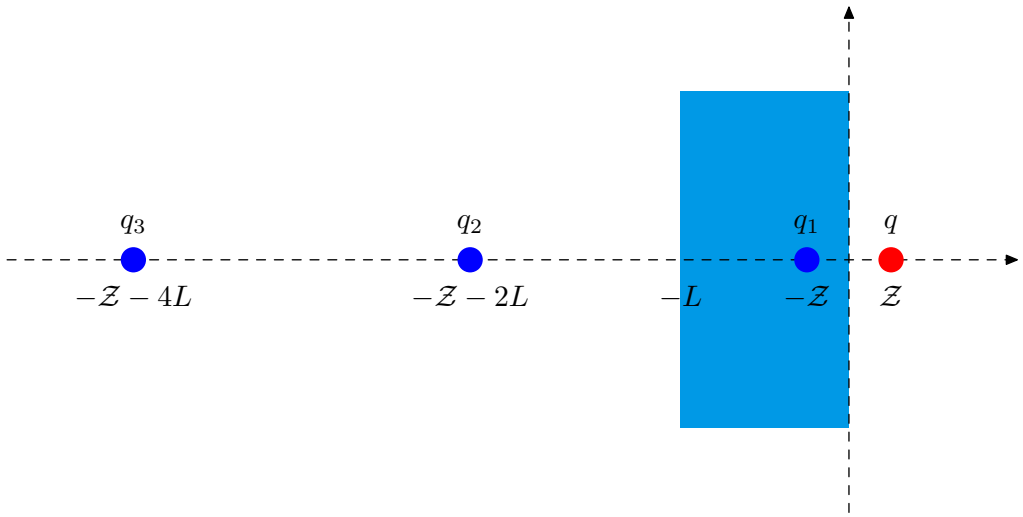

Figure 3.8: Illustrative diagram of some of the image charges produced by a charge q placed at a distance $\mathcal{Z}$ from a dielectric slab of thickness L. Those images that are not drawn are located consecutively at a distance $2L$ farer away from the latest image found.

every $2L$ after the latest image encountered and their magnitudes are given by

$$\begin{aligned} q_1 &= -\frac{\epsilon-1}{\epsilon+1}q \qquad \text{at} \qquad -\mathcal{Z}, \\ q_2 &= \frac{4\epsilon(\epsilon-1)}{(\epsilon+1)^3}q \qquad \text{at} \qquad -(\mathcal{Z}+2L), \\ q_3 &= \frac{4\epsilon(\epsilon-1)^3}{(\epsilon+1)^5}q \qquad \text{at} \qquad -(\mathcal{Z}+4L) \end{aligned}$$

and so on, as it is shown if Fig. 3.8. The charge q_1 corresponds to the first reflection at $z=0$ and q_2 corresponds to the first reflection at $z=-L$. The location of q_2, q_3 and further *images*, can be interpreted as the multiple reflections inside the slab. For q_2 there would be just one reflection at $z=-L$; for q_3 there would be an additional reflection at $z=0$ and then again at $z=-L$; and so on.

So far, as it is shown in Eq. (3.107), we have calculated the electrostatic potential due to the images generated by a charge sitting in front of a dielectric slab, at a distance $\mathcal{Z}$ from its surface. As it was explained at the beginning of this section, these image charges have the same effect as the boundary conditions due to the presence of the slab, and that is why we can replace them for the electrostatic calculation. However,

we are not directly interested in the potential, but in the electrostatic shift of the atomic dipole. It can be derived from the electric potential,

$$\Delta E_{\rm es} = \frac{1}{2}(\mu\cdot\nabla)(\mu\cdot\nabla_o)\Phi_3(\mathbf{r},\mathbf{r}_o)\Big|_{\mathbf{r}\,=\,\mathbf{r}_o} \tag{3.112}$$

$$= \frac{1}{2}\left(|\mu_x|^2\frac{\partial}{\partial x}\frac{\partial}{\partial x_o}+|\mu_y|^2\frac{\partial}{\partial y}\frac{\partial}{\partial y_o}+|\mu_z|^2\frac{\partial}{\partial z}\frac{\partial}{\partial z_o}\right)\Phi_3(\mathbf{r},\mathbf{r}_o)\Big|_{\mathbf{r}\,=\,\mathbf{r}_o} \tag{3.113}$$

where the terms $\mu_\alpha\mu_\beta$ are zero for $\alpha\neq\beta$. Thus, by using the expression for Φ_3 (Eq. (3.107)), one can simply calculate the derivatives in each coordinate. For a charge located at the position $\mathbf{r}=(x_o,y_o,z_o)$, the electric potential will be described by the same Eq. (3.107), but taking $\rho=\sqrt{(x-x_o)^2+(y-y_o)^2}$. Therefore, for the derivative in z one gets

$$\frac{\partial}{\partial z}\frac{\partial\Phi_3}{\partial z_o}\Big|_{\mathbf{r}\,=\,\mathbf{r}_o} = -\frac{q}{4\pi\epsilon_o}\,\frac{\epsilon-1}{\epsilon+1}\int_0^\infty \mathrm{d}k\;k^2\;\frac{1-e^{-2kL}}{1-\left(\frac{\epsilon-1}{\epsilon+1}\right)^2 e^{-2kL}}\;e^{-2\mathcal{Z}k}. \tag{3.114}$$

The derivatives of Φ_3 in x and y turn out to be slightly more complicated, and this is because one has to consider the derivative of the Bessel function, which depends on the two-dimensional coordinate ρ. We have explained the procedure in Appendix C.1, Eqs. (C1)-(C7). Hence, for the derivative in x of the potential we obtain

$$\frac{\partial}{\partial x}\frac{\partial\Phi_3}{\partial x_o}\Big|_{\mathbf{r}\,=\,\mathbf{r}_o} = -\frac{q}{4\pi\epsilon_o}\,\frac{\epsilon-1}{\epsilon+1}\int_0^\infty \mathrm{d}k\;\frac{k^2}{2}\;\frac{1-e^{-2kL}}{1-\left(\frac{\epsilon-1}{\epsilon+1}\right)^2 e^{-2kL}}\;e^{-2\mathcal{Z}k} \tag{3.115}$$

and the same procedure will apply for the derivative in y, obtaining consequently exactly the same result. Therefore, the energy-shift can be written as

$$\Delta E_{\rm es} = -\frac{1}{4\pi\epsilon_o}\,\frac{\epsilon-1}{\epsilon+1}\left(|\mu_z|^2 Q_\perp+\left(|\mu_x|^2+|\mu_y|^2\right)Q_\parallel\right) \tag{3.116}$$

with the functions $Q_\perp$ and $Q_\parallel$ given by the following integrals

$$Q_\perp = \frac{1}{2}\int_0^\infty \mathrm{d}k\, k^2\, \frac{1-e^{-2kL}}{1-\left(\frac{\epsilon-1}{\epsilon+1}\right)^2 e^{-2kL}}\, e^{-2\mathcal{Z}k} \tag{3.117}$$

$$Q_\parallel = \frac{1}{4}\int_0^\infty \mathrm{d}k\, k^2\, \frac{1-e^{-2kL}}{1-\left(\frac{\epsilon-1}{\epsilon+1}\right)^2 e^{-2kL}}\, e^{-2\mathcal{Z}k}. \tag{3.118}$$

It is also convenient to use the identity given in Eq. (3.54) to write the electrostatic contribution in terms of the momentum operator

$$\Delta E_{\mathrm{es}} = -\frac{\alpha}{m^2}\,\frac{\epsilon-1}{\epsilon+1}\sum_j \frac{|p_\perp|^2 Q_\perp + |p_\parallel|^2 Q_\parallel}{E_{ji}^2}, \tag{3.119}$$

in agreement with Eq. (3.79), obtained from our general formula for the energy-shift. The electrostatic shift can be calculated analytically in the limit $L/\mathcal{Z} \to 0$, which can be interpreted as the case of a very thin slab. In order to obtain it, we shall first re-scale $Q_\perp$ as follows

$$Q_\perp = \frac{1}{16\mathcal{Z}^3}\int_0^\infty \mathrm{d}x\, x^2\, e^{-x}\, \frac{1-e^{-xL/\mathcal{Z}}}{1-\left(\frac{n^2-1}{n^2+1}\right)^2 e^{-xL/\mathcal{Z}}}, \tag{3.120}$$

and then simply approximate the exponentials for small arguments. The resulting integral is trivial and gives us

$$Q_\perp(L/\mathcal{Z}\to 0) = \frac{L}{16\mathcal{Z}^4}\int_0^\infty \mathrm{d}x\, \frac{x^3\, e^{-x}}{1-\left(\frac{n^2-1}{n^2+1}\right)^2} = \frac{3L}{32\mathcal{Z}^4}\frac{(n^2+1)^2}{n^2}. \tag{3.121}$$

Thus, substituting into Eq. (3.119), we finally get the electrostatic interaction of an atom in front of a thin dielectric slab

$$\Delta E_{\mathrm{es}} = -\frac{3\alpha(n^4-1)}{16m^2n^2}\,\frac{L}{\mathcal{Z}^4}\sum_j \frac{2|p_\perp|^2 + |p_\parallel|^2}{E_{ji}^2} \tag{3.122}$$

We can note that an analogous result was obtained for the retarded regime: the position of the atom dependence changes from $1/\mathcal{Z}^3$ for a dielectric half space to $L/\mathcal{Z}^4$ for a very thin slab.

Chapter 4

Analysis of results

We have obtained the energy-level shift produced in an atom as a consequence of the presence of a dielectric slab. In order to calculate the shift, we applied second order perturbation theory to the interaction hamiltonian $\mu \cdot \mathbf{E}$. Thus, for a quantum mechanical treatment, the quantisation of the electromagnetic field — in the presence of such a slab— was required and achieved in chapter 2. This procedure allowed us to expand the electric field in terms of normal modes, which were classified into travelling and trapped modes. From the second order in perturbation theory calculation, a sum over intermediate photon states arises and, which was problematic because we had to figure out first the most convenient method to perform such a summation. The reason is that we obtain a sum over discrete trapped modes and an integral over the continuous set of travelling modes, and there is not an *a priori* way to know how to add them together. We derived a good method in section 2.4, and it could be applied quite straightforwardly to the calculation of the energy shift. Moreover, by utilising complex-variable techniques, we succeeded in obtaining a general formula for the atom-slab interaction, as a function of the distance $\mathcal{Z}$ between the atom and the slab, the thickness L and the refractive index n of the slab. The expression for the energy shift is given in Eq. (3.55), with parallel and perpendicular contributions, $S_{\parallel}$ and $S_{\perp}$, given by Eqs. (3.48) and (3.50), respectively.

We have pointed out that two regions are physically interesting: the *retarded* and

the *non-retarded* regime. Therefore we proceeded with an asymptotic analysis of such integrals: The former was characterised by the limit $\xi \to \infty$, and the electrostatic interaction was obtained by considering ξ very small. In both cases we assumed $L \ll \mathcal{Z}$. Hence, we obtained simple formulae, which in principle should be easily applied to particular cases. Thus, if one knows the value of the variables involved, one can simply get a numerical result.

The formulas obtained so far have been summarised in a table, in section 5.1. In the retarded regime the shift is given by Eq. (3.71), for $L \ll \mathcal{Z}$, regardless of how thin the slab is (contrary to conclusions drawn in [120]). This is because the calculation includes the limit $L \to 0$. From this result and the one obtained for the non-retarded regime (Eq. (3.122)), one can conclude that the Casimir-Polder force decays even faster than the one predicted for a half-space, by a factor of $L/\mathcal{Z}$. Thus it should be considered, particularly in recent experiments, where the thickness of the first layer on the top of the substrate utilised for Casimir-Polder measurements[1] has a size that is comparable or much smaller than $\mathcal{Z}$, and can not simply be ignored in theoretical calculations.

Note that we have separated the calculation of the energy shift into retarded and non-retarded regimes in order to obtain more explicit formulae. However, we can take more advantage of Eq. (3.55) and see how the shift varies at any atom-surface separation. We shall calculate numerically (for a fixed thickness L) the integrals contained in the expression for the shift and plot for any separation distance Z. We shall emphasize that the numerical calculations that would be required to obtain the energy-shift for a specific case, can be solved very easily by using standard packages like *Mathematica* or *Maple*.

Then, one could simply plot the energy shift as a function of the atomi-surface separation, however, in order to see more evidently the correction that we have obtained, the convenient method is factorise out a well known result: the force between an atom and a perfect reflector. In such a way, it becomes evident how the correction varies from the non-retarded to the retarded regime. A comparison with the interaction with

[1] See table in section 1.1, of the latest experiments.

a dielectric half-space will be useful as well. We know what the results are for these two cases, so that they would provide us with a verification of the validity of our calculation. We shall derive such limiting cases directly from Eqs. (3.48) and (3.50). By taking the limit $L \to \infty$ we should recover the dielectric half-space result [75] and by letting $n \to \infty$ one should be able to obtain the famous Casimir-Polder result. The former case will be derived in section 4.1 and the latter in section 4.2. Both cases will be analysed in the retarded and non-retarded regimes. Then we shall proceed with some relevant plots, in section 4.3.

4.1 Recovering the dielectric half-space limit

In this section, we intend to recover the results obtained by Wu and Eberlein in [75, 76], where they considered a half-space made of a dielectric that is characterised by a refractive index n, like in our case. We shall treat the retarded and non-retarded regimes separately.

4.1.1 Retarded Regime

In order to analyse this regime, we shall consider the third limit suggested previously: $\tilde{L} \gg \xi \gg 1$. Within these limits, it will be possible to calculate analytically the integrals contained in $S_{\parallel}$ and $S_{\perp}$. Since it is easier to work in polar coordinates we shall start from Eqs. (3.60) and (3.68) for the parallel and perpendicular contributions, respectively.

First of all, we note that the thickness dependence is contained only in the reflection coefficients R_{λ}. It can be seen from Eq. (2.31) that, in the limit $L \to \infty$, one recovers the Fresnel coefficients for a single interface. Alternatively, we can use the expressions (3.61) and (3.62) for the reflection coefficients in polar coordinates, and thus approximate the hyperbolic cotangent function appearing in the denominator by a constant[2]. One can see that, once we have taken this approximation, the expressions are identical to those in Wu's calculation, and thus the derivation will be as described in [76].

[2]See for instance section 4.5 in Ref. [124].

Concerning the limit $\xi \gg 1$ that describes the retarded regime, we shall apply Watson's lemma [127]. This is because the parameter ξ is only included in the argument of the exponential function $e^{-\xi r}$, and thus, one can conclude that the important contribution to the integral comes from small r only. Watson's lemma is equivalent to replacing the numerator by its Taylor series,

$$\frac{1}{x^2+1} \approx 1 - x^2 + x^4 - ... \tag{4.1}$$

Note that even though the denominator contains the factor t^2 multiplying the variable r^2, it does not do any harm to the approximation (4.1), since t goes from 0 to 1. After approximating the coth function, the reflection coefficients $\tilde{R}_\lambda$ only depend on the variable t. Hence, the initial double integral in Eq. (3.60) separates into a product of two single integrals, which are analytically solvable. For the parallel contribution of the shift we get, in the retarded regime,

$$\begin{aligned} S_{\parallel}(L\to\infty) = \frac{1}{4}(n^2-1)\int_0^\infty \mathrm{d}r\; r^3\, e^{-\xi r} \\ \times\left\{\int_0^1 \mathrm{d}t\; \frac{t^4}{(1+\sqrt{1+(n^2-1)t^2})^2} + \int_0^1 \mathrm{d}t\; \frac{n^2+1-t^2}{(n^2+\sqrt{1+(n^2-1)t^2})^2}\right\}. \end{aligned} \tag{4.2}$$

The integral in r can be solved straightforwardly, but for the integration over t it is convenient to do some algebraic manipulation. We shall perform the change of variable that we suggested in page 91: $t \to \tau = \sqrt{1+(n^2-1)t^2}$. In such a way that the integral in τ can be calculated analytically (see page 98 of Ref. [126]). One finally gets that the parallel contribution to the energy shift reads

$$S_{\parallel}(L\to\infty) = \frac{C_4^{\parallel}}{\xi^4}, \tag{4.3}$$

with the coefficient $C_4^{\parallel}$ defined as

$$C_4^{\parallel} = -\frac{1}{2}\Big\{\frac{2n^2+3n-8}{n^2-1} - \frac{3(2n^4-2n^2-1)}{(n^2-1)^{3/2}}\ln(\sqrt{n^2-1}+n) \\ -\frac{6n^4}{(n^2-1)\sqrt{n^2+1}}\ln\left(\frac{\sqrt{n^2+1}+1}{n(\sqrt{n^2+1}+n)}\right)\Big\}, \tag{4.4}$$

as it was shown in [76]. Exactly the same procedure follows for the perpendicular contribution of the energy-level shift of the atom $S_\perp$. The integral (3.50), after the same approximations for L large and r small, can be written as

$$S_\perp(L\to\infty) = \frac{1}{2}(n^2-1)\int_0^\infty \mathrm{d}r\; r^3\, e^{-\xi r}\int_0^1 \mathrm{d}t\; \frac{(1-t^2)(n^2+1-t^2)}{(n^2+\sqrt{1+(n^2-1)t^2})^2}. \tag{4.5}$$

The integral in r can be calculated easily, and the integral in t is performed by changing to the variable τ. Finally, we get that the perpendicular part of the energy-level shift is given by

$$S_\perp(L\to\infty) = \frac{C_4^\perp}{\xi^4}, \tag{4.6}$$

where the coefficient $C_4^\perp$ is exactly the same as the one defined in [76]

$$C_4^\perp = \frac{6n^4-3n^3-2n^2+2}{n^2-1} - \frac{3n^2(2n^4-2n^2+1)}{(n^2-1)^{3/2}}\ln(\sqrt{n^2-1}+n) \\ -\frac{6n^6}{(n^2-1)\sqrt{n^2+1}}\ln\left(\frac{\sqrt{n^2+1}+1}{n(\sqrt{n^2+1}+n)}\right). \tag{4.7}$$

By substituting these results into Eq. (3.55), we can obtain a final expression for the retarded energy shift of an atom near a dielectric half-space, as obtained in [76],

$$\delta E^{\mathrm{ret}} = -\frac{\alpha}{8\pi m^2 \mathcal{Z}^4}\sum_j \frac{C_4^{\parallel}|p_\parallel|^2 + C_4^\perp |p_\perp|^2}{E_{ji}^3}. \tag{4.8}$$

4.1.2 Non-retarded regime

In section 3.6.2 we calculated the non-retarded energy shift of an atom near a dielectric slab. We did it first by following a standard electrostatic calculation, and secondly, by

taking the corresponding limits to out general expression for the shift (3.55). In both cases we obtained that the shift ΔE_{es} is given by Eq. (3.79). Thus, in order to obtain the shift of an atom near a dielectric half-space, it suffices to consider the limit $L \to \infty$ in such an expression. The function $Q_\perp$ defined in page 107 gets simplified after this approximation, and the integral can be trivially solved,

$$Q_\perp(L \to \infty) = \frac{1}{2}\int_0^\infty \mathrm{d}k\; k^2\; e^{-2\mathcal{Z}k} = \frac{1}{8\mathcal{Z}^3}. \tag{4.9}$$

Substituting this result into Eq. (3.119) one gets that the electrostatic energy reads

$$\Delta E_{\text{es}} = \frac{\alpha}{16m^2\mathcal{Z}^3}\,\frac{n^2-1}{n^2+1}\sum_j \frac{2|p_\perp|^2 + |p_\parallel|^2}{E_{ji}^2}, \tag{4.10}$$

as calculated by Wu and Eberlein [76].

4.2 Recovering Casimir and Polder's result: Force on an atom near a perfect reflector

We have included in Appendix A a detailed derivation of the interaction between an atom and a perfect reflector. Thus, we know that the force between them is given by Eq. (A.30), as Casimir and Polder originally obtained. By expanding asymptotically this equation, one can obtain the force in the retarded (A.32) and the non-retarded regimes (A.31).

As a first attempt on recovering the (retarded) Casimir-Polder force, we can simply consider the results obtained in section 4.1.1 for a dielectric half-space, and take the limit $n \to \infty$ in the coefficients $C_\parallel$ and $C_\perp$ (Eqs. (4.4) and (4.7), respectively), as performed in Wu and Eberlein's paper. In the limit those coefficients are reduced to

$$C_4^\parallel(n \to \infty) \sim 2 - \frac{3}{n} \qquad \text{and} \qquad C_4^\perp(n \to \infty) \sim 2 - \frac{3}{2n}, \tag{4.11}$$

and substituting them into the expressions for S_σ we can finally recover the well known

Casimir-Polder result

$$\delta E^{\mathrm{ret}} = -\frac{\alpha}{4\pi m^2 \mathcal{Z}^4} \sum_j \frac{|p_\parallel|^2 + |p_\perp|^2}{E_{ji}^3} + O\left(\frac{1}{n}\right). \tag{4.12}$$

This procedure was performed quite straightforwardly. However, one could also recover the same result from our general formula for the energy shift — for an arbitrary thickness of the dielectric slab. Thus, what we should do, is to consider the limit $n \to \infty$ in Eq. (3.55). As it can be seen, the refractive index-dependence is only included in the reflection coefficients R_λ. Thus, we shall take the limit $n \to \infty$ to Eqs. (3.46) and (3.47). The coth function that appears in the coefficients goes to one (as far as L stays finite), and thus,

$$R_\lambda(n \to \infty) \quad \Longrightarrow \quad r_\lambda(n \to \infty), \tag{4.13}$$

where r_λ is the Fresnel coefficient for one single interface, and such a limit is -1 for the TE polarisation direction and 1 for the TM one. If we substitute the corresponding values in Eq. (3.48) for the parallel part of the energy shift, we solely need to solve

$$S_\parallel(n \to \infty) = \frac{1}{4} \int_0^\infty \mathrm{d}v \int_0^\infty \mathrm{d}s \, \frac{v}{\sqrt{s^2+v^2}} \frac{2s^2+v^2}{1+s^2} \, e^{-\xi\sqrt{s^2+v^2}}, \tag{4.14}$$

which in polar coordinates can also be written as

$$S_\parallel(n \to \infty) = \frac{1}{4} \int_0^\infty \mathrm{d}r \int_0^1 \mathrm{d}t \, \frac{1+t^2}{r^2t^2+1} \, r^3 e^{-\xi r}. \tag{4.15}$$

It seems convenient to start with the integration in t, and especially after some algebraic rearrangements in the integrand we obtain

$$S_\parallel = \frac{1}{4} \int_0^\infty \mathrm{d}r \, r e^{-\xi r} + \frac{1}{4} \int_0^\infty \mathrm{d}r \, r(r^2-1) \, e^{-\xi r} \int_0^1 \mathrm{d}t \, \frac{1}{r^2t^2+1}. \tag{4.16}$$

where the first term turned out to be a trivial integration in t. In the second term we have a relatively simple integral in t, given in Eq. (C.8). Thus the parallel part of the

shift remains in terms of the integral in r

$$S_{\parallel} = \frac{1}{4}\int_0^\infty \mathrm{d}r \ \left[r + (r^2-1)\arctan(r)\right] \ e^{-\xi r}. \tag{4.17}$$

The integration for the first term gives simply $1/\xi^2$. The remaining integrals can be integrated by parts, as it is shown in Eqs. (C.9) and (C.10). Moreover, we can identify in those expressions the *auxiliary function*, defined in section C.3, and thus write $S_{\parallel}$ in terms of its first and second derivatives, given in Eqs. (C.12) and (C.13). The parallel part of the shift is finally written as

$$S_{\parallel} = \frac{1}{2}\left(\frac{f(\xi)}{\xi^3} - \frac{f'(\xi)}{\xi^2} - \frac{f(\xi)}{\xi} + \frac{1}{\xi^2}\right). \tag{4.18}$$

Following the same procedure, we can calculate the perpendicular part of the energy shift

$$S_{\perp} = \frac{1}{2}\int_0^\infty \mathrm{d}v \int_0^\infty \mathrm{d}s \ \frac{v}{\sqrt{s^2+v^2}} \frac{v^2}{1+s^2} \ e^{-\xi\sqrt{s^2+v^2}}, \tag{4.19}$$

which in polar coordinates reads

$$S_{\perp} = \frac{1}{2}\int_0^\infty \mathrm{d}r \int_0^1 \mathrm{d}t \ \frac{1-t^2}{r^2t^2+1} \ r^3 e^{-\xi r}. \tag{4.20}$$

We can rewrite the integrand as we did before, in such a way that the integral in t gets simplified. It turns out to be the same integral given in Eq. (C.8). The remaining integrals in r are exactly Eqs. (C.9) and (C.10). Using the auxiliary functions and its derivatives as we did before we get

$$\begin{aligned} S_{\perp} &= \frac{1}{2}\int_0^\infty \mathrm{d}r \ r(r^2+1) \ e^{-\xi r} \int_0^1 \mathrm{d}t \ \frac{1}{r^2t^2+1} - \frac{1}{2}\int_0^\infty \mathrm{d}r \ re^{-\xi r} && (4.21)\\ &= \frac{1}{2}\int_0^\infty \mathrm{d}r \ \left[(r^2+1)\arctan(r) - r\right] \ e^{-\xi r} && (4.22)\\ &= \frac{f(\xi)}{\xi^3} - \frac{f'(\xi)}{\xi^2}. && (4.23) \end{aligned}$$

Thus, the total result for the Casimir-Polder force, after some further algebraic manip-

ulation in the coefficients $S_{\parallel}$ and $S_{\perp}$ is given by

$$\delta E = -\frac{\alpha}{\pi m^2}\sum_j E_{ji}\left[|p_{\parallel}|^2\left(\frac{\partial^2}{\partial\xi^2}\frac{1}{\xi}+\frac{\partial}{\partial\xi}\frac{1}{\xi^2}+\frac{1}{\xi^3}\right)f(\xi)-2|p_{\perp}|^2\left(\frac{\partial}{\partial\xi}\frac{1}{\xi^2}+\frac{1}{\xi^3}\right)f(\xi)\right], \tag{4.24}$$

in agreement with Eq. (A.26). Performing an asymptotic expansion for the auxiliary functions for $\xi \to \infty$ (see Eq. (C.15)) in order to obtain the result in the retarded regime, we find that both $S_{\parallel}$ and $S_{\perp}$ leading terms are $2/\xi^4$, recovering thus the famous expression (4.12). Also, by expanding the auxiliary functions around 0 (see Eq. (C.15)), one can recover the electrostatic interaction of an atom with a perfect reflector as calculated in previous chapter and given in Eq. (3.1)

4.3 Plots

The expression for the energy-level shift (4.24), as calculated by Casimir and Polder [2], will be very useful in order to show the correction due to the finite thickness of the dielectric that is located near the atom. As we said, by factorising out such a force from our general result (3.55), we can plot a useful parameter that shows how the correction varies with the distance $\mathcal{Z}$.

First of all, with the purpose of understanding the procedure that we will follow, we shall start with a simpler case: the perfect reflector. In order to obtain some useful plots, we shall rewrite the Casimir-Polder interaction in a more convenient way. Then, in section 4.3.2, a similar procedure will be applied to obtain the correction for the atom-slab interaction.

4.3.1 Perfect reflector

In order to rewrite Eq. (4.24) in a more favourable way, we shall bear in mind that the definition of certain parameters, like ξ and $\tilde{L}$, was necessary in previous calculations because they would lead us to an asymptotic analysis of they integrals in play. Nevertheless, at this stage it is more effective to utilise the variables that relate directly

to experiments. Thus, it seems more convenient to use the measurable variables $\mathcal{Z}$, L and the wavelenth of an atomic transition $\bar{\lambda}_{ji}$, as defined in Eq. (3.59). In such a way, we can define the parameter $\tilde{\xi} \equiv \mathcal{Z}/\bar{\lambda}_{ji}$ and use the relation (3.54), given in page 87, in order to transform the expression in terms of the dipole-moment operator. For a perfect reflector we thus have

$$\delta E^{\mathrm{PR}} = -\frac{1}{4\pi\epsilon_o}\sum_j \frac{1}{\bar{\lambda}_{ji}^3}\left(V_{\parallel}^{\mathrm{PR}}|\mu_{\parallel}|^2 + V_{\perp}^{\mathrm{PR}}|\mu_z|^2\right), \tag{4.25}$$

with

$$V_{\parallel}^{\mathrm{PR}} = \frac{1}{8\pi}\left(\frac{\partial^2}{\partial\tilde{\xi}^2}\frac{1}{\tilde{\xi}} + \frac{\partial}{\partial\tilde{\xi}}\frac{1}{\tilde{\xi}^2} + \frac{1}{\tilde{\xi}^3}\right) f(2\tilde{\xi}) \tag{4.26}$$

$$V_{\perp}^{\mathrm{PR}} = -\frac{1}{4\pi}\left(\frac{\partial}{\partial\tilde{\xi}}\frac{1}{\tilde{\xi}^2} + \frac{1}{\tilde{\xi}^3}\right) f(2\tilde{\xi}). \tag{4.27}$$

If we expand the auxiliary functions and its derivatives in Eq. (4.25) for $\tilde{\xi}$ large (use Eq. (C.15)), we obtain that both perpendicular and parallel parts approximate to $1/4\pi\tilde{\xi}^4$. On the other hand, if we expand the expressions for $\tilde{\xi}$ small, by using Eq. (C.16), one gets that in the non-retarded regime the functions are $V_{\parallel}^{\mathrm{PR}} \to 1/16\tilde{\xi}^3$ and $V_{\perp}^{\mathrm{PR}} \to 1/8\tilde{\xi}^3$. We have chosen to divide the functions $V_{\parallel}^{\mathrm{PR}}$ and $V_{\perp}^{\mathrm{PR}}$ given above by their functional dependence as $\tilde{\xi} \to \infty$. This implies that such a product will approach asymptotically to one for large atom-surface separations. On the other hand, as the atom gets closer to the dielectric surface, the product will approach to the lines $\pi\tilde{\xi}/4$ and $\pi\tilde{\xi}/2$, respectively for the parallel and the perpendicular parts. We shall label these new functions as

$$W_{\parallel}^{\mathrm{PR}} = 4\pi\tilde{\xi}^4 V_{\parallel}^{\mathrm{PR}} \qquad \text{and} \qquad W_{\perp}^{\mathrm{PR}} = 4\pi\tilde{\xi}^4 V_{\perp}^{\mathrm{PR}}, \tag{4.28}$$

in such a way that the energy shift can be written as

$$\delta E^{\mathrm{PR}} = -\frac{1}{4\pi\epsilon_o}\sum_j \frac{1}{4\pi E_{ji}\mathcal{Z}^4}\left(W_{\parallel}^{\mathrm{PR}}|\mu_{\parallel}|^2 + W_{\perp}^{\mathrm{PR}}|\mu_z|^2\right). \tag{4.29}$$

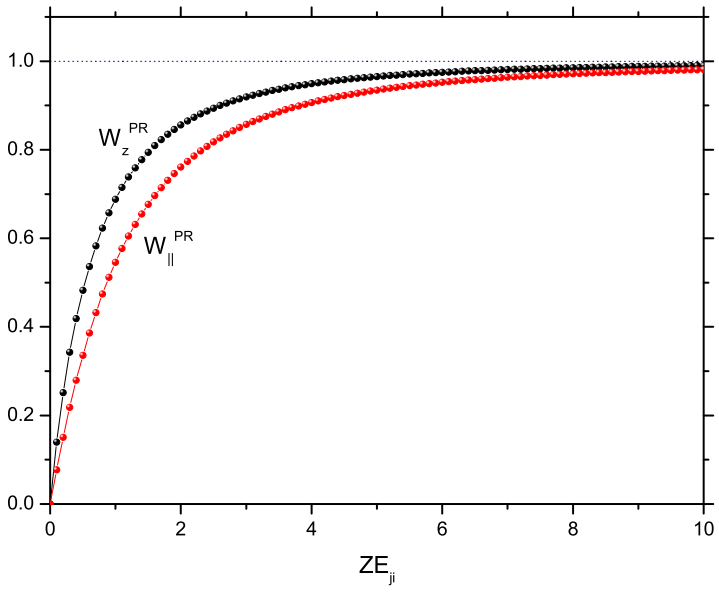

Figure 4.1: The graph shows the functions $W_{\parallel}^{\mathrm{PR}}$ and $W_{\perp}^{\mathrm{PR}}$ for a perfect reflector, as a function of the atom-surface separation (rescaled with E_{ji}). As predicted, the correction approaches to 1 at large distances and to $\pi\tilde{\xi}/4$ and $\pi\tilde{\xi}/2$, respectively in the so called non-retarded regime.

We know that the energy shift for the perfect reflector δE^{PR} behaves like $-1/\mathcal{Z}^3$ in the non-retarded regime, and like $-1/\mathcal{Z}^4$ for large atom-surface separations. Thus, plotting simply δE^{PR} would make difficult to see any difference. Furthermore, it can be seen from Eq. (4.29) that the shift depends on atomic properties. For this reason, it is more convenient to plot the functions $W_{\parallel}^{\mathrm{PR}}$ and $W_{\perp}^{\mathrm{PR}}$ written beside the parallel and perpendicular component of the dipole moment, respectively. Since the shift δE^{PR} in Eq. (4.29) has a factor of $-1/\mathcal{Z}^4$, this implies that for small atom-surface separations, where $\delta E^{\mathrm{PR}} \sim -1/\mathcal{Z}^3$, the functions $W_{\parallel}^{\mathrm{PR}}$ and $W_{\perp}^{\mathrm{PR}}$ go like $\mathcal{Z}$ (with different slope for each polarisation), and in the retarded regime, where $\delta E^{\mathrm{PR}} \sim -1/\mathcal{Z}^4$, the function W_{σ}^{PR} is a constant. In addition, we can see in Fig 4.1 how this correction behaves in between.

4.3.2 Dielectric slab

Following a similar procedure, one can get a more useful expression for the energy shift of an atom due to the presence of the slab. This will be obtained by factoring out the Casimir-Polder dependence, in order to see what the correction is.

The choice of functions W_σ is such that they are dimensionless. They, now labeled as $W_\sigma^{\rm slab}$ in reference to the dielectric slab, play a role analogous to the functions $W_\sigma^{\rm PR}$ in the previous section: they are simply the functions S_σ in Eq. (3.55) but with the Casimir-Polder term $\sim \tilde{\xi}^4$ factored out. Thus, after transforming in terms of the dipole-moment operator, the energy-level shift given in Eq. (3.55) reads

$$\delta E^{\rm slab} = -\frac{1}{4\pi\epsilon_o}\sum_{j\neq i}\frac{1}{4\pi E_{ji}\mathcal{Z}^4}\left(W_\parallel^{\rm slab}|\mu_\parallel|^2 + W_\perp^{\rm slab}|\mu_z|^2\right), \tag{4.30}$$

with parallel part

$$W_\parallel^{\rm slab} = 8\tilde{\xi}^4 S_\parallel = \frac{2\tilde{\xi}^4}{\sqrt{n^2-1}}\int_0^\infty {\rm d}r\int_1^n {\rm d}\tau\,\frac{r^3}{n^2-1+r^2(\tau^2-1)}\frac{\tau}{\sqrt{\tau^2-1}} \times\left(\frac{(n^2-1)(n^4-\tau^2)}{n^4+\tau^2+2n^2\tau\coth(rLE_{ji}\tau)} + \frac{(\tau^2-1)^2}{\tau^2+1+2\tau\coth(rLE_{ji}\tau)}\right)e^{-2r\tilde{\xi}} \tag{4.31}$$

and perpendicular part given by

$$W_\perp^{\rm slab} = 8\tilde{\xi}^4 S_\perp = \frac{4\tilde{\xi}^4}{\sqrt{n^2-1}}\int_0^\infty {\rm d}r\int_1^n {\rm d}\tau\,\frac{\tau}{\sqrt{\tau^2-1}} \times\frac{r^3(n^2-\tau^2)}{n^2-1+r^2(\tau^2-1)}\,\frac{n^4-\tau^2}{n^4+\tau^2+2n^2\tau\coth(rLE_{ji}\tau)}\,e^{-2r\tilde{\xi}}. \tag{4.32}$$

As we did for the perfect reflector case, one can plot the parallel and perpendicular corrections $W_\parallel^{\rm slab}$ and $W_\perp^{\rm slab}$, as a function of the surface-atom separation (scaled with the wavelength of an atomic transition λ_{ji}, in order to get a dimensionless variable). However, since the shift also depends on the thickness of the dielectric slab L (that we shall scale in the same way) and the refractive index n, we shall do this heedfully. Thus, in order to calculate numerically the integrals in Eq. (4.30), by simply using *Maple*, we must separate the graphs into two sets:

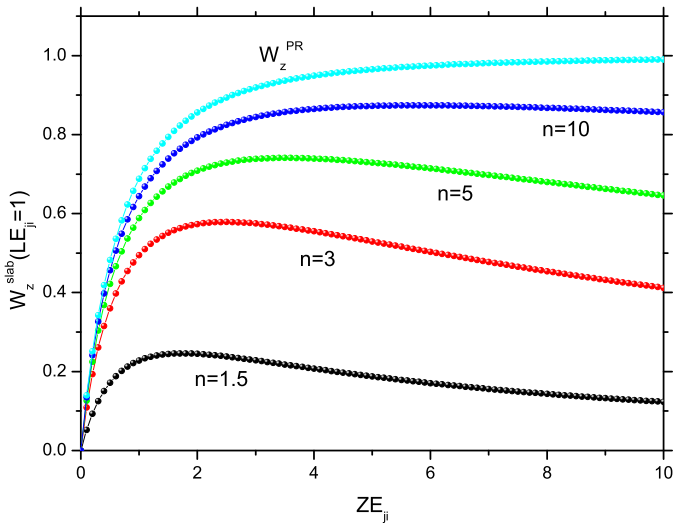

Figure 4.2: The graph shows the function $W_{\perp}^{\text{slab}}$. The slab is taken to have a thickness $LE_{ji} = 1$, and we have varied the value of the refractive index $n = 1.5, 3, 5, 10$. In light blue it is shown the result W_z^{PR} for the perfect reflector ($n \to \infty$).

Fixed thickness

First, by fixing the value of scaled thickness LE_{ji}, one can plot the functions W_{σ}^{slab} of the energy shift for different values of the refractive index n. As it is shown in Fig. 4.2, we have chosen $LE_{ji} = 1$ and calculated numerically Eq. (4.32), by using *Mathematica*, for $n = 1.5, 3, 5, 10$. As we have also plotted the function $W_{\perp}^{PR}$ for a perfect reflector, it can be clearly seen how they approach to the latter as $n \to \infty$.

The same procedure is followed in order to calculate the parallel correction. By fixing the thickness of the slab and solving numerically Eq. (4.31) for the same values of n, one can plot $W_{\parallel}^{\text{slab}}$ as shown in Fig. 4.3. Note that this plot looks very similar to the previous one, however it has a different slope.

Using the same values for n, we have also plot $W_{\perp}^{\text{slab}}$ and $W_{\parallel}^{\text{slab}}$ for $LE_{ji} = 10$, in Fig. 4.4 and 4.5, respectively, and for LE_{ji} =0.1 in Fig. 4.6 and 4.7, respectively.

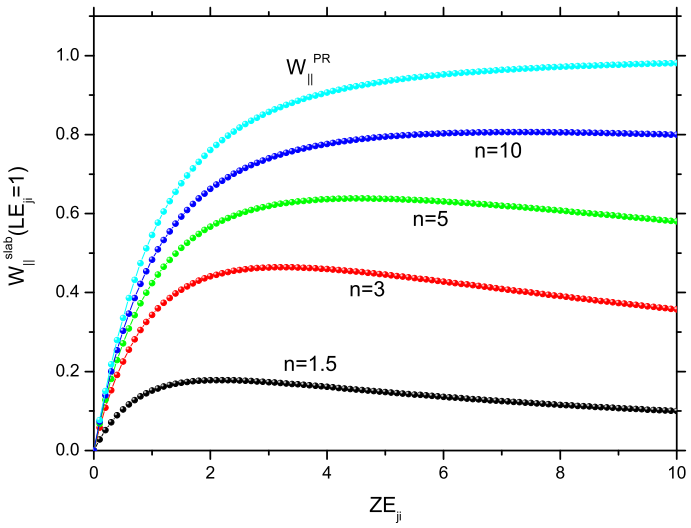

Figure 4.3: The graph shows the function $W_{\parallel}^{\text{slab}}$. The slab is taken to have a thickness $LE_{ji} = 1$, and we have varied the value of the refractive index $n = 1.5, 3, 5, 10$. In light blue it is shown the result $W_{\parallel}^{\text{PR}}$ for the perfect reflector ($n \to \infty$).

Fixed refractive index

For the second set of graphs, it is necessary to fix the value of the refractive index n. We have arbitrarily chosen first $n = 2$ in order to calculate numerically the integrals in Eqs. (4.32) and (4.31), and then plot separately for a scaled thickness $LE_{ji} = 0.1$, 1, 5, 10. The functions $W_{\perp}^{\text{slab}}$ and $W_{\parallel}^{\text{slab}}$, are shown in Fig. 4.8 and 4.9, respectively.

Furthermore, we have taken the limit $L \to \infty$ in Eq. (4.32), in such a way that we can approximate the cotangent function by one. Note that in that limit, $\coth(rL)$ will be one except at $r = 0$, but this term would be negligible compared to r^3 in the numerator and thus we can proceed without problem. The resulting integral in Eq. (4.32) can be solved numerically in *Mathematica* for $n = 2$, and we have labeled it as $W_{\perp}^{\text{HS}}$. In order to compare it with the graphs obtained for various thickness, we have also plot the function $W_{\perp}^{\text{HS}}$ in Fig. 4.8, in light blue. Note that as the value of L increases, the branch gets closer to the result obtained for a dielectric half-space, which in this case approaches asymptotically to .53. If we had chosen a larger value for

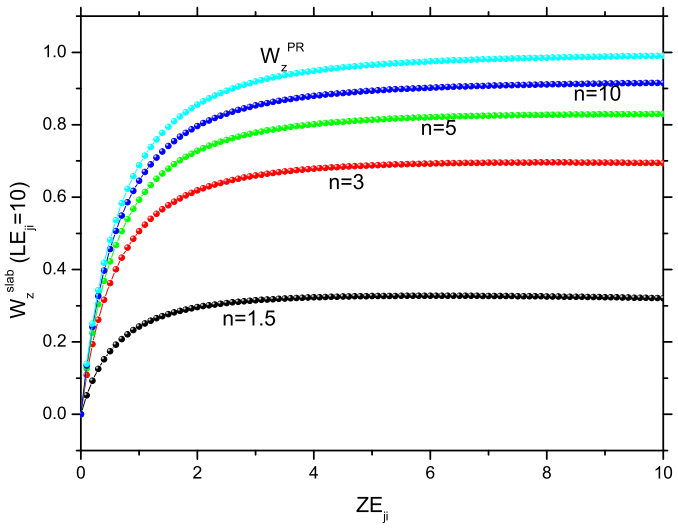

Figure 4.4: The graph shows the function $W_{\perp}^{\text{slab}}$. The slab is taken to have a thickness $LE_{ji} = 10$, and we have varied the value of the refractive index $n = 1.5, 3, 5, 10$. In light blue it is shown the result W_z^{PR} for the perfect reflector ($n \to \infty$).

the refractive index n this asymptote would be shifted up, but never further than one (which gives the perfect reflector result shown in Fig. 4.1). The corresponding graph for $W_{\parallel}^{\text{HS}}$ is added in Fig. 4.9.

Using the same values for LE_{ji}, we have plot $W_{\perp}^{\text{slab}}$ and $W_{\perp}^{\text{slab}}$ for $n = 5$, in Fig. 4.10 and 4.11, respectively.

4.4 Comparison with previous work

Only a very few works in which the interaction between an atom and a slab is calculated can be found in the literature. The one that we could consider the most important, due to its high applicability, is the work done by Buhmann *et al* [128]. We have given more details of such a work in chapter 1 of this thesis. In summary, they utilised lowest-order perturbation theory and linear response theory to calculate the van der Waals potential of a ground-state atom placed within an arbitrary dispersing and absorbing magnetodielectric multilayer system. Their general formula can be analysed for some

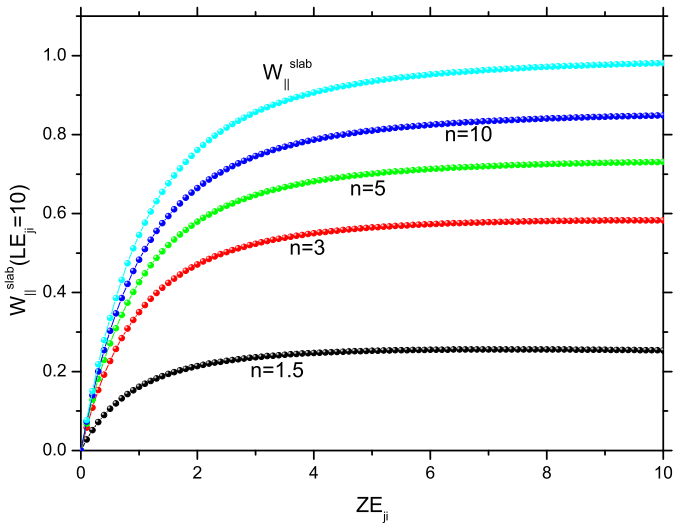

Figure 4.5: The graph shows the function $W_{\parallel}^{\text{slab}}$. The slab is taken to have a thickness $LE_{ji} = 10$, and we have varied the value of the refractive index $n = 1.5, 3, 5, 10$. In light blue it is shown the result for the perfect reflector ($n \to \infty$).

special cases and simplified, i.e., for one material half-space and for a plate of finite thickness. They are particularly interested in the behaviour due to both the electric and magnetic permittivities, and realised that there is an optimal plate thickness for creating a maximum potential wall. They claimed that their expression for the Casimir-Polder potential of an atom near a plate of finite thickness reduces to the result given in Ref. [83], in the special case of a dielectric plate. In order to get a more explicit formula, they consider the limit of an asymptotically thin plate, in the retarded regime. The result obtained, as given in Eq. (218) in [7], reads

$$U(\mathcal{Z}) = -\frac{\hbar c \alpha(0)}{160\pi^2\varepsilon_0}\frac{L}{\mathcal{Z}^5}\left[\frac{14\varepsilon^2(0)-9}{\varepsilon(0)} - \frac{6\mu^2(0)-1}{\mu(0)}\right], \tag{4.33}$$

where $\alpha(0)$ is the static polarisability. They also calculated the interaction in the non-retarded limit, where they could distinguish between a purely dielectric plate and a purely magnetic one. For the dielectric case, by direct comparison with out results, it can be seen that they have a dependence of the order $L/\mathcal{Z}^5$, as we do.

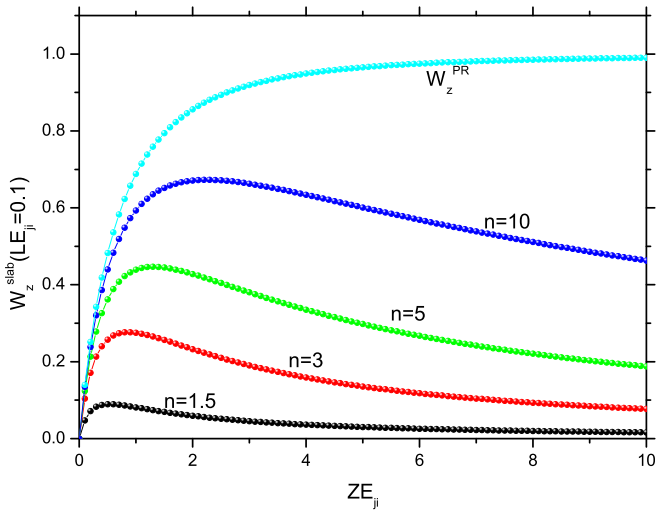

Figure 4.6: The graph shows the function $W_{\perp}^{\rm slab}$. The slab is taken to have a thickness $LE_{ji} = 0.1$, and we have varied the value of the refractive index $n = 1.5, 3, 5, 10$. In light blue it is shown the result $W_z^{\rm PR}$ for the perfect reflector ($n \to \infty$).

In order to reduce, from Eq. (4.33), to the case of a dielectric plate, we shall substitute $\mu(0) = 1$. Moreover, since the static refractive index of the medium is $n(0) = \sqrt{\varepsilon(0)\mu(0)}$, we can simply substitute $\varepsilon(0) = n^2$ into the expression above. Note that, unlike our treatment, they have considered an atom with isotropic polarisability, i.e, the same at all directions. Thus, Eq. (4.33) simply reduces to

$$U(\mathcal{Z}) = -\frac{\hbar c\alpha(0)}{160\pi^2 n^2 \varepsilon_0}\frac{L}{\mathcal{Z}^5}(n^2-1)(9+14n^2). \tag{4.34}$$

We should be able to compare this formula with our result, by using Eq. (3.71) for the interaction between an atom and a thin slab. Since it is written in terms of the matrix elements of the momentum operator, it is convenient to use relation (3.54) to convert them into those of the dipole moment operator,

$$\delta E = -\frac{(n^2-1)}{160\pi^2 n^2 \varepsilon_o}\frac{L}{\mathcal{Z}^5}\sum_{j\neq i}\frac{(5+9n^2)|\mu_{\parallel}|^2 + 2(4+5n^2)|\mu_{\perp}|^2}{E_{ji}}. \tag{4.35}$$

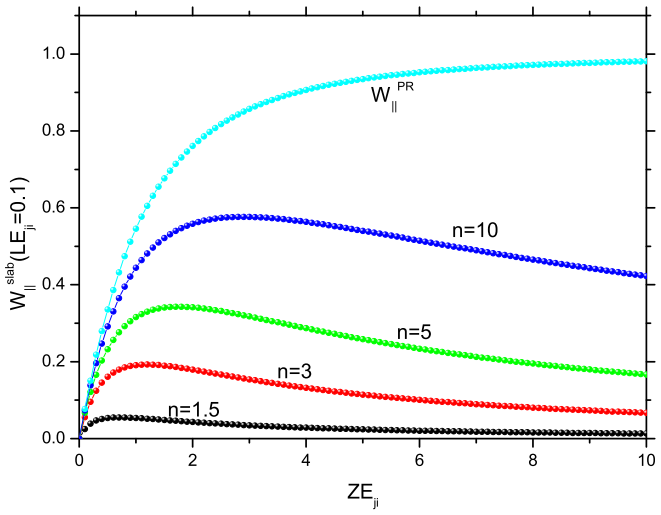

Figure 4.7: The graph shows the function $W_{\parallel}^{\text{slab}}$. The slab is taken to have a thickness $LE_{ji} = 0.1$, and we have varied the value of the refractive index $n = 1.5, 3, 5, 10$. In light blue it is shown the result $W_{\parallel}^{\text{PR}}$ for the perfect reflector ($n \to \infty$).

Then we can use the relation for the polarisability of an isotropic atom [3]

$$\alpha(\omega) = \frac{2}{3} \sum_j \frac{E_{ji} |\boldsymbol{\mu}|^2}{E_{ji}^2 - \omega^2}, \tag{4.36}$$

with $|\boldsymbol{\mu}|^2 = |\mu_x|^2 + |\mu_y|^2 + |\mu_z|^2$ and $|\mu_x|^2 = |\mu_y|^2 = |\mu_z|^2$. Thus the static polarisability can be written as

$$\alpha(0) = 2 \sum_{j \neq i} \frac{|\mu_z|^2}{E_{ji}}, \quad \text{or} \quad \alpha(0) = \sum_{j \neq i} \frac{|\mu_{\parallel}|^2}{E_{ji}}. \tag{4.37}$$

With this our result reduces to

$$\delta E = -\frac{\alpha(0)}{160\pi^2 n^2} \frac{L}{\mathcal{Z}^5} (n^2 - 1)(9 + 14n^2), \tag{4.38}$$

which agrees with Eq. (4.34) in our choice of units $\hbar = 1 = c$ and $\varepsilon_o = 1$.

[3] See for instance page 243 in [3].

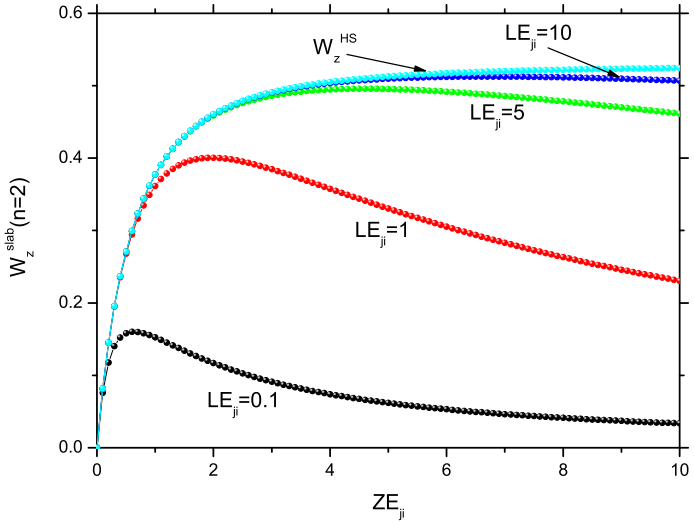

Figure 4.8: The graph shows the function $W_{\perp}^{\text{slab}}$ for different thickness of the slab. In this specific case, the dielectric is characterised by a refractive index $n = 2$ so $W_{\perp}^{\text{slab}}$ can be obtained numerically for different thickness. We have chosen LE_{ji} = 0.1,1,5,10. The curve in light blue comes from the dielectric half-space result.

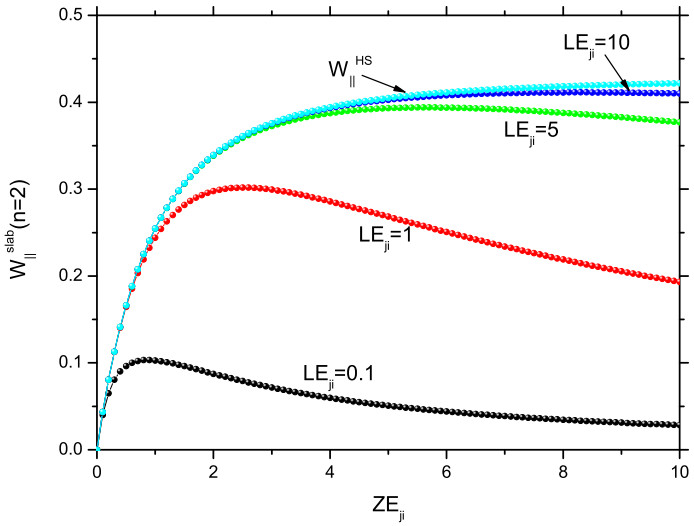

Figure 4.9: The graph shows the function $W_{\parallel}^{\text{slab}}$ for different thickness of the dielectric slab ($n = 2$). As above, numerical values $LE_{ji} = 0.1, 1, 5, 10$ are used.

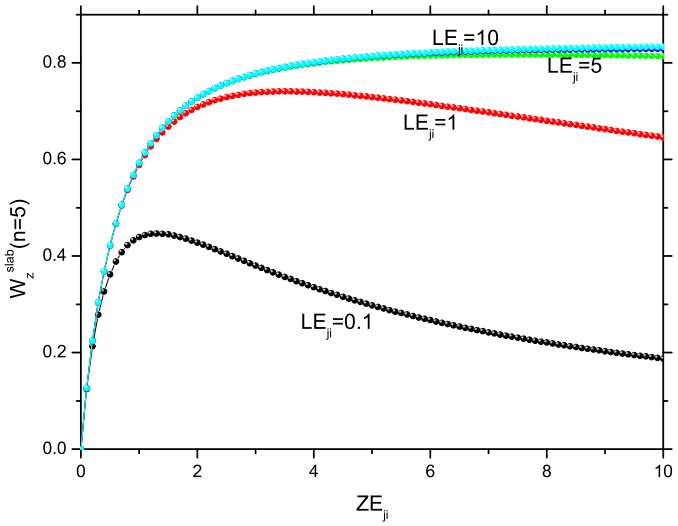

Figure 4.10: The graph shows the function $W_{\perp}^{\text{slab}}$ for a dielectric with refractive index $n = 5$. $W_{\perp}^{\text{slab}}$ is shown for different thickness $LE_{ji} = 0.1,1,5,10$. The curve in light blue comes from the dielectric half-space result.

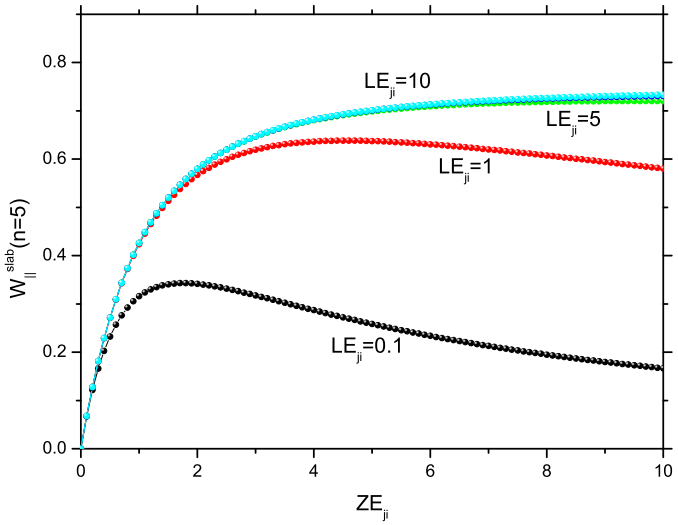

Figure 4.11: The graph shows the function $W_{\parallel}^{\text{slab}}$ for different thickness of the dielectric slab ($n = 5$). As above, numerical values $LE_{ji} = 0.1, 1, 5, 10$ are used.

Chapter 5

Summary and outlook

In this thesis, we have have calculated the energy-level shift of an atom located near a non-dispersive and non-dissipative dielectric slab. We have considered an atom in its ground state, and the system was studied at zero temperature. The dielectric slab is characterised by a refractive index n, which is real and the same for all the frequencies. Although this is a simplified model, it constitutes an improvement over the unrealistic perfect reflector model, as it allows for imperfect reflectivity and evanescent waves. Most importantly, the simplicity and high symmetry of the geometry utilised allow us to quantise the electromagnetic field by explicit mode expansion, which facilitates exact analytic calculations. Many powerful methods to study quantum electrodynamics near media with diverse properties and geometries have been developed in the past [129]. We have mentioned some of them in section 1.2.2, emphasizing that their importance is mainly due to their wide applicability (i.e., they are capable of including absorption and dissipation). However, the problem that they present, unlike the treatment in terms of an explicit mode expansion, is that applying these methods to a particular problem generally necessitates extensive numerical calculations. As we are wishing to obtain simple formulas that can be applied very easily to current experiments (see page 18), it is convenient to follow a quantisation by explicit mode expansion.

The energy-level shift is a purely quantum mechanical effect and arises from the interaction of the atom with the electromagnetic field fluctuations, which in turn are

affected by the presence of the slab. Therefore, a quantisation of the electromagnetic field in the presence of a layered system was vital in order to work out the shift. Even though the field quantisation for this system has been analysed previously [78], we decided to show in this work a complete derivation of the normal modes. The reason for this is because there has been an ambiguity in the results presented so far (a wrong normalisation constant was given for the TM polarisation in Ref. [78]). Also, the absence of the proof of the completeness of the electromagnetic field modes and the use of certain constants (i.e., the density of modes) without sufficient justification, made their procedure unsuitable for indiscriminate copying.

By solving the Helmholtz equation and imposing the corresponding boundary conditions that result from Maxwell's equations, it could be shown that the field modes comprise of travelling and trapped modes. The travelling modes have a continuous range of frequencies, and are composed of incident, reflected and transmitted parts (at each interface). The trapped modes arise due to the solutions of the Helmholtz equation with purely imaginary normal wave vector outside the slab. They are subject to repeated total internal reflection inside the dielectric, and emerge as an evanescent field outside the slab. Also, they only exist at certain discrete frequencies which depend on their polarisation direction and parity and are obtained through the dispersion relations.

In order to calculate the energy-level shift, we applied second-order perturbation theory to the interaction Hamiltonian $H_I = -\mu \cdot \mathbf{E}(\mathbf{r}, t)$, corresponding to the electric-dipole interaction, which is the lowest-order in the multipole Hamiltonian. In this equation, $\mu = e(\mathbf{r} - \mathbf{r}_o)$ is the electric-dipole moment operator of the atomic electron and $\mathbf{E}(\mathbf{r}, t)$ the transverse electric field, which can be expanded in terms of travelling and trapped modes. The advantage of working with this Hamiltonian, over the conventional minimal-coupling Hamiltonian $H_I = \mathbf{p} \cdot \mathbf{A}$, is that it does not explicitly contain the electrostatic interaction between the atomic dipole and its image charges inside the dielectric.

A typical second-order perturbative calculation in quantum electrodynamics, like

the one required in this work for the Casimir-Polder interaction between the atom and the dielectric slab, involves a product of mode functions and a sum over intermediate photon states (as shown in Eq. (3.12)). As these modes have different nature, the shift automatically splits into two contributions: one from the continuous set of travelling modes and the other from the discrete set of trapped modes.

A problem arose when we had to add both contributions together, as it was difficult to know *a priori* how to add the travelling and the trapped modes with the correct relative weightings. As the completeness condition (2.15) — which must be satisfied — contains such a sum over all the modes, we decided to embark on this calculation. The procedure, as we hoped, would guide us to see the convenient way to treat such a sum.

In order to perform the proof of the completeness in an unambiguous way, it was necessary to introduce a quantisation box. In such a way, all modes became discrete, and we could add them unequivocally. Then, by taking the limit of an infinite quantisation volume, we recovered the original modes, as obtained in free space, and hence a correct way to sum them (without guessing the weighting constants, in contrast to previous work [78]).

What we found out is that the integral in k_z, that corresponds to the contribution from the travelling modes, could be transformed into a sum over residues around the poles of the reflection coefficients R_{TE} and R_{TM}. This sum was equal (but with opposite sign) to the contribution coming from the trapped modes, which allowed us to prove the completeness of the modes.

However, the most important benefit that we got out of the completeness calculation was that we realised that by following the procedure in reverse, one could see the sum over trapped modes as a contour integral in the complex k_z plane. This means that we came out with a convenient method of summing over all modes. In general, for any

function $Q(k_z, \mathbf{k}_\parallel)$ contained in the integrand

$$\int \mathrm{d}^2\mathbf{k}_\parallel \sum\!\!\!\!\!\!\int_{k_z\lambda} Q(k_z, \mathbf{k}_\parallel)\ \sqrt{\varepsilon} f^i_{\mathbf{k}\lambda}(\mathbf{r})\ \sqrt{\varepsilon} f^{*j}_{\mathbf{k}\lambda}(\mathbf{r}') \Bigg|_{\text{all modes}} \tag{5.1}$$

in which $f_{\mathbf{k}\lambda}(\mathbf{r})$ are the normal modes of the system, one can calculate the sum over all modes by applying Eq. (2.116). Note that it is important to ensure that the function $Q(k_z, \mathbf{k}_\parallel)$ is analytic in the vicinity of the poles of the reflection coefficients R_{TE} and R_{TM} on the positive imaginary k_z axis.

The calculation of the energy-level shift could then be achieved more easily, in a clever and sophisticated way, as an application of our method. The shift, written as an integral along the new path shown in Fig. 2.11, is given by Eq. (3.32). Furthermore, in order to solve this integral we applied complex variable techniques, resulting in the general expression (3.32), with parallel and perpendicular components given by Eqs. (3.48) and (3.50) respectively.

Finally, in order to obtain more explicit expressions, we analysed the final result by separating the analysis in two groups, depending on whether the retardation of the electromagnetic interaction mattered. When the retardation can be neglected, the interaction is purely electrostatic, and is due to the interaction between the atomic dipole and its images on the other side of the interface (as drawn in Fig. 3.8). On the other hand, when the separation $\mathcal{Z}$ between the atom and the slab is large compared with the wavelength λ_{ij} of an atomic transition, retardation had to be taken into account. In order to analyse this regime, we proceeded with an asymptotic analysis of the integral (3.32). It had been stated in Ref. [120], that the result should depend on the thickness of the slab, as there was a discrepancy between the force due to a thick slab and the one produced by a thin sheet. Nevertheless, we found that this was not the case, and the result was the same for all thicknesses, including the limit of an infinitely thin sheet. Also, we have managed to recover results obtained previously for a dielectric half-space [75], and the well-known result of Casimir and Polder for a perfect reflector. We have summarised all the results obtained in the following table

5.1. Note that the formula that describes the energy-level shift between an atom and a thin dielectric slab is a very simple expression and thus could be applied quite easily to current experimental research. This is very important, as experiments that intend to measure the Casimir-Polder force are becoming more precise, especially due to the use of cold atoms. Moreover, they no longer simply use a thick dielectric substrate, but utilise a very thin layer of other material on the top, and that layer interacts with the atom.

5.1 Summary of results

The following table shows the results obtained

Atom-surface interaction $\delta E(\mathcal{Z}, n, L)$	Retarded regime	General formula	Non-retarded regime
Finite slab with $L \ll \mathcal{Z}$	(3.71)	(3.55)	(3.79) $\rightarrow$ (3.122)
Half-space ($L \rightarrow \infty$)	(4.8)	(3.55)	(4.10)
Perfect conductor ($n \rightarrow \infty$)	(4.12)	(3.55)	(A.31)

5.2 Outlook

Since we have found a very convenient way to add a discrete and a continuous set of modes, in principle, the result (2.116) could be applied to a series of problems for the same model and geometry. For instance, we could calculate the correction due to finite temperature, by simply including the Planck distribution

$$N_\nu = \frac{1}{e^{\omega_\nu/T} - 1} \tag{5.2}$$

into the expression of the shift, as it was calculated for the dielectric half-space case [111]. We have to be careful on how to apply the method though (i.e., checking that the function Q in Eq. (2.116 is analytic)), as the calculation will also involve a sum over the Matsubara frequencies (i.e., poles located on the imaginary ω-axis).

Appendix A

Casimir-Polder force for a plane

The force between a ground state atom and a perfect reflector was first calculated by Casimir and Polder [2], by using perturbation theory. In order to facilitate the understanding of the problem presented in this thesis, we shall reproduce Casimir and Polder's result. The reason is that the method followed here, for the ideal case, is exactly the same required in our calculation for the interaction between an atom and a slab. However, we shall describe the procedure with less detail in this Appendix, since we have left those details for the main part of this thesis.

The Casimir-Polder force is due to the interaction of the atom with the electromagnetic field fluctuations, which are affected by the presence of the boundary, i.e., perfect reflector. Thus, a quantisation of the field in the presence of such a boundary is required. For instance, it is well known that one can write the vector potential for the free electromagnetic field in terms of plane waves

$$\mathbf{A}(\mathbf{r},t)=\sum_{\lambda}\int\frac{\mathrm{d}^3\mathbf{k}}{(2\pi)^{3/2}}\frac{1}{\sqrt{2\omega\epsilon_o}}\left(\hat{\mathbf{e}}_\lambda a_{\mathbf{k}\lambda}e^{-\mathrm{i}\omega t+\mathrm{i}\mathbf{k}\cdot\mathbf{r}}+\hat{\mathbf{e}}^*_\lambda a^\dagger_{\mathbf{k}\lambda}e^{\mathrm{i}\omega t-\mathrm{i}\mathbf{k}\cdot\mathbf{r}}\right), \tag{A.1}$$

where the polarisation vectors $\hat{\mathbf{e}}_\lambda$ are given by Eqs. (2.19) and (2.20), for the TE and TM polarisation respectively (see page 30). For convenience in the rest of the

calculation, we shall write them in the following way

$$\hat{\mathbf{e}}_1 = \frac{1}{k_\parallel}(\mathbf{k} \times \hat{\mathbf{e}}_z) \qquad \text{and} \qquad \hat{\mathbf{e}}_2 = \frac{k_z}{k_\parallel k}\mathbf{k}_\parallel - \frac{k_\parallel}{k}\hat{\mathbf{e}}_z, \tag{A.2}$$

where $\hat{\mathbf{e}}_z$ is the unit vector pointing out in the z direction, and $\mathbf{k} = (\mathbf{k}_\parallel, k_z)$ is the wave vector in free space (following the same notation as used before). The vector field, as written in Eq. (A.1), describes the electromagnetic field in free space. However, in order to take into account the chosen boundary, the field must satisfy the boundary conditions imposed by the reflecting surface. From Maxwell Eqs. (2.1)–(2.4), these are given by,

$$E_x = 0 = E_y \qquad \text{and} \qquad B_z = 0 \tag{A.3}$$

at $z = 0$, where the interface is located.

It is necessary to obtain an expression for the vector potential $\mathbf{A}(\mathbf{r}, t)$ in terms of the normal modes $\mathbf{f}_{\mathbf{k}\lambda}(\mathbf{r})$, as in Eq. (2.10). For this we shall only make sure that the electromagnetic field satisfies the boundary conditions (A.3), for each polarisation direction λ. For example, for the TE polarisation we have,

$$e^{-\mathrm{i}\omega t}\frac{\mathbf{k} \times \hat{\mathbf{e}}_z}{k_\parallel} e^{\mathrm{i}\mathbf{k}_\parallel \cdot \mathbf{r}_\parallel} \sin k_z z \tag{A.4}$$

in order to satisfy the condition $E_\parallel = 0$ at $z = 0$. The z-component of the magnetic field can be obtained from the vector potential above, by using $\mathbf{B} = \nabla \times \mathbf{A}$. Thus,

$$B_z = \frac{\partial A_y}{\partial x} - \frac{\partial A_x}{\partial y} \sim \sin k_z z, \tag{A.5}$$

ensuring the condition (A.3) for the magnetic field at the interface. A similar procedure is done for the second polarisation, described by the vector $\hat{\mathbf{e}}_2$. In order to satisfy the condition $E_\parallel = 0$ at $z = 0$ we get

$$e^{-\mathrm{i}\omega t}\left(\frac{k_z}{k_\parallel k}\mathbf{k}_\parallel \sin k_z z + \mathrm{i}\frac{k_\parallel}{k}\hat{\mathbf{e}}_z \cos k_z z\right) e^{\mathrm{i}\mathbf{k}_\parallel \cdot \mathbf{r}_\parallel}, \tag{A.6}$$

and $B_z = 0$ will be satisfied anyway. Since we have now all expressions needed, we can finally define the mode functions. We shall do this in the following section, and also, introduce the electric field in terms of such normal modes.

A.1 Mode functions

The mode functions for an electromagnetic field bounded by a perfectly conducting plate are divided in two, depending on the polarisation direction of the light. In the TE polarisation, as concluded above, they read

$$\mathbf{f}_{\mathbf{k}}^{(1)} = 2\frac{\mathbf{k}\times\hat{\mathbf{e}}_z}{k_\parallel}e^{\mathrm{i}\mathbf{k}_\parallel\cdot\mathbf{r}_\parallel}\sin k_z z, \tag{A.7}$$

and for the TM polarisation

$$\mathbf{f}_{\mathbf{k}}^{(2)} = 2e^{\mathrm{i}\mathbf{k}_\parallel\cdot\mathbf{r}_\parallel}\left(\frac{k_z}{k_\parallel k}\mathbf{k}_\parallel\sin k_z z + \mathrm{i}\frac{k_\parallel}{k}\hat{\mathbf{e}}_z\cos k_z z\right), \tag{A.8}$$

with $\mathbf{k}_\parallel \in \Re^2$ and $k_z \geq 0$. The factor of 2 that we have added into their definitions is due to the fact, as explained in chapter 2, that these mode functions must be orthonormal, i.e., satisfy the condition

$$\int \mathrm{d}^3\mathbf{r}\ \mathbf{f}^*_{\mathbf{k}\lambda}(\mathbf{r})\cdot\mathbf{f}_{\mathbf{k}'\lambda'}(\mathbf{r}) = (2\pi)^3\delta^{(3)}(\mathbf{k}-\mathbf{k}')\delta_{\lambda\lambda'}. \tag{A.9}$$

It can be proven that $\mathbf{f}_{\mathbf{k}}^{(1)}$ and $\mathbf{f}_{\mathbf{k}}^{(2)}$ form a complete set of modes, i.e., that satisfy the completeness relation

$$\int \mathrm{d}^3\mathbf{k} f^i_{\mathbf{k}\lambda}(\mathbf{r})\ f^{*j}_{\mathbf{k}\lambda}(\mathbf{r}') = (\delta_{ij} - \Delta^{-1}\partial_i\partial_j)\delta^{(3)}(\mathbf{r}-\mathbf{r}'), \tag{A.10}$$

Then, we can finally write the vector potential in terms of the normal modes

$$\mathbf{A}(\mathbf{r},t) = \sum_\lambda \int \mathrm{d}^2\mathbf{k}_\parallel \int \mathrm{d}k_z \frac{1}{(2\pi)^{3/2}}\frac{1}{\sqrt{2\omega\epsilon_o}}\ a_{\mathbf{k}\lambda}e^{-\mathrm{i}\omega t}\ \mathbf{f}_{\mathbf{k}\lambda}(\mathbf{r}) + \text{H.C.}, \tag{A.11}$$

where H.C. is the hermitian conjugate, and the electric field is obtained straightforwardly, by using Eq. (2.7), bearing in mind that we are working in the Coulomb gauge, where $\Phi = 0$, we get

$$\mathbf{E}(\mathbf{r},t) = \mathrm{i}\sum_{\lambda}\int \mathrm{d}^2\mathbf{k}_{\parallel}\int \mathrm{d}k_z \frac{1}{(2\pi)^{3/2}}\sqrt{\frac{\omega}{2\epsilon_o}}\, a_{\mathbf{k}\lambda}e^{-\mathrm{i}\omega t}\,\mathbf{f}_{\mathbf{k}\lambda}(\mathbf{r}) - \mathrm{H.C.} \tag{A.12}$$

A.2 Perturbative calculation

We have now obtained the electric field in terms of the spatial modes, thus we can proceed with the calculation of the energy-level shift. By applying second order perturbation theory to the interaction Hamiltonian

$$H^{\mathrm{int}} = -\boldsymbol{\mu}\cdot\mathbf{E}(\mathbf{r},t), \tag{A.13}$$

we obtain

$$\Delta E = -\sum_{\lambda}\int \mathrm{d}^2\mathbf{k}_{\parallel}\int \mathrm{d}k_z \sum_{j\neq i}\frac{\left|\left\langle j;1_\nu|\boldsymbol{\mu}\cdot\hat{\mathbf{E}}(\mathbf{r},t)|i;0\right\rangle\right|^2}{E_j - E_i + \omega_\nu}, \tag{A.14}$$

as it has been derived in chapter 3. Within the electric dipole approximation, we can simplify the expression, for each component of the field, to

$$\Delta E = -\frac{1}{(2\pi)^3}\sum_{\iota}\sum_{j\neq i}\sum_{\lambda}\int \mathrm{d}^2\mathbf{k}_{\parallel}\int \mathrm{d}k_z \frac{\omega}{2\epsilon_o}\frac{1}{E_{ji}+\omega}\,|f^{(\lambda)}_{\mathbf{k}\iota}|^2\,|\langle j|\mu_\iota|i\rangle|^2 \tag{A.15}$$

We shall substitute each component of the mode functions. Then, in order to perform the double integral in $\mathbf{k}_{\parallel}$, we use the polar coordinates

$$\int \mathrm{d}^2\mathbf{k}_{\parallel} = \int_0^{\infty}\mathrm{d}k_{\parallel}k_{\parallel}\int_0^{2\pi}\mathrm{d}\phi \tag{A.16}$$

with $k_{\parallel} = k_x\cos\phi$ and $k_{\parallel} = k_y\sin\phi$. The integral in the azimuthal angle ϕ can be calculated straightforwardly, as we only need to know

$$\int_0^{2\pi}\mathrm{d}\phi\ \sin^2\pi = \int_0^{2\pi}\mathrm{d}\phi\ \cos^2\pi = \pi. \tag{A.17}$$

Thus, the energy-level shift is given by

$$\Delta E = -\frac{1}{(2\pi)^3}\sum_{j\neq i}\int_0^\infty \mathrm{d}k_\parallel k_\parallel \int_0^\infty \mathrm{d}k_z \frac{\omega}{2(E_{ji}+\omega)}\Big\{4\pi|\mu_x|^2\left(1+\frac{k_z^2}{k^2}\right)\sin^2 k_z z \\ +4\pi|\mu_y|^2\left(1+\frac{k_z^2}{k^2}\right)\sin^2 k_z z + 8\pi|\mu_z|^2\frac{k_\parallel^2}{k^2}\cos^2 k_z z\Big\}, \tag{A.18}$$

where, in order to simplify our notation, we have defined

$$|\mu_\iota|^2 \equiv |\langle j|\mu_\iota|i\rangle|^2 \qquad \text{with} \qquad \iota = x, y, z. \tag{A.19}$$

A.3 Renormalisation

In order to obtain the energy-level shift due solely to the presence of the reflecting surface, we shall remove the contribution that arises from the free space electromagnetic fluctuations, i.e. the Lamb shift. It is given by,

$$\Delta E^{\text{free}} = -\frac{1}{(2\pi)^3}\sum_{j\neq i}\int_0^\infty \mathrm{d}k_\parallel \int_0^\infty \mathrm{d}k_z \frac{k_\parallel\omega}{2(E_{ji}+\omega)} \\ \times\left(2\pi|\mu_x|^2\left(1+\frac{k_z^2}{k^2}\right)+2\pi|\mu_y|^2\left(1+\frac{k_z^2}{k^2}\right)+4\pi|\mu_z|^2\frac{k_\parallel^2}{k^2}\right), \tag{A.20}$$

and thus the renormalised shift reads,

$$\begin{aligned}\Delta E^{\text{ren}} &= \Delta E - \Delta E^{\text{free}} \\ &= -\frac{1}{2(2\pi)^3}\sum_{j\neq i}\int_0^\infty \mathrm{d}k_\parallel \int_0^\infty \mathrm{d}k_z \frac{k_\parallel\omega}{2(E_{ji}+\omega)}\Big[|\mu_x|^2\left(1+\frac{k_z^2}{k^2}\right)(2\sin^2 k_z z-1) \\ &\quad +|\mu_y|^2\left(1+\frac{k_z^2}{k^2}\right)(2\sin^2 k_z z-1)+2|\mu_z|^2\frac{k_\parallel^2}{k^2}(2\cos^2 k_z z-1)\Big].\end{aligned} \tag{A.21}$$

This equation can be solved analytically after performing some algebraic manipulation. We shall derive an exact expression for the shift in the following section.

A.4 Algebraic manipulation

In order to simplify the expression above we can use some identities for the trigonometric functions. Moreover, it can be seen that the x and y components of the shift can be treated together if we define $|\mu_\parallel|^2 = |\mu_x|^2 + |\mu_y|^2$. Thus,

$$\Delta E^{\text{ren}} = -\frac{1}{2(2\pi)^3}\sum_{j\neq i}\int_0^\infty \mathrm{d}k_\parallel \int_0^\infty \mathrm{d}k_z \frac{k_\parallel \omega}{2(E_{ji}+\omega)} \times \left(2|\mu_z|^2\frac{k_\parallel^2}{k^2}\cos 2k_z z - |\mu_\parallel|^2\left(1+\frac{k_z^2}{k^2}\right)\cos 2k_z z\right). \tag{A.22}$$

To perform the double integral we shall transform to polar coordinates: $k_\parallel = k\sin\theta$ and $k_z = k\cos\theta$, such that

$$\int_0^\infty \mathrm{d}k_\parallel \int_0^\infty \mathrm{d}k_z = \int_0^\infty \mathrm{d}k\; k \int_0^{\pi/2} \mathrm{d}\theta, \tag{A.23}$$

thus

$$\Delta E^{\text{ren}} = -\frac{1}{2(2\pi)^3}\sum_{j\neq i}\int_0^\infty \mathrm{d}k k^3 \int_0^{\pi/2} \mathrm{d}\theta\, \frac{\sin\theta}{E_{ji}+k} \times \left[2|\mu_z|^2\sin^2\theta\cos(2kz\cos\theta) - |\mu_\parallel|^2\left(1+\cos^2\theta\right)\cos(2kz\cos\theta)\right]. \tag{A.24}$$

It is quite useful to make a final change of variable. If we define $t = \cos\theta$ we get

$$\Delta E^{\text{ren}} = -\frac{1}{8\pi^2}\sum_{j\neq i}\int_0^\infty \mathrm{d}k \int_0^1 \mathrm{d}t\, \frac{k^3}{E_{ji}+k} \times \left\{2|\mu_z|^2(1-t^2)\cos(2kzt) - |\mu_\parallel|^2(1+t^2)\cos(2kzt)\right\}. \tag{A.25}$$

The integral in t can be solved analytically, and hence the expression for the energy-shift is reduced to

$$\Delta E^{\text{ren}} = -\frac{1}{8\pi^2}\sum_{j\neq i}\int_0^\infty \mathrm{d}k \frac{k^3}{E_{ji}+k}\Big\{|\mu_z|^2\left(\frac{\sin(2kz)}{2k^3z^3} - \frac{\cos(2kz)}{k^2z^2}\right) + |\mu_\parallel|^2\left(\frac{\sin(2kz)}{4k^3z^3} - \frac{\cos(2kz)}{2k^2z^2} - \frac{\sin(2kz)}{kz}\right)\Big\}. \tag{A.26}$$

However, as we are expecting to find a solution in terms of the auxiliary function, as defined in section 5.2.12 of Ref. [124]

$$f(x) \equiv \int_0^\infty \mathrm{d}t \frac{\sin t}{x+t}, \tag{A.27}$$

we can intuit that a quickly way to obtain them is by rewriting the sine and cosine functions in Eq. (A.26), in terms of their derivatives in z. For example, the perpendicular part of the shift can be rewritten as

$$\begin{aligned}\int_0^\infty \mathrm{d}k \frac{k^3}{E_{ji}+k}\left(\frac{\sin(2kz)}{2k^3z^3} - \frac{\cos(2kz)}{k^2z^2}\right) \\ = -\int_0^\infty \mathrm{d}k \frac{1}{E_{ji}+k}\left(\frac{\sin(2kz)}{2z^3} + \frac{\partial}{\partial z}\frac{\sin(2kz)}{2z^2}\right) \\ = -\frac{1}{2}\left(\frac{1}{z^3} + \frac{\partial}{\partial z}\frac{1}{z^2}\right)\int_0^\infty \mathrm{d}k \, \frac{\sin(2kz)}{E_{ji}+k}.\end{aligned} \tag{A.28}$$

We shall do similar manipulation for the parallel component of the shift. After some extensive algebraic manipulation we obtain,

$$\begin{aligned}\int_0^\infty \mathrm{d}k \frac{k^3}{E_{ji}+k}\left(\frac{\sin(2kz)}{4k^3z^3} - \frac{\cos(2kz)}{2k^2z^2} - \frac{\sin(2kz)}{kz}\right) \\ = \int_0^\infty \mathrm{d}k \frac{k^3}{E_{ji}+k}\left(\frac{\partial^2}{\partial z^2}\frac{\sin(2kz)}{4k^3z} + \frac{\cos(2kz)}{2k^2z^2} - \frac{\sin(2kz)}{4k^3z^3}\right) \\ = \frac{1}{4}\left(\frac{1}{z^3} + \frac{\partial}{\partial z}\frac{1}{z^2} + \frac{\partial^2}{\partial z^2}\frac{1}{z}\right)\int_0^\infty \mathrm{d}k \, \frac{\sin(2kz)}{E_{ji}+k}.\end{aligned} \tag{A.29}$$

Replacing the auxiliary function as defined in Eq. (A.27), we finally obtain

$$\Delta E^{\mathrm{ren}} = -\frac{1}{32\pi^2}\sum_{j\neq i}\left\{|\mu_\parallel|^2\left(\frac{1}{z^3} + \frac{\partial}{\partial z}\frac{1}{z^2} + \frac{\partial^2}{\partial z^2}\frac{1}{z}\right) - 2|\mu_z|^2\left(\frac{1}{z^3} + \frac{\partial}{\partial z}\frac{1}{z^2}\right)\right\} f(2zE_{ji}), \tag{A.30}$$

in agreement with Eq. (4.24)

A.5 Asymptotics

Note that the equation above is a general expression for the energy-level shift of an atom as a function of its distance from the surface of the reflecting plate. If we wish to obtain separate expressions for the retarded and the non-retarded regime, as it is normally presented, we shall expand the auxiliary function $f(x)$ for large and small x. In Appendix C we have given how the function $f(x)$ behaves in these limits. At small x, the expansion of the auxiliary function is given by Eq. (C.16). Thus, by substituting this into Eq. (A.30) we get

$$\Delta E^{\mathrm{es}} = -\frac{1}{64\pi\epsilon_o z^3}\left(|\mu_{\parallel}|^2 + 2|\mu_z|^2\right), \tag{A.31}$$

which is the correct electrostatic result (3.1). In order to recover the retarded regime, we shall substitute Eq. (C.15) into Eq. (A.30). The result is

$$\Delta E^{\mathrm{CP}} = -\frac{\hbar c}{16\pi^2\epsilon_o z^4}\sum_{j\neq i}\frac{|\mu_{\parallel}|^2 + |\mu_z|^2}{E_{ji}}, \tag{A.32}$$

which is the correct Casimir-Polder limit, in agreement with Eq. (4.12).

Appendix B

Transformation of the interaction Hamiltonian

In this appendix we shall explain how to transform the minimal coupling Hamiltonian $\mathbf{p} \cdot \mathbf{A}$ into the electric-dipole interaction $H_I = -\boldsymbol{\mu} \cdot \mathbf{E}(\mathbf{r}, t)$, which corresponds to the lowest-order in the multipole Hamiltonian [114, 116].

B.1 The electric-dipole approximation

Let us consider a single bound electron with binding potential energy $V(x) = e\phi(x)$ and suppose that the distances over which the bound electron can move in this potential are small compared with the wavelength of any field with which the electron undergoes a significant interaction. We can thus make what is called the electric-dipole approximation, which means that we can ignore the spatial variations of $\mathbf{A}$ in the interaction and simply evaluate $\mathbf{A}$ at a fixed position e.g. at the centre of the region over which the electron is free to move classically.

We can consider an overall neutral system, localized about the coordinate origin, and assume that all particles are sufficiently near to one another so that the Coulomb interaction is a very good approximation to their interaction. If such a system corresponds to an atom, which is small compared to the wavelength of the relevant electromagnetic

field, we can thus assume that all charges within the atom see practically the same field (or almost). This means that we can Taylor expand the fields around the centre of the atom,

$$A(\mathbf{r}) = A(0) + \mathbf{r} \cdot \nabla \mathbf{A}(0) + \cdots \tag{B.1}$$

$$\phi(\mathbf{r}) = \phi(0) + \mathbf{r} \cdot \nabla \phi(0) + \cdots \tag{B.2}$$

This expansion gives rise to the multipole moments of increasing order. We shall retain only the lowest order terms in this expansion and substitute these fields into the Hamiltonian (3.4). Hence, it can be approximated to

$$H = \sum_{\alpha} \frac{1}{2m} [\mathbf{p}_\alpha - q_\alpha \mathbf{A}(0)]^2 + V_{\text{Coul}}(\mathbf{r}) + \sum_{\alpha} q_\alpha r_\alpha \cdot \nabla \phi(0,t) \tag{B.3}$$

where $\{q_\alpha\}$ is the assembly of charges within the atom. The last term correspond to the electrostatic interaction, and we shall note that the first term of the expansion for ϕ, i.e. $\sum_\alpha q_\alpha \phi(0,t) = 0$ because the sum over all charges is zero. The lowest-order in the expansion is the electric dipole moment, which is defined as

$$\boldsymbol{\mu} = \sum_{\alpha} q_\alpha r_\alpha \tag{B.4}$$

to rewrite the Hamiltonian as

$$H = \sum_{\alpha} \frac{1}{2m} [\mathbf{p}_\alpha - q_\alpha \mathbf{A}(0)]^2 + V_{\text{Coul}}(\mathbf{r}) + \boldsymbol{\mu} \cdot \nabla \phi(0,t) \tag{B.5}$$

B.2 Electric Dipole interaction

Furthermore, we can use the generator $X(\mathbf{r},t)$ defined by

$$X(\mathbf{r},t) = -\mathbf{r} \cdot \mathbf{A}(0,t) \tag{B.6}$$

Hence, the new potentials are given by

$$\mathbf{A}(\mathbf{r},t) \rightarrow \mathbf{A}'(\mathbf{r},t) = \mathbf{A}(\mathbf{r},t) - \mathbf{A}(0,t) \tag{B.7}$$

$$\phi(\mathbf{r},t) \rightarrow \phi'(\mathbf{r},t) = \phi(\mathbf{r},t) + \mathbf{r}\cdot\dot{\mathbf{A}}(0,t), \tag{B.8}$$

which is the so-called Göpper-Mayer transformation. It yields to,

$$\mathbf{A}'(0,t) = 0, \tag{B.9}$$

$$\nabla\phi'(0,t) = \nabla\phi(0,t) + \dot{\mathbf{A}}(0,t) = -\mathbf{E}(0,t), \tag{B.10}$$

where $\mathbf{E}(0,t)$ is the total electric field at 0. Substituting these potentials into the Hamiltonian (B.5), we finally get

$$H = \sum_\alpha \frac{1}{2m}[\mathbf{p}_\alpha - q_\alpha\mathbf{A}(0)]^2 + V_{\text{Coul}}(\mathbf{r}) - \boldsymbol{\mu}\cdot\mathbf{E}(0,t). \tag{B.11}$$

This equation has the advantage of making explicit the electric dipole interaction between d and $\mathbf{E}$.

In quantum theory, the transition between the usual description and the Göpper-Mayer transformation is realised by the unitary transformation

$$T(t) = \exp\left\{-\frac{\mathrm{i}}{\hbar}\boldsymbol{\mu}\cdot\mathbf{A}(0,t)\right\} = \exp\left\{-\frac{\mathrm{i}}{\hbar}\sum_\alpha q_\alpha r_\alpha\cdot\mathbf{A}(0,t)\right\}. \tag{B.12}$$

It is possible to study directly the effect of this unitary transformation on the initial representation[1].

A generalisation of the Göpper-Mayer transformation which no longer describes the system of charges through their dipole moment, but takes into account the precise distribution of charges and currents is the Power-Zienau transformation [115]. We can use this approach to get a multipole expansion of the interaction between the system of charges and the electric and magnetic field.

[1] See for instance page 121 in Ref. [3]

Appendix C

Some useful mathematics

C.1 Bessel Functions

Section 6.554, Eq. 1, in [126]

$$\int_0^\infty \mathrm{d}x x \frac{J_o(yx)}{\sqrt{x^2+z^2}} = \frac{e^{-yz}}{y}, \tag{C.1}$$

In order to obtain Eq. (3.115) that leads us to the electrostatic interaction in 3.6.2, we require the derivative of the Bessel function $J_o(z)$, which can be found in Eq. 9.1.28 in Ref. [124]

$$J_o'(z) = -J_1(z), \tag{C.2}$$

using the chain rule we obtain

$$\frac{\partial}{\partial x_o} J_o(k\rho) = -kJ_1(k\rho)\frac{\partial \rho}{\partial x_o} = -kJ_1(k\rho)\frac{x_o - x}{\rho}, \tag{C.3}$$

and using the same formula again in order to obtain the second derivative

$$\frac{\partial}{\partial x}\left(\frac{\partial}{\partial x_o} J_o(k\rho)\right) = \frac{\partial J_1(k\rho)}{\partial(k\rho)}(x-x_o)^2\frac{k^2}{\rho^2} + J_1(k\rho)\frac{k}{\rho} - J_1(k\rho)(x-x_o)^2\frac{k}{\rho^3}. \tag{C.4}$$

By using the identity 9.1.27 in [124]

$$\frac{\partial J_1(x)}{\partial x} = J_o(x) - \frac{J_1(x)}{x}, \tag{C.5}$$

one can further simplify the expression above, to obtain

$$\frac{\partial}{\partial x}\left(\frac{\partial}{\partial x_o} J_o(k\rho)\right) = \left(J_o(k\rho)\frac{k^2}{\rho^2} - 2J_1(k\rho)\frac{k}{\rho^3}\right)(x - x_o)^2 + J_1(k\rho)\frac{k}{\rho} \tag{C.6}$$

As it can be seen in Eq. (3.113) of page 106, what we actually need is the limit $\rho \to 0$. We can use

$$\lim_{\rho\to 0} \frac{J_1(k\rho)}{\rho} = \frac{k}{2}$$

into the equation above to finally get

$$\left.\frac{\partial^2 J_o(k\rho)}{\partial x\, \partial x_o}\right|_{\rho \to 0} = \frac{k^2}{2}, \tag{C.7}$$

which gives us the result shown in Eq. (3.115).

C.2 Integrals

In order to recover the Casimir-Polder force between an atom and a perfect mirror, we require the following integrals, taken from section 2.124 in Ref. [126],

$$\int_0^1 \mathrm{d}t\, \frac{1}{r^2t^2 + 1} = \frac{1}{r}\arctan(r). \tag{C.8}$$

In order to calculate Eq. (4.17) we shall integrate by parts

$$\int_0^\infty \mathrm{d}r\ \arctan(r)\, e^{-\xi r} = \arctan(r)\, \frac{e^{-\xi r}}{\xi}\bigg|_0^\infty + \frac{1}{\xi}\int_0^\infty \mathrm{d}r\, \frac{e^{-\xi r}}{1 + r^2} \tag{C.9}$$

$$\int_0^\infty \mathrm{d}r\, r^2 \arctan(r)\, e^{-\xi r} = -(r^2\xi^2 + 2r\xi + 2)\arctan(r)\, \frac{e^{-\xi r}}{\xi^3}\bigg|_0^\infty + \frac{1}{\xi}\int_0^\infty \mathrm{d}r\, \frac{r^2 e^{-\xi r}}{1 + r^2} + \frac{2}{\xi^2}\int_0^\infty \mathrm{d}r\, \frac{r\, e^{-\xi r}}{1 + r^2} + \frac{2}{\xi^3}\int_0^\infty \mathrm{d}r\, \frac{e^{-\xi r}}{1 + r^2}. \tag{C.10}$$

Notice that the first term in each integral vanishes after evaluation in the limits.

C.3 Auxiliary Function

The definition for the auxiliary function has been taken from section 5.2.12 in Ref. [126],

$$f(z) = \int_0^\infty \mathrm{d}y \, \frac{e^{-zy}}{1+y^2} = ci(z)\sin(z) - si(z)\cos(z). \tag{C.11}$$

Also, from the equation above, we can write its first and second derivatives,

$$\int_0^\infty \mathrm{d}y \, \frac{y\, e^{-zy}}{1+y^2} = -\frac{\partial}{\partial z}\int_0^\infty \mathrm{d}y \, \frac{e^{-zy}}{1+y^2} = -f'(z) \tag{C.12}$$

$$\int_0^\infty \mathrm{d}y \, \frac{y^2\, e^{-zy}}{1+y^2} = \frac{\partial^2}{\partial z^2}\int_0^\infty \mathrm{d}y \, \frac{e^{-zy}}{1+y^2} = f''(z) \tag{C.13}$$

And we can rewrite the second derivative as follows,

$$\begin{aligned}\int_0^\infty \mathrm{d}y \, \frac{y^2\, e^{-zy}}{1+y^2} &= \int_0^\infty \mathrm{d}y \, \frac{(y^2+1-1)\, e^{-zy}}{1+y^2} \\ &= \int_0^\infty \mathrm{d}y \, e^{-zy} - \int_0^\infty \mathrm{d}y \, \frac{e^{-zy}}{1+y^2} = \frac{1}{z} - f(z).\end{aligned} \tag{C.14}$$

C.3.1 Asymptotics

For large values of the argument of the auxiliary function, from Eq. 5.2.34 in [124]

$$f(z) \sim \frac{1}{z}\left(1 - \frac{2!}{z^2} + \frac{4!}{z^4} - ...\right) \qquad z \gg 1 \tag{C.15}$$

and for very small arguments we can approximate

$$f(z) \sim \frac{\pi}{2} \qquad z \ll 1 \tag{C.16}$$

Bibliography

[1] K. Autumn, Y. Liang, S. Hsieh, W. Zesch, W. Chan, T. Kenny, R. Fearing, and R. Full. Adhesive force of a single gecko foot-hair. *Nature*, 405(6787):681–685, 2000.

[2] H. Casimir and D. Polder. The influence of retardation on the London-van der Waals forces. *Phys. Rev.*, 73(4):360–372, 1948.

[3] P. Milonni. *The Quantum Vacuum. An introduction to Quantum Electrodynamics.* Academic Press, New York, 1994.

[4] J. Israelachvili. *Intermolecular and surface forces.* Academic Press, London, second edition, 1991.

[5] D. Langbein. *Theory of Van der Waals attraction.* Springer, New York, 1974.

[6] H. Margenau and N. Kestner. *Theory of intermolecular forces.* Pergamon, Oxford, second edition, 1971.

[7] S. Buhmann and D. Welsch. Dispersion forces in macroscopic quantum electrodynamics. *Progress in quantum electronics*, 31:51–130, 2007.

[8] G. Navascues. Liquid surfaces. theory of surface-tension. *Rep. Prog. Phys.*, 42: 1131, 1979.

[9] L. Bruch, M. Cole, and E. Zaremba. Physical adsorption: Forces and phenomena. *Journal of Chemical Education*, 75:1557, 1997.

[10] H. Kellay, J. Meunier, and B. Binks. Wetting properties of n-alkanes on AOT monolayers at the brine-air interface. *Phys. Rev. Lett.*, 69(8):1220–1223, 1992.

[11] J. Jackson. *Classical Electrodynamics*. Wiley, New York, third edition, 1999.

[12] F. London. *Z. Phys. Chem. B*, 11:222, 1930.

[13] F. London. On centers of van der Waals attraction. *J. Phys. Chem.*, 46(2): 305–316, 1942.

[14] A. McLachlan. Retarded dispersion forces between molecules. *Proc. R. Soc. London Ser. A*, 271:387, 1963.

[15] H. Casimir and D. Polder. The influence of retardation on the London-van der Waals forces. *Nature*, 158(4022):787–788, 1946.

[16] H. Casimir and D. Polder. *Proc. K. Ned. Akad. Wet.*, 60:793, 1948.

[17] E. Power and S. Zienau. The general theory of van der Waals forces. *Nuovo Cim.*, 6(1):7–17, 1957.

[18] I. Dzialoshinskii. Account of retardation in the interaction of neutral atoms. *Soviet Physics JETP-USSR*, 3:977–979, 1957.

[19] C. Mavroyannis and M. Stephen. Dispersion forces. *Mol. Phys.*, 5:629–638, 1962.

[20] P. Milonni. Casimir effects. *Phys. Scr.*, 76:C167, 2007.

[21] E. Lifshitz. The theory of molecular attractive forces between solids. *Sov. Phys. JETP*, 2:73, 1956.

[22] H. Casimir. On the attraction between two perfectly conducting plates. *Proc. Kon. Ned. Akad. Wet*, 51:793–795, 1948.

[23] I. Brevik, S. Ellingsen, and K. Milton. Thermal corrections to the Casimir effect. *New J. Phys.*, 8(236), 2006.

[24] B. Geyer, G. Klimchitskaya, and V. Mostepanenko. Casimir force under the influence of real conditions. *Int. J. Mod. Phys. A*, 16:3291–3308, 2001.

[25] A. Contreras-Reyes and W. Mochán. Surface screening in the Casimir force. *Phys. Rev. A*, 72(3):034102, 2005.

[26] A. Lambrecht, P. Neto, and S. Reynaud. The casimir effect within scattering theory. *New J. Phys.*, 8(243), 2006.

[27] W. Mochán and C. Villarreal. Casimir effect for arbitrary materials: contributions within and beyond the light cone. *New J. Phys.*, 8(242), 2006.

[28] G. Barton. Frequency shifts near an interface: Inadequecy of two-level atomic models. *J. Phys. B: Atom. Molec. Phys.*, 7(16):2134–2142, 1974.

[29] G. Barton. Quantum electrodynamics of spinless particles between conducting plates. *Proc. R. Soc. London Ser. A*, 320:320, 1970.

[30] C. Mavroyannis. The interaction of neutral molecules with dielectric surfaces. *Mol. Phys.*, 6:593–600, 1956.

[31] M. Babiker and G. Barton. Quantum frequency shifts near a plasma surface. *J. Phys. A*, 9:129, 1976.

[32] C. Eberlein and M. Janowicz. Interaction of an atom with a small dispersive and absorptive dielectric body. *Phys. Rev. A*, 67(6):063816, 2003.

[33] S. Buhmann, H. Dung, T. Kanipf, and D. Welsch. Casimir-Polder interaction of atoms with magnetodielectric bodies. *Eur. Phys. J. D*, 35(1):15–30, 2005.

[34] S. Lamoreaux. Casimir forces: Still surprising after 60 years. *Physics Today*, 60: 40, 2007.

[35] D. Raskin and P. Kusch. Interaction between a neutral atomic or molecular beam and a conducting surface. *Phys. Rev.*, 179(3):712–721, 1969.

[36] A. Shih, D. Raskin, and P. Kusch. Investigation of the interaction potential between a neutral molecule and a conducting surface. *Phys. Rev. A*, 9(2):652–662, 1974.

[37] A. Anderson, S. Haroche, E. Hinds, W. Jhe, and D. Meschede. Measuring the van der Waals forces between a Rydberg atom and a metallic surface. *Phys. Rev. A*, 37:3594, 1988.

[38] V. Sandoghdar, C. Sukenik, E. Hinds, and S. Haroche. Direct measurement of the van der Waals interactions between an atom and its images in a micron-sized cavity. *Phys. Rev. Lett.*, 68(3432), 1992.

[39] C. Sukenik, M. Boshier, D. Cho, V. Sandoghdar, and E. Hinds. Measument of the Casimir-Polder force. *Phys. Rev. Lett.*, 70(5), 1993.

[40] M. Kasevich, K. Moler, E. Riis, E. Sundermann, D. Weiss, and S. Chu. Applications of laser cooling and trapping. *Atom. Phys.*, 12, 1991.

[41] A. Landragin, J. Courtois, G. Labeyrie, N. Vansteenkiste, C. Westbrook, and A. Aspect. Measurement of the van der Waals force in an atomic mirror. *Phys. Rev. Lett.*, 77(8):1464–1467, 1996.

[42] R. Grisenti, W. Schöllkopf, J. Toennies, G. Hegerfeldt, and T. Köhler. Determination of atom-surface van der Waals potentials from transmission-grating diffraction intensities. *Phys. Rev. Lett.*, 83(9):1755–1758, 1999.

[43] M. Boustimi, B. Viaris de Lesegno, J. Baudon, J. Robert, and M. Ducloy. Atom symmetry break and metastable level coupling in rare gas atom-surface van der Waals interaction. *Phys. Rev. Lett.*, 86(13):2766–2769, 2001.

[44] F. Shimizu. Specular reflection of very slow metastable neon atoms from a solid surface. *Phys. Rev. Lett.*, 86(987), 2001.

[45] T. Pasquini, Y. Shin, C. Sanner, M. Saba, A. Schirotzek, D. Pritchard, and

W. Ketterle. Quantum reflection from a solid surface at normal incidence. *Phys. Rev. Lett.*, 93(22):223201, 2004.

[46] V. Druzhinina and M. DeKieviet. Experimental observation of quantum reflection far from threshold. *Phys. Rev. Lett.*, 91(19):193202, 2003.

[47] Y. Lin, I. Teper, C. Chin, and Vuleti'c. Impact of the Casimir-Polder potencial and Johnson noise on Bose-Einstein condensate stability near surfaces. *Phys. Rev. Lett.*, 92(5):050404, 2004.

[48] H. Oberst, Y. Tashiro, K. Shimizu, and F. Shimizu. Quantum reflection of he-* on silicon. *Phys. Rev. A*, 71(5):052901, 2005.

[49] D. Dalvit, P. Maia, A. Lambrecht, and S. Reynaud. Probing quantum-vacuum geometrical effects with cold atoms. *Phys. Rev. Lett.*, 100(040405), 2008.

[50] Lamb and Retherford. Fine structure of the hydrogen atom by a microwave method. *Phys. Rev.*, 72:241–243, 1947.

[51] A. Salam, H. Bethe, P. Dirac, W. Heisenberg, E. Wigner, O. Klein, and E. Lifshitz. *From a life of Physics.* World Scientific, 1980.

[52] H. Bethe. The electromagnetic shift of energy levels. *Phys. Rev.*, 72(4):339–341, 1941.

[53] R. Feynman. Development of space-time view of quantum electrodynamics. *Science*, 153:699, 1966.

[54] U. Leonhardt and T. Philbin. Quantum levitation by left-handed metamaterials. *New J. Phys.*, 9(254), 2007.

[55] F. Rosa, D. Dalvit, and P. Milonni. Casimir-Lifshitz theory and metamaterials. *Phys. Rev. Lett.*, 100(183602), 2008.

[56] H. Chan, V. Aksyuk, R. Kleiman, D. Bishop, and F. Capasso. Nonlinear micromechanical Casimir oscillator. *Phys. Rev. Lett.*, 87(21):211801, 2001.

[57] H. Chan, V. Aksyuk, R. Kleiman, D. Bishop, and F. Capasso. Quantum mechanical actuation of microelectromechanical systems by the Casimir force. *Science*, 291(5510):1941–1944, 2001.

[58] C Eberlein and R Zietal. Force on a neutral atom near conducting microstructures. *Phys. Rev. A*, 75(032516), 2007.

[59] A. Migdall, J. Prodan, W. Phillips, T. Bergeman, and H. Metcalf. First observation of magnetically trapped neutral atoms. *Phys. Rev. Lett.*, 54(24):2596–2599, 1985.

[60] E. Cornell and C. Wieman. Nobel lecture: Bose-einstein condensation in a dilute gas, the first 70 years and some recent experiments. *Rev. Mod. Phys.*, 74(3): 875–893, 2002.

[61] W. Ketterle. Nobel lecture: When atoms behave as waves: Bose-einstein condensation and the atom laser. *Rev. Mod. Phys.*, 74(4):1131–1151, 2002.

[62] S. Dimopoulos and A. Geraci. Probing submicron forces by interferometry of bose-einstein condensed atoms. *Phys. Rev. D*, 68(12):124021, 2003.

[63] C. Pethick and H. Smith. *Bose-Einstein Condensation in Dilute Bose Gases*. Cambridge University Press, first edition, 2002.

[64] L. Pitaevskii and S. Stringari. *Bose-Einstein Condensation*. Clarendon Press, Oxford, first edition, 2003.

[65] D. Harber, J. Obrecht, J. McGuirk, and E. Cornell. Measurement of the Casimir-Polder force through center-of-mass oscillations of a Bose-Einstein condensate. *Phys. Rev. A*, 72:033610, 2005.

[66] J. Obrecht, R. Wild, M. Antezza, L. Pitaevskii, S. Stringari, and E. Cornell. Measurement of the temperature dependence of the Casimir-Polder force. *Phys. Rev. Lett.*, 98:063201, 2007.

[67] M. Antezza, L. Pitaevskii, and S. Stringari. Effect of the Casimir-Polder force on the collective oscillations of a trapped Bose-Einstein condensate. *Phys. Rev. A*, 70:053619, 2004.

[68] A. Mohapatra and C. Unnikrishnan. Measurement of the van der Waals force using reflection of cold atoms from magnetic thin-film atom mirrors. *Europhys. Lett.*, 73:839–845, 2006.

[69] V. Ivanov, R. Cornelussen, H. van den Heuvell, and Spreeuw R. Observation of modified radiative properties of cold atoms in vacuum near a dielectric surface. *J. Opt. B*, 6:454–459, 2004.

[70] J. Fortagh and C. Zimmermann. Magnetic microtraps for ultracold atoms. *Review of Modern Phys.*, 79(1):235–289, 2007.

[71] C. Henkel, S. Potting, and M. Wilkens. Spin coupling between cold atoms and the thermal fluctuations of a metal surface. *Appl. Phys. B*, 69(5–6):379–387, 1999.

[72] M. Jones, C. Vale, D. Sahagun, B. Hall, and E. Hinds. Spin coupling between cold atoms and the thermal fluctuations of a metal surface. *Phys. Rev. Lett.*, 91 (8), 2003.

[73] D. Harber, J. McGuirk, J. Obrecht, and E. Cornell. Thermally induced losses in ultra-cold atoms magnetically trapped near room-temperature surfaces. *J. Low Temp. Phys.*, 133:229–238, 2003.

[74] A. Leanhardt, Y. Shin, A. Chikkatur, D. Kielpinski, W. Ketterle, and D. Pritchard. Bose-Einstein condensates near a microfabricated surface. *Phys. Rev. Lett.*, 90(10):100404, 2003.

[75] C. Eberlein and S. Wu. Methods of asymptotic analysis in cavity quantum electrodynamics. *Phys. Rev. A*, 68:033813, 2003.

[76] S. Wu and C. Eberlein. Quantum electrodynamics of an atom in front of a non-dispersive dielectric half-space. *Proc. R. Soc. Lond. A*, 455:2487–2512, 1999.

[77] H. Khosravi and R. Loudon. Vacuum field fluctuations and spontaneous emission in a dielectric slab. *Proc. R. Soc. Lond. A*, 436:373–389, 1992.

[78] H. Khosravi and R. Loudon. Vacuum field fluctuations and spontaneous emission in the vicinity of a dielectric surface. *Proc. R. Soc. Lond. A*, 433:337–352, 1991.

[79] W. Żakowicz and A. Błędowski. Spontaneous emission in the presence of a dielectric slab. *Phys. Rev. A*, 52:1640–1650, 1995.

[80] H. Urbach and A. Rikken. Spontaneous emission from a dielectric slab. *Phys. Rev. A*, 57(5):3913–3929, 1998.

[81] E. Yablonovitch, T. Gmitter, and R. Bhat. Inhibited and enhanced spontaneous emission from optically thin AlGaAs/GaAs double heterostructures. *Phys. Rev. Lett.*, 61(22):2546–2549, 1988.

[82] G. Rikken. Spontaneous emission from stratified dielectrics. *Phys. Rev. A*, 51(6): 4906–4909, 1995.

[83] F. Zhou and L. Spruch. Van der Waals and retardation (Casimir) interactions of an electron or an atom with multilayered walls. *Phys. Rev. A*, 52(1):297–310, 1995.

[84] M. Böstrom and B. Sernelius. Van der Waals energy of an atom in the proximity of thin metal films. *Phys. Rev. A*, 61:052703, 2000.

[85] H. Nha and W. Jhe. Cavity quantum electrodynamics between parallel diectric surfaces. *Phys. Rev. A*, 54(2):3505–3512, 1996.

[86] A. McLachlan. Van der Waals forces between an atom an a surface. *Mol. Phys.*, 7(4):381–388, 1963.

[87] G. Agarwal. Quantum electrodynamics in the presence of dielectrics and conductors: Theory of dispersion forces. *Phys. Rev. A*, 11(1):243–251, 1975.

[88] G. Agarwal. Quantum electrodynamics in the presence of dielectrics and conductors: General theory for spontaneous emission in finite geometries. *Phys. Rev. A*, 12(4):1475–1497, 1975.

[89] J. Wylie and E. Slipe. Quantum electrodynamics near an interface. *Phys. Rev. A*, 30(3):1185–1193, 1984.

[90] J. Wylie and E. Slipe. Quantum electrodynamics near an interface ii. *Phys. Rev. A*, 32(4):2030–2043, 1985.

[91] C. Eberlein and D. Robaschik. Quantum electrodynamics in the presence of a dielectric. *J. Phys. A: Math. Gen.*, 39:6293–6298, 2006.

[92] N. Bogoliubov and D. Shirkov. *Introduction to the theory of quantized fields.* Wiley, New Yrok, third edition, 1980.

[93] N. Kapany and J. Burke. *Optical waveguides.* Academic Press, New York, 1972.

[94] D. Marcuse. *Theory of dielectric optical waveguides.* Academic Press, New York, 1974.

[95] E. Hecht. *Optics.* Addison-Wesley, Reading, Mass., fourth edition, 2002.

[96] Greiner W and J. Reinhardt. *Field quantization.* Springer, Berlin, 1996.

[97] S. Siklos and C. Eberlein. On the asymptotics of a class of two-dimensional fourier integrals. *J. Phys. A: Math. Gen.*, 32(18):3433–3439, 1999.

[98] N. Ashcroft and D. Mermin. *Solid State Physics.* Hot-Saunders International Editions, New York, 1976.

[99] C. Carniglia and L. Mandel. Quantization of evanescent electromagnetic waves. *Phys. Rev. D*, 3:280–296, 1971.

[100] I. Bialynicki-Birula and J. Brojan. Completeness of evanescent waves. *Phys. Rev. D*, 5:485–487, 1972.

[101] M. Goldgberger and K. Watson. *Collision theory*. John Wiley & Sons, Inc, 1964.

[102] M. Born and E. Wolf. *Principles of optics: Electromagnetic theory of propagation, interference and diffraction of light*. Addison-Wesley, Reading, Mass., sixth edition, 1980.

[103] R. Silverman. *Introductory Complex Analysis*. Dover, New York, 1972.

[104] G. Arfken. *Mathematical methods for physicists*. Academic Press, Orlando, third edition, 1985.

[105] A. Contreras-Reyes and C. Eberlein. Completeness of evanescent modes in layered dielectrics. Submitted to Phys. Rev. A, 2008.

[106] J. Sakurai. *Modern Quantum Mechanics*. Addison-Wesley, Reading, Mass., 1994.

[107] K. Cho. *Optical Response of nanostructures*. Springer, Berlin, 2003.

[108] J. Lennard-Jones. Processes of adsorption and diffusion on solid surfaces. *Transaction of the Faraday Society*, 28:0333–0358, 1932.

[109] C. Cohen-Tannoudji, J. Dupont-Roc, and G. Grynberg. *Phtotons and atoms. Introduction to Quantum Electrodynamics*. Wiley-Interscience Publication, New York, 1964.

[110] R. Loudon. *The quantum theory of light*. Clarendon Press, Oxford, second edition, 1983.

[111] S. Wu and C. Eberlein. Quantum electrodynamics of an atom in front of a non-dispersive dielectric half-space ii. effects of finite temperature. *Proc. R. Soc. Lond. A*, 1931:2487–2512, 2000.

[112] J. Annett and P. Echenique. Van der Waals interaction between an atom and a surface at finite separations. *Phys. Rev. B*, 34(10):6853–6859, 1986.

[113] S. Scheel, L. Knöll, D. Welsch, and S. Barnett. Quantum local-field corrections and spontaneous decay. *Phys. Rev. A*, 60(2):1590–1597, 1999.

[114] E. Power. *Introductory Quantum Electrodynamics*. Longmans, 1964.

[115] E. Power and S. Zienau. Coulomb gauge in non-relativistic quantum electrodynamics and the shape of spectral lines. *Philos. Trans. R. Soc. London A*, 251: 427, 1959.

[116] D. P. Craig and T. Thirunamachandran. *Molecular Quantum Electrodynamics*. Academic Press, New York, 1984.

[117] E. Power and T. Thirunamachandran. Quantum electrodynamics in a cavity. *Phys. Rev. A*, 25(5):2473–2484, 1982.

[118] C. Eberlein and D. Robaschik. Quantum electrodynamics near a dielectric halfspace. *Phys. Rev. D*, 73:025009, 2006.

[119] P. Morse and H. Feshbach. *Methods of theoretical physics*, volume 1. McGraw-Hill Book Company, Inc, 1953.

[120] M. Bordag. Reconsidering the quantization of electrodynamics with boundary conditions and some measurable consequences. *Phys. Rev. D*, 70:085010, 2004.

[121] M. Bordag. Interaction of a charge with a thin plasma sheet. *Phys. Rev. D*, 76: 065011, 2007.

[122] G. Barton. Casimir effects for a flat plasma sheet I. Energies. *J. Phys. A: Math*, 38(13):2997–3019, 2005.

[123] G. Barton. Casimir effects for a flat plasma sheet II. Fields and stresses. *J. Phys. A*, 38(13):3021–3044, 2005.

[124] M. Abramowitz and I. Stegun. *Handbook of mathematical functions*. Dover, New York, ninth edition, 1970.

[125] Eisenschitz and F. London. *Z. Phys.*, 60:491, 1930.

[126] I. Gradshteyn and I. Ryzhik. *Table of Integrals, series and products*. Academic Press, London, sixth edition, 2000.

[127] C. Bender and S. Orszag. *Advanced mathematical methods for scientists and engineers*. McGraw-Hill, 1978.

[128] S. Buhmann, D. Welsch, and T. Kampf. Ground-state van der Waals forces in planar multilayer magnetodielectrics. *Phys. Rev. A*, 72(3):032112, 2005.

[129] A. Abrikosov, L. Gorkov, and I. Dzyaloshinski. *Methods of Quantum Field Theory in Statistical Physics*. 1975.